Characterization of early mouse mesenchymal stem/progenitor cells for generating cartilage and study their role in endochondral ossification

Inauguraldissertation

zur Erlangung der Würde eines Doktors der Philosophie

vorgelegt der

Philosophisch-Naturwissenschaftlichen Fakultät

der Universität Basel

von

Sumit Jaiswal

aus Indien

Basel, 2016

Genehmigt von der Philosophisch-Naturwissenschaftlichen Fakultät
auf Antrag von

Prof. Dr. Rolf Zeller (Dissertationsleiter und Fakultätsverantwortlicher),

Prof. Dr. Ivan Martin (Korreferent)

Basel, den 23. Februar 2016

Prof. Dr. Jörg Schibler

Dekan

1. Table of Contents

2. Summary

Mesenchymal stem/ stromal cells (MSCs) isolated from mice have allowed to address some of the major issues that could not be investigated by using human MSCs. For this thesis, a thorough characterization of a previously described mouse MSC population, namely PαS MSCs (identified by expression of both PDGFRα and Sca1 antigens) was done. Using a developmental approach, the MSC-like cells were also identified in embryonic stages. We identified 4 subpopulations of PαS cells, based on the expression of the CD90 and CD73 markers. The flow-cytometry based analysis revealed different time points of the emergence of the different subpopulations of these cells during ontogeny. Using a Sox9-*GFP* reporter line, we were able to correlate these changes with the predominant chondrogenic and osteogenic processes during progression of mouse development and endochondral ossification.

A developmental paradigm was used to characterize the "stem" like properties of PαS subpopulations in vitro from postnatal day P2, since a significant increase of this population was observed from E18.5 until P2 after birth. The conditions of the in vitro trilineage differentiation and chondrogenic differentiation were refined to achieve better results by mimicking the molecular pathways operating during limb development. Two subsets of PαS cells were discriminated by the expression of CD90 marker (PαS$^+$CD90$^+$ and PαS$^+$CD90$^-$ subsets). These subsets were assessed for their in vivo fate by engrafting cartilage templates generated from these cells subcutaneously in nude mice. Strikingly, the cartilage models generated from the PαS$^+$CD90$^+$ subset remodeled completely to undergo endochondral ossification and the resulting bone ossicles were invaded by host-derived bone marrow cells. On the other hand, the cartilage models generated from the PαS$^+$CD90$^-$ subset appeared to remodel only partially. No endochondral ossification was observed, but the expression of Sox9 persisted, which pointed to maintenance of chondrogenic potential. As in vivo functions of MSCs may depend on their interaction with HSCs in the stem cell niche, cartilage

templates generated from PαS subsets isolated at embryonic day E18.5 were also engrafted. This developmental stage coincides with migration of the first HSCs from fetal liver to the bone marrow. The remodeling of cartilage into bone was reduced and only small bone ossicles formed when cartilage templates from PαS$^+$CD90$^+$ cells were implanted.

Thus, this study focuses on extensive characterization of PαS cells to identify new subpopulations and refining the conditions of multilineage differentiation in these subpopulations with a developmental approach. Emergence of these subpopulations during mouse development to contribute towards cartilage and bone lineage was determined by studying in detail their in vivo fates during endochondral ossification.

3. List of Abbreviations

7-AAD	7-aminoactinomycin D	**IBMX**	3-isobutyl-1-methylxanthine
AER	Apical ectodermal ridge	**IHC**	Immunohistochemistry
ALP	Alkaline phosphatase	**IHH**	Indian hedgehog
BMP	Bone morphogenetic protein	**IP**	Intraperitoneal
BMSC	Bone marrow stromal cell	**ISCT**	International Society for Cellular Therapy
BrdU	5-bromo-2'-deoxyuridine		
BSA	Bovine serum albumin	**LMP**	Limb bud mesenchymal progenitor
C/EBPα	CCAAT/enhancer binding protein alpha	**LNGFR**	Low-affinity nerve growth factor receptor
cAMP	Cyclic adenosine 3′,5′-monophosphate	**LPA**	Linear polyacrylamide
CAR	CXCL12-abundant reticular	**Ly6**	Lymphocyte antigen 6
CD	Cluster of differentiation	**MCAM**	Melanoma cell adhesion molecule
CFU-F	Colony-forming unit fibroblast	**MMP**	Matrix metalloproteinase
CLP	Common lymphoid progenitor	**mSSC**	Mouse skeletal stem cell
CMP	Common myeloid progenitor	**Mx1**	Myxoma Resistance Protein 1
CMV	Cytomegalovirus	**OA**	Osteoarthritis
CREB	cAMP response element-binding protein	**OCP**	Osteo-chondroprogenitor
		OCR	Osteochondroreticular
CXCL12	C-X-C motif chemokine 12	**OCT**	Optimum cutting temperature
DAPI	4′,6-Diamidin-2-phenylindol	**PDGFRα**	Platelet-derived growth factor receptor-alpha
DEPC	Diethylpyrocarbonate		
DMEM	Dulbecco's modified eagle's medium	**PFA**	Paraformaldehyde
DMSO	Dimethyl sulfoxide	**PI3K3**	Phosphatidylinositol-3 kinase
DPBS	Dulbecco`s phosphate buffered saline	**PPARγ**	Peroxisome proliferator-activated receptor gamma
ECM	Extracellular matrix		
EDTA	Ethylenediaminetetraacetic acid	**Prx1**	Paired related homeobox 1
EpCAM	Epithelial cell adhesion molecule	**PTHrP**	Parathyroid hormone-related protein
ESC	Embryonic stem cell	**Runx2**	Runt-related transcription factor 2
FACS	Fluorescence Activated Cell Sorting	**Sca1**	Stem cell antigen 1
FBS	Fetal bovine serum	**SDS**	Sodium dodecyl sulfate
FGF	Fibroblast growth factor	**SHH**	Sonic hedgehog
FSC	Forward scatter	**SSC**	Side scatter
GAG	Glycosaminoglycan	**Tgfbr**	Transforming growth factor beta receptor
GPI-AP	glycosyl phosphatidylinositol-anchored cell surface protein		
		TGFβ	Transforming growth factor beta
HBSS	Hanks' balanced salt solution	**VCAM-1**	Vascular cell adhesion molecule 1
hESC	Human embryonic stem cell	**VEGF**	Vascular endothelial growth factor
HLA	Human Leukocyte Antigen	**ZPA**	Zone of polarizing activity
hPC	Human pluripotent cell	**α-MEM**	alpha-Minimum essential medium
HSPC	Hematopoietic stem/progenitor cell		

4. Introduction

4.1 What is defined as Mesenchymal stromal/ stem cells?

4.1.1 Historical perspective

The term 'MSCs' was coined by Caplan for mesenchymal stem cells that are precursors of bone, cartilage and other mesodermal tissues (Caplan, 1991). These cells were speculated to reside in bone marrow (BM), which was used to determine its osteogenic potential (Tavassoli and Crosby, 1968; Bianco et al., 2008). Friedenstein and coworkers showed for the first time that the osteogenic potential of cells from bone marrow was actually inherent in a fraction of BM cells that adhered to the plastic in culture and have fibroblastic morphology (Friedenstein et al., 1968). These cells were able to give rise to colonies when plated in vitro that were termed as colony-forming unit fibroblasts (CFU-F). The CFU-F cell populations from bone marrow are thought to contain stem cells of non-hematopoietic lineage, the MSCs (Friedenstein et al., 1970, reviewed by Friedenstein et al., 1992).

4.1.2 Definition of 'MSC'

MSCs are defined as stem cells of non-hematopoietic lineage that adhere to plastic, are able to give rise to CFU-Fs and are multipotent (Pittenger et al., 1999). Owing to heterogeneity in unfractionated MSC populations derived from bone marrow, common criteria to identify these cells are difficult. The minimal criteria to define MSCs by International Society for Cellular Therapy (ISCT) are illustrated in Fig. 1 (Dominici et al., 2006):
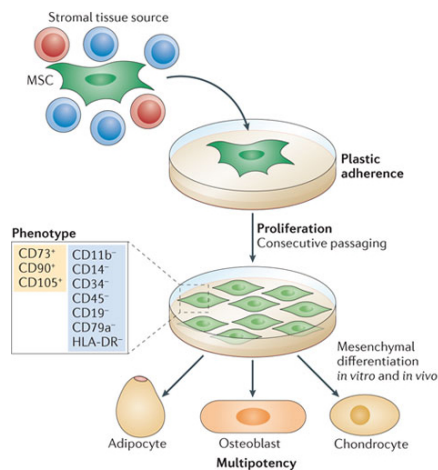
Fig. 1 ISCT's minimal criteria to define 'MSCs':
- Adherence to plastic

- Expression of specific surface antigens (positive for: CD105, CD90 and CD73; negative for: CD45, CD34, CD11b, CD19 and HLA class II/ HLA-DR)

- Multilineage differentiation potential into: osteoblasts, adipocytes and chondrocytes. Adapted from (Le Blanc and Mougiakakos, 2012)

The listed markers in Fig. 1 do not identify a homogeneous mesenchymal stem cell population (Sabatini et al., 2005). In addition, *ex vivo* expansion of MSCs cause chromosomal abnormalities that could transform these cells such that they can no longer be considered as MSCs. Human MSCs display osteogenic potential at single cell level (Sacchetti et al., 2007). Nonetheless, the term 'MSCs' has remained controversial as a definitive proof of their "stemness" by single-cell in vivo transplantation experiments has not been achieved (reviewed by Bianco et al., 2013).

4.2 Human MSCs (hMSCs): concepts of tissue regeneration and its limitations

Most of the criteria used to define MSCs were based on studies using human MSCs (hMSCs) and bone marrow cells. Initially, studies conducted with the aim to use hMSCs for 'cell replacement' therapies were hampered by the use of undefined MSC populations. Additional studies identified other tissue sources (e.g. dental pulp (Gronthos et al., 2002), umbilical cord blood (Erices et al., 2000), adipose tissue (Zuk et al., 2002) and skin (Shih et al., 2005), etc.) as sources for MSCs. The self-renewal capacity and multilineage potential of these MSCs varied a lot depending on the tissue sources (Sarugaser et al., 2009, reviewed by Keating, 2012). In addition, another consideration for regenerative therapy in using MSCs is their potential immunomodulatory properties, as these cells are known to influence the innate and adaptive immune system by altering the expression of

inflammatory cytokines (Le Blanc and Ringden, 2007; Nauta and Fibbe, 2007; Uccelli et al., 2008, Tolar et al., 2010, Chen et al., 2011, reviewed by Keating, 2012). Due to such limitations arising from undefined MSC populations, it was important to further characterize the hMSCs before using them as a cell source for therapeutic applications. Identification of additional MSC markers provided further functional insights into the nature of these cells. In addition to the markers mentioned before, several markers are expressed in human and mouse MSCs that are listed in Table 4.1:

Markers	Full-form/ Alternate Names	Reference
CD90	Thy1	(Dominici et al., 2006)
CD73	Nt5e, Ecto-59-nucleotidase	(Dominici et al., 2006)
CD105	Endoglin	(Dominici et al., 2006)
H-2-D	H-2Db MHC class I alloantigen	(Dominici et al., 2006)
CD49a	Alpha 1 beta 1 integrin	(Boiret et al., 2005)
CD49e	Itga5, Integrin alpha-5, Fibronectin receptor	(Colter et al., 2001)
CD29	Itgb1, Integrin beta-1	(Delorme et al., 2008)
CD44	Hyaluronate receptor	(Delorme et al., 2008)
CD51	Itgav, Integrin alpha-v, Vitronectin receptor	(Foster et al., 2005)
STRO-1		(Simmons and Torok-Storb, 1991)
CD140a	Pdgfra, PDGF Receptor alpha	(Delorme et al., 2008)
CD140b	Pdgfrb, PDGF Receptor beta	(Tokunaga et al., 2008)
CD106	Vcam1, Vascular Cell Adhesion Molecule 1	(Delorme et al., 2008)
CD271	LNGFR, Low-affinity nerve growth factor receptor or LNGFR	(Mabuchi et al., 2013)
CD146	MCAM, melanoma cell adhesion molecule	(Sacchetti et al., 2007)
CD200	OX-2 membrane glycoprotein	(Peister et al., 2004)
SSEA-4	Stage Specific Embryonic Antigen 4	(Gang et al., 2007)
CD47	Itgp, Integrin-associated protein	(Foster et al., 2005)
Sca1	Stem cell antigen 1	Morikawa et al., 2009
Nestin		(Mendez-Ferrer et al., 2010)
Mx1	Myxoma Resistance Protein 1, Interferon-induced GTP-binding protein	(Park et al., 2012)
Prx1	Paired related homeobox 1	(Logan et al., 2002)
LepR	CD295, Leptin Receptor	(Zhou et al., 2014)

Table 4.1. List of markers that are expressed by human and mouse MSCs.

CD146 (melanoma cell adhesion molecule or MCAM) expressing hMSCs are isolated from the sub-endothelial fraction of human bone marrow stroma (Sacchetti et al., 2007). These cells form fibroblastic colonies and are distinct from other types of osteogenic fibroblast-like cells. Upon subcutaneous implantation into nude mice, the CD146-positive cells form bony ossicles infiltrated by hematopoietic cells derived from the host. These findings provided a better understanding of the roles of bone marrow stromal cells (BMSCs) in establishing a hematopoietic microenvironment in vivo. Pinho and coworkers showed that a subset of CD146^{+} cells in the BM express Nestin, CD51 and PDGFRα and have a high self-renewal potential as assessed by transplantation in immunodeficient mice (Pinho et al., 2013). These cells are also able to form bony ossicles that recruit murine hematopoietic cells enriched in HSPCs (hematopoietic stem/progenitor cells). Another study identified an hMSC population by a combination of LNGFR, VCAM-1 and THY-1 markers that allows enrichment of a highly clonogenic population of hMSCs from bone and marrow (Mabuchi et al., 2013). These findings provide a deep insight into the possible origin, localization and roles of MSCs in the BM stroma and their interactions with HSPCs to regulate the activity of stem cell niche. MSCs are now routinely isolated from bone marrow using FACS based prospective isolation that is based on a combination of surface markers (Fig. 2).
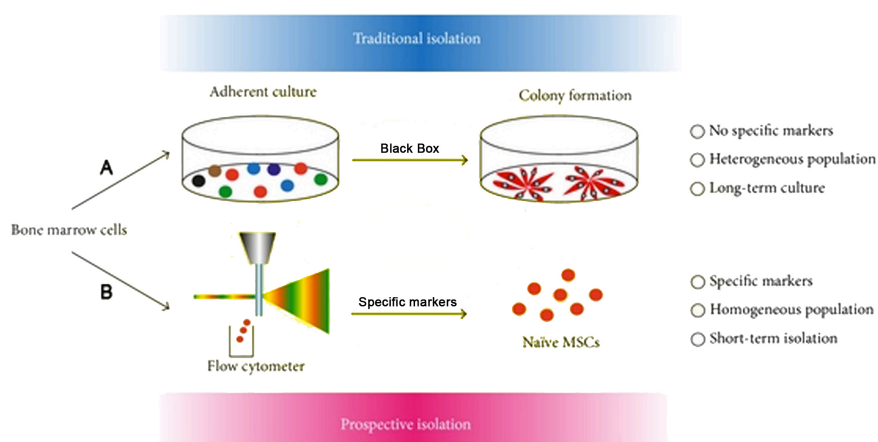
Fig. 2. Isolation of MSCs. **(A)** Classical method relies on plastic adherence of BM cells followed by long-term expansion to eliminate the majority of non-adherent hematopoietic cells and select adherent colony forming cells as MSCs. **(B)** FACS based isolation of hMSCs using

standard surface markers, without the need for long-term culture. This procedure allows isolation of naïve, more homogeneous and multipotent MSCs, free of contaminating hematopoietic cells. Adapted from (Mabuchi et al., 2013).

Despite of recent progresses, the field addresses several limitations for identification of hMSCs. These cells still remain a very heterogeneous population, which may also lead to donor-to-donor variations in regenerative therapy. The in vitro expanded hMSCs may not recapitulate the in vivo physiological conditions and fate-mapping studies are not possible to track the role of hMSCs in vivo at the level of single cell.

4.3 Mouse MSCs (mMSCs): Tools, genetic aspects and recent progress in the field

As the rather complex architecture of bone, bone marrow and stem cell niches were uncovered, it was envisaged that MSCs likely reside in these niches as distinct cell populations with specific roles. To study this further, the mouse model was used as an attempt to identify the corresponding mouse MSC populations, gain insight into their functional roles and study their short and long-term contributions to different developing tissues by cell lineage-tracing experiments. In addition, the available mouse models provide excellent sources to identify novel surface markers for better MSC populations. Mice can easily be genetically modified and fluorescent reporter lines can be used for cell lineage tracing which provides important insights into the stemness and fates of non-committed MSCs and mesenchymal progenitors committed to specific lineages.

4.3.1 Identification of new surface markers for mMSCs

Identification of murine MSC markers began with the observation that unfractionated mouse bone marrow also contains adherent cells with clonogenic capacity in culture. These studies also showed that distinct stem cells in the bone marrow give rise to either hematopoietic or mesenchymal stem cells (Koide et al., 2007). Besides these standard markers used to define MSCs (Dominici et al., 2006), additional markers used to study human

MSCs are also differentially expressed in mouse mesenchymal cell populations. A list of the markers used to characterize mouse MSCs is provided in Table 4.1.

The combination of PDGFRα and Sca1 (PαS) marks a specific MSC-like subpopulation in the bone marrow and among the cells isolated from compact bone (Morikawa et al., 2009; Houlihan et al., 2012). These cells are highly enriched for CFU-Fs, proliferate fast and can be induced to differentiate into chondrocytes, osteocytes and adipocytes (trilineage differentiation). In agreement with what has been shown for CD146$^+$ human MSCs, these studies point to an interactive role of mMSCs in regulating and maintaining the hematopoietic stem cell niche (Morikawa et al., 2009; Mabuchi et al., 2013). The identification of PαS cells is one of the first steps in the direction to identify a bona-fide mMSC population in mouse adult bones. However, Sca1 is not expressed in hMSCs, which renders direct comparison of human MSC populations with Sca1$^+$ mouse MSCs difficult. Recently, CD200 marker, which is expressed by human bone marrow cells with osteogenic properties (Delorme et al., 2008), has been used as a part of a signature (CD45$^-$Ter119$^-$AlphaV$^+$Thy$^+$6C3$^-$CD105$^+$CD200$^+$) to identify mouse skeletal stem cells (mSSCs) with stem cell-like properties. These mSSCs self-renew, are multipotent and differentiate predominantly into cartilage upon engraftment in the kidney capsule of immunosuppressed mice (Chan et al., 2015). These mSSCs are defined as rare pro-chondrogenic progenitors residing in the bone marrow.

4.3.2 Mouse genetic tools to study the fates of mMSCs in vivo

While it is impossible to study the lineage commitment of hMSCs, mice are well suited for this purpose by combining inducible fluorescent proteins expression to track the fates of specific cell populations for fate mapping (Mendez-Ferrer et al., 2010; Park et al., 2012; Greenbaum et al., 2013; Zhou et al., 2014). One of the major breakthroughs is the identification of a MSC population marked by Nestin expression (nestin-GFP mice). Nestin positive cells encompass cells from bone marrow fraction with CFU-F activity and also

reside in the BM stroma to support the hematopoietic stem cell niche (Mendez-Ferrer et al., 2010). Nestin positive cells form non-adherent mensenspheres and display self-renewal capacity in serial transplantation experiments. *Nes*-GFP$^+$ cells also express several other markers of HSC maintenance, some of which are also expressed by PαS cells. Some of these markers of HSC maintenance are listed in Table 4.2:

Markers	Full-form/ Alternate Names	Reference
Cxcl12	C-X-C motif chemokine 12, Stromal-derived factor-1 (SDF-1)	(Greenbaum et al., 2013)
Kitl	Stem cell factor/kit-ligand	(Mendez-Ferrer et al., 2010)
Angpt1	Angiopoietin-1	(Sacchetti et al., 2007)
Il-7	Interleukin-7	(Mendez-Ferrer et al., 2010)
Vcam1	Vascular cell adhesion molecule-1	(Mabuchi et al., 2013)
Spp1	Osteopontin	(Mendez-Ferrer et al., 2010)

Table 4.2. List of markers that are expressed by MSCs during HSC maintenance.

Specific depletion of Nestin positive cells results in severe reduction (by ~50%) of bone marrow HSCs (CD48$^-$Lin$^-$Sca-1$^+$c-kit$^+$ (LSK) cells and CD150$^+$ CD48$^-$ LSK cell). These HSCs also have low capacity to home in the bone marrow. Interestingly, an MSC subpopulation based on expression of CD51 and PDGFRα (CD51$^+$PDGFRα$^+$ double positive cells) are a fraction of nestin$^+$ cells in mice and can be isolated from human (Pinho et al., 2013). These evidences show a possible interaction of HSCs with MSCs to maintain the stem cell niche in bone marrow.

In addition, a recently published study used a more progenitor/ stem cell like *Mx1*$^+$ bone marrow stromal cells that are fate-restricted and have perivascular origin. These cells replace the osteoblastic cells during mice development and take part in bone maintenance and regeneration (Park et al., 2012). The *Mx1*$^+$ cells replaces the osterix labeling preosteoblasts and can be transplanted at the site of bone injury to migrate and recover injured bones. Another study used a fraction of stromal cells in bone marrow that expresses CXCL12 (stromal-derived factor-1, SDF-1) that are abundant in the perivascular compartment of bone marrow. CXCL12 is a factor that is known to have

supportive role in maintaining HSCs and lymphoid progenitors in the bone marrow (Tokoyoda et al., 2004). The study shows that specific deletion of *Cxcl12* in bone marrow subpopulations leads to the loss of hematopoietic progenitor cells (HPCs) and B-lymphoid progenitors from the bone marrow. These data suggest that the expression of CXCL12 is essential in maintaining HSC pool and involves the stromal component in the bone marrow for its development and maintenance. Interestingly, in this study, it is also shown that about 50% of PαS cells are targeted by *Prx1-Cre* that included a subpopulation of cells expressing intermediate levels of CXCL12 (Greenbaum et al., 2013).

Furthermore, Leptin Receptor (LepR) was recently shown to mark ~0.3% of the bone marrow cells, mainly in arterioles and sinusoids. LepR can be used for FACS sorting to isolate highly clonogenic population of MSCs that co-expressed PDGFRα, CD51 and Prx1 (Zhou et al., 2014). LepR$^+$ cells were previously also identified in perivascular stromal cells and these cells were shown to produce *Stem cell factor* (*Scf)* and *Cxcl12* within the bone marrow compartment (Ding and Morrison, 2013). Fate mapping of LepR$^+$ cells in *Lepr-cre; tdTomato; Col2.3-GFP* triple transgenic mice showed that these cells are a very rare population prior to birth. However, in 2 months old mice, LepR$^+$ cells were easily detectable in the bone marrow fraction of the meta- and diaphysis that increased sharply with age. Clonal expansion of LepR$^+$ cells in culture and their subsequent subcutaneous engraftment resulted in formation of bony ossicles with host-derived hematopoiesis. LepR$^+$ cells also contributed to the bone, cartilage and adipocyte compartment following intra-femoral injection in sub-lethally irradiated mice. In older mice, LepR$^+$ cells were detected mostly in bone marrow adipocytes, while the adipocytes in the periosteum did not contain LepR$^+$ cells, which pointed to a distinct origin of these cells.

These lineage-tracing studies show that the MSCs that reside in the bone marrow stroma contribute predominantly to the osteocyte and adipocyte, but less to chondrogenic lineage. Recently, it was shown that expression of the bone morphogenetic protein (BMP) antagonist Gremlin 1 (Grem1$^+$) marks

osteochondroreticular (OCR) stem cells within the bone marrow (Worthley et al., 2015). Grem1$^+$ cells are distinct from perisinusoidal *Nes-GFP*$^+$ cells and are able to give rise to osteoblasts, chondrocytes and reticular marrow stromal cells, but not adipocytes. Of note, Gremlin 1 is required for skeletal development (Zuniga, 2015) and bone homeostasis postnatally (Canalis et al., 2012).

Together, these and many other studies have provided deep insights into the molecular signature and potential diversity of MSCs. Identification of new surface markers resulted in isolation and characterization of different subpopulations of MSCs. Mouse PαS cells isolated from compact long bones are a rare subpopulation that appear to satisfy many of the defining criteria for MSCs based on their properties. However, in vivo marker and fate mapping analysis also shows that the in vivo functionality of MSC subpopulations may differ from their in vitro properties. This is a likely consequence of these MSCs interacting with HSCs, being part of stem cells in the niche and/ or other stromal cells in the niche. Most importantly, these studies also provided the insight into the ontology of the different MSC subpopulations during fetal and postnatal mouse development. Whether the mouse MSC populations and their roles are orthologous to human MSCs remain to be determined.

4.4 Origin for tissues of mouse MSCs

Most of the markers expressed by MSCs are also expressed by other cell types, such as fibroblasts. It has, thus, become an important topic of debate to discuss the origin of MSCs in order to specify the site of the tissue as a source of specific type of MSCs.

4.4.1 Recent efforts to localize MSCs in bone marrow

Recent efforts have indicated that MSCs may reside in the perivascular space of bone marrow (Morikawa et al., 2009; Mendez-Ferrer et al., 2010). Others indicated subendothelial region in the BM sinusoids as the origin of MSCs (Sacchetti et al., 2007). During embryonic development, the primitive skeletal stem and progenitor cells likely reside outside the bone marrow cavity in the

perichondrium and periosteum. The primitive bone marrow stromal cells and the skeletal progenitor cells invade the developing cavity as the blood vessels are formed (Fig. 3). The MSCs located in the bone marrow after birth reside in the proximity of the blood vessels of subendothelial origin that are called sinusoids. However, it has been difficult to locate these cells in vivo. MSCs interact with HSCs and other hematopoietic cells in and around the sinusoids to maintain a niche microenvironment that support hematopoiesis, as well as development of osteoblasts and adipocytes (Fig. 3A, B). The development of bone marrow stoma is a complex process and the HSCs-MSCs interactions regulate the niches located in the perivascular space of the bone marrow stroma (reviewed by Bianco et al., 2013) (Fig. 3). The complexity of the bone marrow stroma is increasingly revealed by the identification of an increasing number of types and subpopulations of MSCs that function in regulating the stroma composition, together with their functional interaction with HSCs. Hence, a better understanding of the structure and function of BM stroma is a pre-requisite for attempts to mobilize these cells for regenerative medicine.
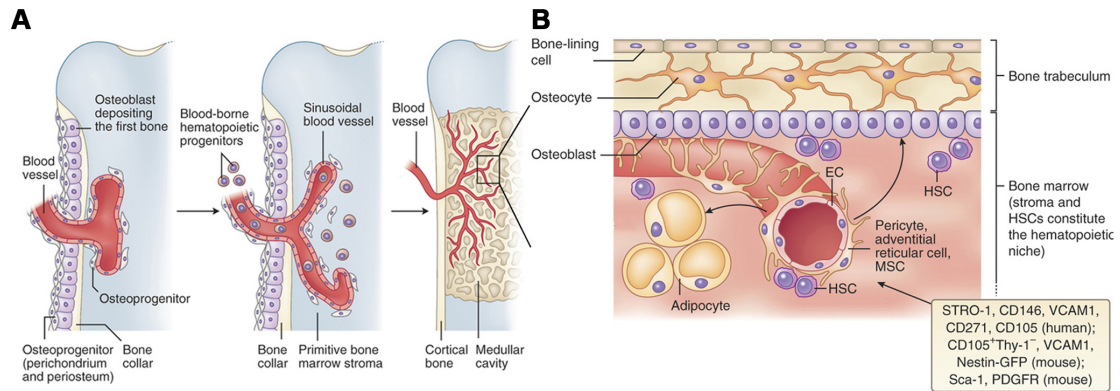
Fig. 3. MSCs in the bone marrow stroma. **(A)** Blood vessels invade the primitive stroma cavity while skeletal progenitors generate osteoblasts to form bone and bone collar. Hematopoietic progenitors occupy the space in the sinusoidal blood vessel, along with primitive bone marrow stroma. **(B)** The MSCs reside in the perisinusoidal space and interact with HSC and other hematopoietic cells. Osteoblasts mature into osteocytes and form the bone trabeculum. Pericytes and adventitial reticular cells form a niche with HSCs and MSCs, which express a combination of markers (yellow box). Adipocytes fill the bone marrow stroma. Adapted from (Bianco et al., 2013).

4.4.2 Adipogenic differentiation: Late fates of MSCs in bone marrow?

The adipogenic differentiation of MSCs in vitro follows the step-wise induction that differentiate MSCs into preadipocytes, which then mature into adipocytes that accumulate lipid droplets that are synthesized and stored in adipocytes. Several studies have shown that insulin, in combination with Dexamethasone and indomethacin induces differentiation of MSCs into adipocytes in culture (Zuk et al., 2002; Zhang et al., 2012). Dexamethasone, a synthetic glucocorticoid agonist acts as a stimulating agent (Grigoriadis et al., 1988) while indomethacin, a non-steroidal anti-inflammatory drug, induces *PPARγ* (Peroxisome proliferator-activated receptors alpha and gamma, (Lehmann et al., 1997)). Insulin binds to IGF-1 (insulin-like growth factor-1), the receptors of which are expressed by preadipocytes. This induces phosphorylation of the cAMP response element-binding protein (CREB) via cAMP and phosphatidylinositol-3 kinase (PI3K). CREB activates the expression of the CCAAT/enhancer binding protein alpha (C/EBPα) and PPARγ, which together promote adipogenesis (Hammarstedt et al., 2005; Rosen, 2005).

The differentiation of MSCs into adipocytes has been linked to aging. LepR$^+$ MSCs were shown to contribute to the adipocyte lineage in adult bone marrow. This contribution of LepR$^+$ cells increased in older mice upon injury (Zhou et al., 2014). It has been suggested that osteogenic and adipogenic fates are determined at the expense of each other and mainly regulated by the balance of the *Runx2* and *PPARγ* transcriptional regulators (Pei and Tontonoz, 2004; Muruganandan et al., 2009; James, 2013). The bone regenerative capacity declines with age, while the adipogenic fates become more prominent. This "adipogenic switch" of MSCs results in increased production of fat cells in the aging bone marrow (Pei and Tontonoz, 2004; Muruganandan et al., 2009, Lepperdinger, 2011; reviewed by James, 2013).

4.5 Limb development: patterning, proliferation and differentiation

The vertebrate limb bud has been used as a genetic model to study the molecular pathways involved in transcriptional regulation of cell proliferation and specification (Fig. 4). As most cells in the developing limb bud are of

mesenchymal origin, molecular pathways involved in proliferation and specification of these limb bud mesenchymal progenitors (LMPs) are likely of relevance to chondrogenic and osteogenic differentiation of MSCs. Fig. 4 summarizes the patterning of embryonic limb formation that leads to development of skeletal elements in adult:
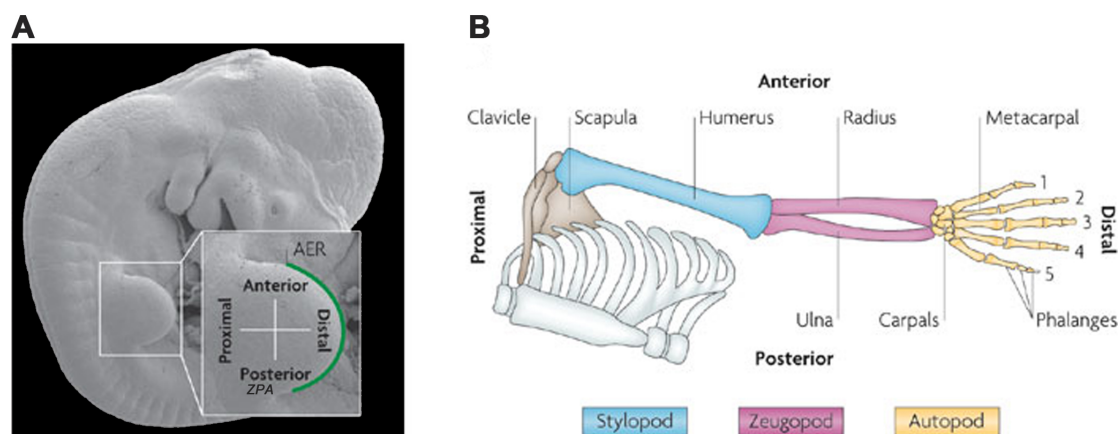
Fig. 4 Limb bud development. **(A)** SEM image of a mouse embryo at E10.5 stage. The enlarged inset shows the forelimb bud with the proximo-distal (PD) and antero-posterior (AP) limb bud axes. The apical ectodermal ridge (AER) is indicated in green and the zone of polarizing activity (ZPA) is in the posterior mesenchyme. **(B)** The skeletal elements of a human arm. The stylopod forms humerus, the most proximal element; zeugopod forms the radius (anterior) and ulna (posterior); autopod forms the wrist (carpals), palm (metacarpals) and digit bones (phalanges) (Zeller et al., 2009).

4.5.1 Molecular pathways regulating mesenchymal cell proliferation in developing limbs

During the onset of limb bud, the distal most part of ectodermal epithelial layer forms apical ectodermal ridge (AER), which secretes several FGFs. These FGFs act as survival and proliferation factors for the underlying mesenchymal progenitors and instruct PD limb bud outgrowth and patterning (Niswander et al. 1994; Mariani et al., 2008). FGFs also maintain the expression of sonic hedgehog (SHH) in the posterior mesenchyme, which together with the BMP antagonist Grem1 assure survival and proliferation of LMPs, while BMPs induce their chondrogenic differentiation (reviewed by Zeller et al., 2009; Zuniga, 2015). In addition, ectodermal Wnts and AER-FGFs act in a synergistic manner to promote the proliferation and maintenance of

multilineage potential of LMPs in the distal mesenchyme of limb bud (Ten Berge et al., 2008). While LMPs in the distal mesenchyme continue to proliferate, cells in the proximal limb bud are no longer under the influence of Wnt and FGF signaling, and initiate chondrogenic differentiation under the influence of TGFβ/BMP signaling.

4.5.2 Parallels between LMP and MSC proliferation

The regulatory molecules that control the proliferation of LMPs have been used for promoting proliferation of MSCs in culture. In particular, their potential for long-term in vitro expansion and keeping these cells in undifferentiated state has been explored. However, these in vitro studies gave conflicting results. For example, treatment with Wnt3a to hMSCs in culture induced increased alkaline phosphatase (ALP) expression and decreased lipid droplet formation, which is due to Wnt3a inducing osteo-lineage commitment (Qiu et al., 2007). This study contradicted previous findings, which showed that Wnt3a is able to suppress osteogenic differentiation of hMSCs (Boland et al., 2004). FGF2 increases in vitro proliferation of the hMSCs, but again induces cells toward osteogenic lineage (Ito et al., 2007). These contradictory results in MSCs drove a sequential approach of exogenous application of these growth factors that mimic endogenous molecular pathways. Efforts are being made to provide the MSCs in culture as an indispensable source of multipotent stem/progenitor cells. These results underline the requirement of exposing MSCs to growth factors sequentially in a precise, time-controlled manner.

4.6 Developmental regulation of the growth plate cartilage during endochondral ossification

Endochondral ossification is the developmental program that controls long bone formation. This is the process by which cartilage templates undergo hypertrophy and are remodeled into bony tissue and longitudinal growth of bone progresses. The step-wise remodeling of the cartilage template into bone during endochondral ossification contrasts with the direct formation of

osteoblasts from mesenchymal condensation, without formation of a cartilage intermediate, which is called as intramembranous ossification.

While endochondral ossification is typical for e.g. all limb skeletal bones, the flat bones of e.g. skull form by intramembranous ossification. The mesenchymal condensations are first step towards formation of the cartilage template required for the development of the endochondral skeleton. The following sections give an overview of molecular regulation of different steps during endochondral ossification:

4.6.1 Role of *Sox* transcription factors in mesenchymal cell condensation and chondrogenic differentiation

Following proliferative expansion of LMPs, several transcriptional regulators drive their specification towards osteo-chondrogenic progenitors in spatio-temporally controlled manner. During osteo-chondrogenic commitment, LMPs start to express *Sox9* and initiate mesenchymal condensation (Ng et al., 1997; Zhao et al., 1997). The *Sox9* transcriptional regulator belongs to the HMG-box class DNA-binding protein that binds to the CCTTGAG sequence and is a master regulator of chondrogenesis (Akiyama et al., 2005). This study shows that conditional inactivation of *Sox9* during limb bud development disrupts the mesenchymal cell condensation and formation of the cartilage templates of the future bone.

Sox5 and *Sox6* transcriptional regulators are also required for chondrogenesis after the initial mesenchymal condensation (Smits et al., 2001). This combination of Sox transcriptional regulators, i.e, the "Sox trio" (*Sox5*, *Sox6* and *Sox9*) is essential for chondrogenic differentiation. In particular, *Sox9*, which is activated first, controls the expression of *Sox5* and *Sox6* during subsequent steps of chondrogenic differentiation. The "Sox trio" promotes chondrocyte proliferation and suppresses their progression to hypertrophic stages and osteoblast differentiation (Fig. 5) (Ikeda et al., 2005).
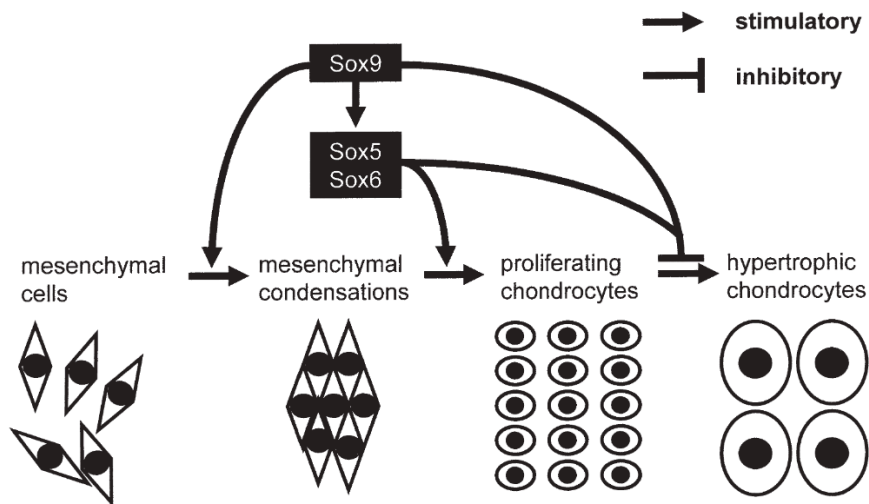
Fig. 5. Role of Sox5, Sox6 and Sox9 in chondrogenic differentiation. Sox9 is essential before and after mesenchymal condensation; Sox5 and Sox6, the expression of which is controlled by Sox9, allow progression to proliferating chondrocytes. The Sox trio inhibits hypertrophy and further stages of chondrogenic differentiation (Ikeda et al., 2005).

4.6.2 Molecular pathways controlling cartilage differentiation

Chondrocytes in the developing cartilage templates are arranged in morphologically distinct zone, consisting of resting, proliferating and hypertrophic chondrocytes (Fig. 6) (Kozhemyakina et al., 2015).
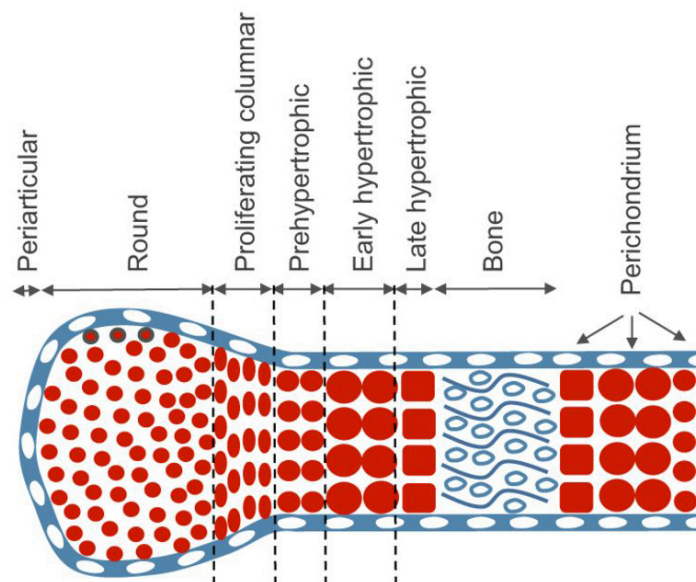
Fig. 6 distinct transition zones of developing cartilage template during long bone development. Adapted from (Kozhemyakina et al., 2015).

In addition to *Sox* transcription factors, chondrocytes express Collagen type-II and Aggrecan. The transforming growth factor β (TGFβ) superfamily that includes TGFβs and BMP ligands, together with *Sox9* have been shown to regulate the differentiation of LMPs to chondroblasts and chondrocytes. TGFβ/BMP ligands bind to type I and type II serine/threonine kinase receptors and signal transduction involves the activation and nuclear localization of phosphorylated Smad proteins, which regulate the expression target genes (Derynck and Zhang, 2003; Shi and Massague, 2003; Feng and Derynck, 2005). Combined deletion of SMADs 1, 5 and 8 in developing chondrocytes results in severe chondrodysplasia, in which the cartilage of the limbs are malformed and abnormal growth in long bone leads to shortened limbs. The result indicates that BMP signaling is essential for maintenance of chondrogenic fates (Retting et al., 2009). Similarly, SMAD4, a core mediator of canonical TGFβ/BMP signaling, is required for the formation of the Sox9-positive digit ray primordia. Its inactivation in mouse limb buds blocks the aggregation of Sox9-positive osteo-chondrogenic progenitors and results in loss of collagen type-II (Retting et al., 2009; Benazet et al., 2012). These studies corroborate the essential roles and interactions of *Sox9* and TGFβ/BMP signaling for initiating chondrogenesis. Three BMP ligands (BMP2, BMP4 and BMP7) are expressed in the limb bud and regulate chondrogenic differentiation. Deletion of *Bmp2* and *Bmp4* in the limb bud mesenchyme results in the loss of specific pre-cartilaginous condensations (Bandyopadhyay et al., 2006). Moreover, inactivation of both BMP receptors, BMPR1A and BMPR1B, results in loss of *Sox9* expression and severe chondrodysplasia (Baur et al., 2000; Yi et al., 2000; Ovchinnikov et al., 2006). Further, genetic analysis showed that these BMP receptors have overlapping functions during chondrogenesis (Yoon et al., 2005). Using retroviral vectors to misexpress the BMP antagonist Noggin in chick limb buds, BMP ligands were shown to be required in a 2-step process of cartilage development, as the antagonist blocks both mesenchymal condensation and chondrogenic differentiation (Pizette and Niswander, 2000; Yoon et al., 2005). BMP signaling interacts with *Sox* genes to induce the expression of *Col2a1* and *Aggrecan* during progression of cartilage differentiation (Chimal-Monroy et al., 2003).

Furthermore, LMPs isolated from the proximal and distal limb bud from mouse embryo at E10.5 stage displayed distinct aggregation and condensation behaviors in culture. These cells appeared to have acquired distinct identities that allow them to sort themselves in culture, in agreement with the distinct identities of the future skeletal elements (Barna and Niswander, 2007). Inhibition of BMP signaling resulted in disruption of compaction and absence of cartilage nodules (Fig. 7).
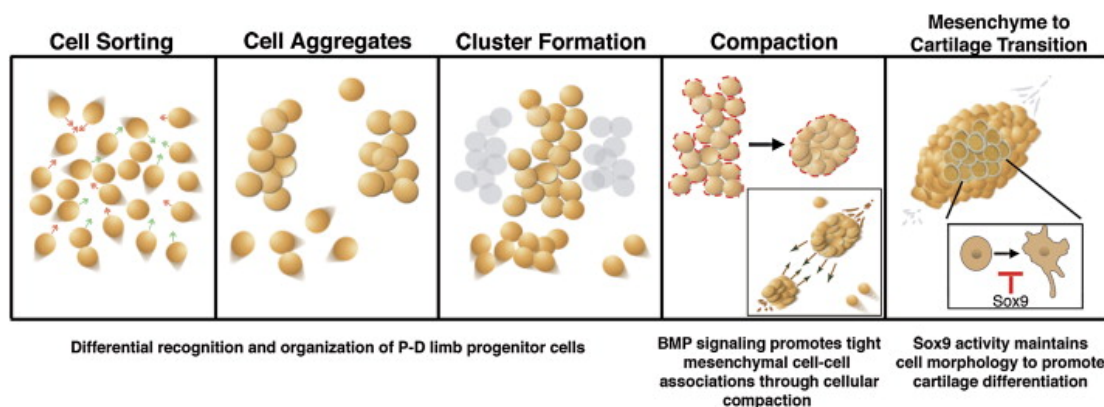
Fig. 7. Scheme of the cellular events LMPs undergo during osteo-chondrogenic commitment and formation of cartilage templates. Red arrows: movement of proximal limb progenitors; Green arrows: movement of distal limb progenitors (Barna and Niswander 2007).

In addition, experimental evidence indicates that exposure of mesenchymal cells to TGFβ signaling primes LMPs for BMP-induced cartilage condensation (Karamboulas et al., 2010). When limb buds were dissected for distal and proximal LMPs and cultured in micromass, LMPs responded to BMP4 in differential manner. While the chondrogenic activity was lowered in LMPs from distal mesenchyme, it remained unaffected in the LMPs from proximal mesenchyme. When LMPs were isolated from the intermediate mesenchyme, the chondrogenic activity lowered by a lesser extent compared to that of LMPs from distal mesenchyme. This revealed a dose-dependent effect of BMP on the two LMP populations in the limb mesenchyme. The authors show that exposure of LMPs from distal limb bud to the TGFβ1 for only 4 hours is sufficient to overcome anti-chondrogenic effect of the BMP4 in culture. Furthermore, simultaneous addition of TGFβ1 and BMP4 inhibits

chondrogenesis, indicating that a sequential exposure of these molecules is required for positive modulation of chondrogenesis. Indeed, inhibition of TGFβ signaling results in loss of chondrogenesis response to BMP4, which points to the fact that TGFβ signaling primes LMPs for BMP-induced chondrogenesis. Supporting these results is the observation that all three TGFβ ligands are expressed in the mesenchyme of early limb buds. SMAD3, a downstream mediator of TGFβ signaling, is also expressed in the pre-chondrogenic mesenchyme (Lorda-Diez et al., 2009). Inactivation of *Tgfbr2* in the limb bud mesenchyme results in defective development of long bones and joints (Seo and Serra, 2007), pointing to its requirement for chondrogenic differentiation.

Sequential exposure of human and mouse MSCs to signals that induce formation of cartilage have had limited success. BM-derived hMSCs have been shown to respond to TGFβ signaling in pellet based culture setups and differentiate into hypertrophic cartilage (Pittenger et al., 1999). Priming of hMSCs in 3D culture with Wnt3a improves their responsiveness to TGFβ1-induced chondrogenesis (Centola et al., 2013). The role of BMPs in chondrogenic differentiation of MSCs has remained largely elusive. Attempts to study the role of BMPs in osteogenic differentiation of hMSCs were non-conclusive, but it was shown that BMPs induce the expression of the antagonist Noggin (Balk et al., 1997; Diefenderfer et al., 2003; Osyczka et al., 2004). These results indicated that changes in extracellular signals alter the response of MSCs to BMPs and result in auto-regulation of BMP activity. Efforts to induce the afore-mentioned signaling pathway in a step-wise manner to mimic the developmental signaling networks and guide the MSCs towards their definitive fates are currently underway.

4.6.3 The growth plate: distinctive features of articular and growth plate cartilage

Based on functional properties, two distinct types of cartilage exist, namely, articular and growth plate cartilage. Articular cartilage consists of less proliferative and long-term stable chondrocytes that do not undergo hypertrophy. Articular chondrocytes neither produce extensive extracellular

matrix nor undergo apoptosis under normal conditions. They express the typical chondrocyte markers *Col2a1* and *Acan*, in combination with sulfated glycosaminoglycans (GAGs). Progressive degradation of articular chondrocytes in joints, e.g. by apoptosis or progressive hypertrophy, results in osteoarthritis (OA). This disease is characterized by degenerating joints, accumulation of matrix-degrading enzymes, an increase in ossification and calcification.

In contrast, growth plate chondrocytes are short-term proliferating chondrocytes that undergo hypertrophy and secrete large quantities of extracellular matrix, which ultimately results in their increased apoptosis. Continuation of hypertrophy results in remodeled cartilage, in which most of the extracellular matrix is eliminated by matrix-degrading enzymes, eventually promoting the longitudinal growth of the long bone rudiments (reviewed by Kronenberg, 2003). Genes expressed by chondrocytes during hypertrophy include *collagen type X* (*Col10a1*), *Indian hedgehog* (*Ihh*), *alkaline phosphatase* (*Alp*), *matrix metalloproteinase* (*MMP-13*), *vascular endothelial growth factor* (*VEGF*) and *parathyroid hormone-related protein receptor* (*PTHrP-R*) (Yoo et al., 1998; Sekiya et al. 2002; Pelttari et al., 2006).

4.6.4 The signaling networks that regulate growth plate development

The growth plates are located under the epiphyseal plate of developing bone (Fig. 8). Growth plate cells are arranged in vertical columns in a highly anisotropic manner, giving it a unique morphology (Kember and Sissons, 1976; Rodriguez et al., 1992). Eventually, the proliferating chondrocytes flatten and transit to a pre-hypertrophic state. Signals then induce the transition from pre-hypertrophic to the hypertrophic stage, which is accompanied by an increase in volume due to increased extracellular matrix secretion and mineralization.
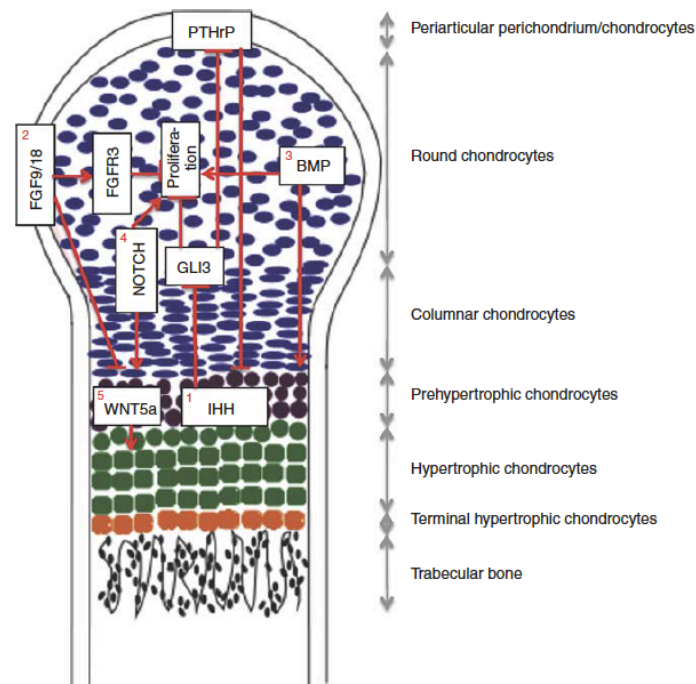
Fig. 8 Longitudinal section through a growth plate of mouse long bone depicting extracellular signals that regulate its development (E15.5 – E19). **(1)** IHH and PTHrP act synergistically towards chondrocyte proliferation and maturation through a negative-feedback mechanism. IHH stimulates PTHrP transcription through derepression of GLI3, which mediates chondrocyte proliferation. PTHrP suppresses chondrocyte maturation associated with IHH expression. **(2)** FGFR3 is a likely receptor for FGF9/18 to suppress chondrocyte proliferation in the growth plate late **(3)** BMPs expressed by both chondrocytes and perichondrial cells promote proliferation and maturation. **(4)** NOTCH signaling in chondrocytes promotes proliferation and maturation. **(5)** WNT5A expressed by pre-hypertrophic chondrocytes stimulates hypertrophy (Long and Ornitz, 2013).

Several molecular cascades instruct to control the process of endochondral ossification. *Indian hedgehog* (*Ihh*), a hedgehog ligand and master regulator of bone development, is expressed by pre-hypertrophic chondrocytes located close to the proliferation zone, whereas parathyroid hormone-related protein (PTHrP) is expressed by peri-articular chondrocytes (Bitgood and McMahon, 1995). It has been shown that IHH stimulates PTHrP expression in peri-articular chondrocytes, which results in a feedback loop that regulates the growth plate and bone formation (Fig. 8) (Van den Heuvel and Ingham, 1996; St-Jacques et al., 1999; Kindblom et al., 2002). PTHrP promotes the proliferation of chondrocytes in the growth plate and their hypertrophy is triggered when PTHrP levels fall below a critical threshold. This shows that a high PTHrP levels inhibit chondrocyte hypertrophy. The interaction of IHH with

PTHrP during chondrocyte proliferation counteracts the inhibitory role of the GLI3 repressor in this process (Fig. 8) (Hilton et al., 2005). In particular, inactivation of both GLI3 and IHH restores the proliferation defects, disruption of PTHrP expression and hypertrophy observed in *Ihh* deficient limbs. These results are in agreement with the proposal that IHH and PTHrP regulate chondrocyte proliferation and maturation in a synergistic manner (reviewed by Long and Ornitz, 2013). In addition, the functions of FGF signaling, in particular FGF receptors Fgfr1 and Fgfr3, in regulating pre-hypertrophic and hypertrophic chondrocytes has also been analysed (Peters et al., 1992; Deng et al., 1996; Ornitz and Marie, 2002; reviewed by Long and Ornitz, 2013). Conditional deletion of *Fgfr1* in chondrocytes delays the maturation of hypertrophic chondrocytes (Jacob et al., 2006), while deletion of Fgfr3 keeps chondrocytes in a proliferative state (Eswarakumar and Schlessinger, 2007). Finally, Sox9 keeps the chondrocytes in proliferative state and interfere with their progression to hypertrophic states (Dy et al., 2012).

4.6.5 Osteoblast development and endochondral ossification

The hypertrophic chondrocytes mature and direct the mineralization of the surrounding matrix by osteoblasts. This results in a physiological environment that attracts invasion of blood vessels by vascular endothelial growth factors (VEGFs) and other signals (reviewed by Kronenberg, 2003). The invading chondroclasts and osteoclasts start to degrade the matrix, while the adjacent perichondrial cells differentiate into osteoblasts. This results in formation of the bone collar that will develop into cortical bone (Mackie et al., 2011). Hypertrophic chondrocytes undergo apoptosis and the remaining matrix provides the scaffold for osteoblasts and invading blood vessels that continues mineralization of the extracellular matrix (ECM) (reviewed by Long and Ornitz, 2013).

Several molecular pathways regulate osteoblast differentiation and functions during endochondral ossification. Inactivation of IHH disrupts osteoblast differentiation and *Runx2* (*Runt-related transcription factor 2*) activation in the perichondrial progenitors, which is essential for osteoblast differentiation

(Long et al., 2004). Additional functions of IHH signaling in promoting chondrocyte hypertrophy independent of PTHrP have also been evidenced (Mak et al., 2008). A recent study showed that IHH impacts on the *Col10a1* promoter via *Gli* transcriptional regulators or indirectly via the *Runx2/Smad* pathway (Amano et al., 2014). The *Osx* transcriptional regulator acts downstream of Runx2 and BMPs are critical to osteoblast differentiation (Nakashima et al., 2002). In particular, threshold levels of BMP2 and BMP4 are required for the transition from Runx2 to Osterix positive cells (Bandyopadhyay et al., 2006).

Thus, Fig. 9 summarizes all the steps of endochondral ossification:
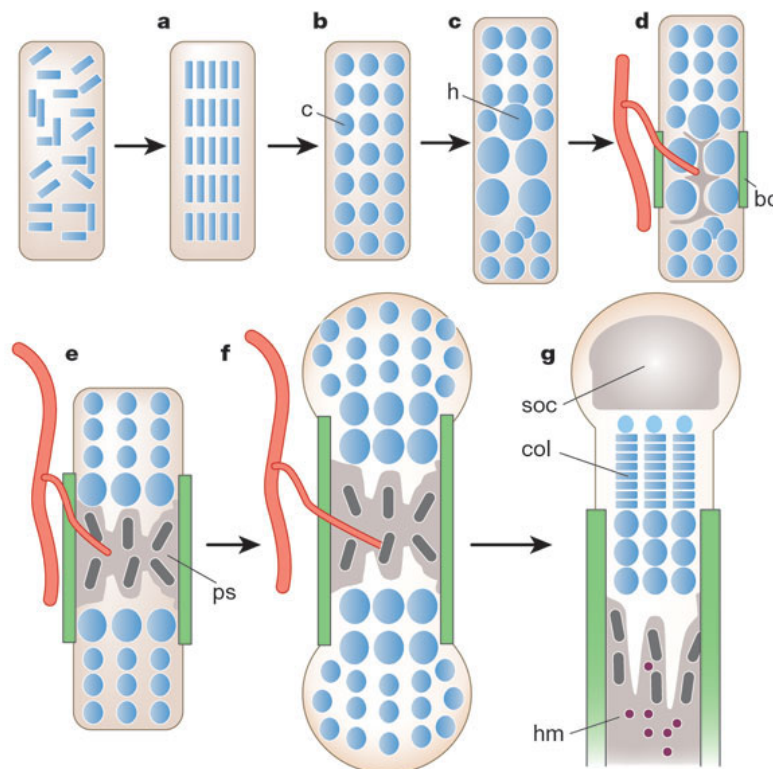
Fig. 9. (**a**) Mesenchymal cells condense and rearrange in orderly manner. (**b**) Condensed cells differentiate into chondrocytes (c). (**c**) Chondrocytes in the center stop their proliferation and become hypertrophic (h). (**d**) Adjacent perichondrial cells differentiate into osteoblasts, forming the bone collar (bc). Apoptosis and mineralization of hypertrophic chondrocytes lead to physiological changes, which begin to attract blood vessels. (**e**) Vascular invasion and osteoblasts promote formation of the primary spongiosa (ps). (**f**) Proliferating chondrocyte underline the longitudinal growth. (**g**) Hypertrophic program in chondrocytes along with vascular invasion and osteoblast activity leads to formation of secondary ossification centres at the distal ends of the bone rudiment (soc). The growth plates formed are by proliferating

columnar chondrocytes (col). The hematopoietic compartment of the bone marrow (hm) invades the marrow space along with stromal cells. (Kronenberg, 2003).

4.6.6 Hematopoiesis during endochondral ossification

The process by which hematopoietic stem cells (HSCs) differentiate and form all types of blood cells is called as hematopoiesis. HSCs and Hematopoietic cells from fetal liver migrate to the marrow space of endochondral bone via the invading blood vessels. In this process, HSCs continuously give rise to common myeloid progenitors (CMPs) and common lymphoid progenitors (CLPs). CMPs differentiate further to generate erythrocytes, platelets, macrophages, neutrophils, eosinophils, basophils and megakaryocytes. CLPs differentiate into natural killer cells, T-cell progenitors that would mobilize from bone marrow and complete their differentiation in the thymus and B-cell progenitors that would complete their program of differentiation in bone marrow. Dendritic cells arise both from CMPs and CLPs (Miyamoto et al., 2002; Iwasaki and Akashi, 2007; Kondo, 2010; reviewed by Weissman and Shizuru, 2008). Functional HSCs in bone marrow of mice is observed by E17.5 stage and is mainly residing in the endosteal region, at the interphase between bone and BM (Christensen et al., 2004). During hematopoiesis, HSCs in bone marrow interact with stromal cells and establish the stem cell niche and maintain a steady state (Greenbaum et al., 2013; Chan et al., 2015).

4.7 Guiding MSCs towards endochondral ossification

During chondrogenic differentiation in vitro, the BM-derived MSCs display features of growth plate chondrocytes (Pelttari et al., 2008; Steinert et al., 2009; Scotti et al., 2010; Caron et al., 2012). However, the hypertrophic program in differentiating chondrocytes is triggered in a rather uncontrolled manner. In vitro studies using hMSCs, cultured in three-dimensional (3D) constructs have been used for directed, step-wise induction of chondrogenesis, hypertrophy and finally bone formation (Ichinose et al., 2005; Sasaki et al., 2012). These experiments reveal the importance of the 3D environment in attempting to mimic in vivo physiological conditions. In

addition, endochondral ossification must be paralleled by hematopoiesis to form functional bone. Cartilage templates made from human BM-MSCs are capable of recapitulating the embryonic process of endochondral ossification following their subcutaneous implantation in the immunosuppressed nude mouse model (Scotti et al., 2010). As the process involves vascularization, endothelial cells were indeed detected in the resulting bony ossicles. In addition, osteoclasts were detected, which are key to active matrix degradation during endochondral ossification. The importance of MSCs and osteoprogenitors in regulating the hematopoietic stem cell niche has also been addressed for both human and murine model of endochondral ossification (Chan et al., 2009). Others studies point to the necessity of chondrogenic priming of MSCs in vitro to stimulate bone regeneration in vivo (Farrell et al., 2011; Van der Stok et al., 2014). Priming MSCs with IL-1β (interleukin-1β) in hypertrophic medium prior to implantation results in enhanced vascularization and osteoclast activity and enlarged bone marrow regions (Scotti et al., 2013). Another study indicates that chondrocytes derived from MSCs can revert back to their stromal phenotypes, which supports hematopoiesis and homing of hematopoietic stem cells (Serafini et al., 2014).

While MSCs can be differentiated into osteoblasts and recapitulate aspects of endochondral ossification, the generation of e.g. growing and stable cartilage templates to much better mimic bone growth has not been accomplished. Fate mapping studies in the mouse begin to provide a deeper understanding of functions and fates of mesenchymal progenitor cells in growing bone with respect to their osteogenic or chondrogenic lineage contributions. Using *Col2-creER*; *R26R*–tdTomato double transgenic reporter mice in combination with a *Col1(2.3kb)*-GFP allele to mark osteoblastic cells, it was shown that the cartilage and perichondrium compartments arise early during embryonic development as precursors of the Osterix^{+} cells (Mizoguchi et al., 2014). After birth, these cells give rise to chondrocytes, osteoblasts, osteocytes and *Cxcl12*-expressing stromal cells within the marrow space. Similar results were obtained by fate mapping of *Sox9–creER* positive cells. These results indicate that the Sox9 positive osteo-chondrogenic progenitors give rise to

chondrocytes, osteoblasts and stromal cells during endochondral bone development. These studies are highly relevant to gain insight into the nature of the progenitor cells best suited for bone regeneration and generating stable cartilage. Very recently, evidence for achieving stable cartilage was obtained by CD200$^+$ cells in combination with other surface markers from mice (Chan et al., 2015). Based on their emergence with other skeletal stem cells during development, these skeletal progenitor cells could be potentially used to engineer bone or cartilage by modulating there exposure to morphogenetic signals. Interestingly, both mouse and human cells express CD200. These findings provide insight into the underlying cellular mechanisms and may aid in developing protocols to harness well-characterized mesenchymal and skeletal stem/ progenitor cells for cartilage and bone engineering in the long term.

5. Aims of the thesis

Tissue engineering approaches using MSCs and mesenchymal progenitor cells for regenerative therapy have indicated several limitations of MSCs to be used for therapeutic purposes. These limitations occur predominantly due to heterogeneity in MSC populations, donor-to-donor variations, uncontrolled differentiation in vitro and in vivo, and physiological differences between in vitro and in vivo functionality of these cells. MSCs from murine model have recently gained popularity to address some of these issues. It allows using sophisticated genetic tools to visualize cells for fate mapping studies. In addition, possibility of using a developmental engineering approach from in vivo studies in mice allows to gain insight into the lineage commitment of these cells. Recently, PαS cells were identified in mice that fitted best with the criteria to define MSCs and were chosen as candidate cells for this study.

Few major aims that were developed for the thesis are as follows:

1) To characterize in detail the adult PαS cells and its ontogenic analysis during mouse development, using standard markers of MSCs.

2) To refine the existing conditions under which PαS cells could be guided to a controlled differentiation into cartilage and other lineages in vitro.

3) To analyze the in vivo fate of cartilage templates derived from PαS cells and its subsets. The key question was to analyse whether the PαS cells and its subsets, upon in vivo engraftment, retained stable cartilage phenotype or remodeled into a functionalized bone, so as to prove them as a better model population of MSCs for engraftment.

Characterization of freshly isolated cells allowed generating a 'CD signature' of PαS cells. These signatures could be tracked in the cells in culture to envisage any differences from endogenous PαS cells, especially with respect to their multilineage differentiation potential. Ontogenic analysis allowed to track the earliest possible emergence of PαS cells and its subsets during mouse development.

MSCs, which mainly consist of progenitor populations, may determine their lineage commitment very early in development. A refinement of lineage differentiation protocol, in particular towards chondrogenic lineage, allows the possibility to recapitulate the development processes undergoing in vivo. For the thesis, several culture conditions and differentiation conditions were tested for PαS cells to improve the quality of cartilage templates generated in vitro. Although generating stable cartilage by subcutaneous implantation of PαS cells remains challenging, striking differences were observed between the in vivo engrafted postnatal subsets of PαS cells and cells isolated prior to birth. These results will be described and discussed in detail in this thesis.

6. Results

6.1 Isolation, characterization and ontogenic analysis of PαS mouse mesenchymal stromal/stem cells

6.1.1 Mice as a source of mesenchymal stromal/stem cells (MSCs)

Ever since the therapeutic potential of MSC was realized, efforts have been made to isolate and characterize these cells from humans and mice in order to explore their potential for cartilage/bone engineering and regenerative medicine. Bone marrow aspirates have been one of the predominant sources of human MSCs (hMSCs). The classical methods of isolation of hMSCs from bone marrow have relied on their adherence to plastic and their fibroblast-like morphology (Friedenstein et al., 1970). In culture, MSCs display a so-called colony-forming units-fibroblasts (CFU-F) property (Friedenstein et al., 1970) and they have the capacity to differentiate into multiple lineages, namely chondrocytes, osteocytes and adipocytes. Because of the inherent heterogeneity of the adherent hMSCs and the associated variability in cellular phenotypes (Gothard et al., 2013; Hagmann et al., 2013), further characterization and purification of hMSCs is an essential step for their use in therapeutic approaches. Advances were also hampered by difficulties in isolating rodent bone-marrow mesenchymal cells. During the past 10 years, several surface markers amenable to flow cytometry have been identified that are expressed in MSCs. Standard cell surface markers used to identify hMSCs include CD146, CD73, CD90, CD29, CD44, CD140b, CD105, CD106 and CD271. Since none of these markers could identify a homogeneous MSC population, a combination of different standard markers is used to purify and define different bone-derived MSC populations by fluorescence-activated cell sorting (FACS). However, the potential essential roles of these cell surface markers in the etiology of hMSCs is not yet well understood. Moreover, genetic models that could be used to trace the origin and identify the bona-fide mesenchymal stem/ early progenitor populations and delineate essential developmental pathways involved in determining their functions are not available for humans. Therefore, the mouse is an essential animal model to

isolate and study mouse MSCs (mMSCs) due to its manifold genetic tools. Mouse genetics provides an exciting approach to gain further insight into mMSC functions in vivo and for detailed characterization of their pluripotent differentiation potential. Several of the standard surface markers are expressed both by mouse and human MSCs, such that findings from the mouse can be transferred to the study of hMSCs.

6.1.2 Challenges in isolation of mouse MSCs

Since 1961, when Friedenstein described and coined the term mesenchymal stem cells, several methods to isolate MSCs have been described (Simmons and Torok-Storb, 1991; Sacchetti et al., 2007, Bianco et al., 2008). Originally, hMSCs were isolated due to their capacity to adhere to plastic, whereas the non-adherent hematopoietic cells were washed away after few passages. Unlike hMSCs in culture, mMSCs isolated using the same procedure were contaminated with remaining hematopoietic cells (Phinney et al., 1999; Rombouts and Ploemacher, 2003). Fig. 9 shows mesenchymal cells isolated from bone marrow of adult mice (BL6, 8 weeks old), which were kept in culture for 4 weeks. During culture, their initial fibroblastic morphology changed (Fig. 10A, B) and these cultures still contained a considerable fraction of CD45$^+$ hematopoietic cells (Fig. 10C).
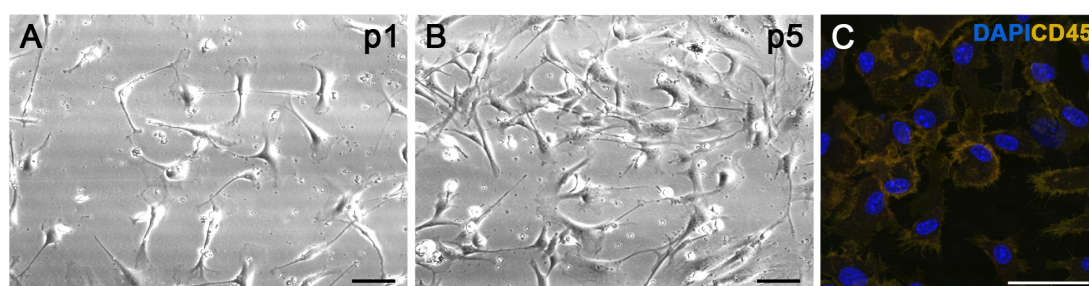
Fig 10. Plastic-adherent mouse bone marrow (BM) mesenchymal cells are contaminated with CD45$^+$ hematopoietic cells. (A) BM cells initially display a typical fibroblastic morphology (passage p1). **(B)** This morphology was changed in later passages (p5). **(C)** Immunofluorescent detection of CD45$^+$ hematopoietic cells (p5). The majority of cells are CD45 positive (yellow). Nuclei are detected by Hoechst (blue). Scale bar = 50 µm. (n ≥ 6 independent BM cultures).

Bone-derived mesenchymal cells are located in the endosteum and perivascular compartments of the bone marrow (Crisan et al., 2008; Morikawa et al. 2009; Mendez-Ferrer et al., 2010; Nakamura et al., 2010). Most of the markers reported are expressed by human mesenchymal cells isolated from bone marrow aspirates (i.e. the perivascular compartment). Mesenchymal cells attached to the endosteum can only be retrieved by protease treatment. For this reason, the mesenchymal cells from endosteal compartment have only recently been studied in the mouse. This compartment is enriched for novel types of mesenchymal cells with multi-lineage differentiation potential (Morikawa et al., 2009; Chan et al., 2015). Furthermore, recent in vivo studies in mouse models have addressed the functions of different MSC subsets and their contributions to cartilage and skeletal lineages and tissue during embryonic and postnatal development and tissue homeostasis (Park et al., 2012; Greenbaum et al., 2013; Mizoguchi et al., 2014; Zhou et al., 2014; Chan et al., 2015).

In particular, Sca1 (stem cell antigen 1), a mouse stem cell marker expressed in hematopoietic stem cells, endothelial cells and other cell types (Ortega et al., 1986) and PDGFRα (platelet derived growth factor-alpha), an early mesodermal marker (Takakura et al., 1997), were used together to identify a rare MSC population (PαS) in the non-hematopoietic lineage of adult mouse (8-11 weeks of age) (Morikawa et al., 2009; Houlihan et al., 2012). This PαS MSC population undergoes robust trilineage differentiation and displays the highest CFU-F efficiency among the known mouse MSC subsets.

6.1.3 Isolation and characterization of adult PαS mouse MSCs

PαS cells are present at very low frequency in the adult mouse bones and bone marrow (Morikawa et al., 2009). Several reports in the literature have established that mesenchymal stromal cells lose their multi-lineage differentiation potential upon prolonged expansion in culture. Therefore, we have characterized freshly isolated PαS cells with respect to their expression of mesenchymal CD markers by FACS analysis to establish a "CD signature" that could be tracked during expansion in culture and correlated with their

multi-lineage differentiation potential. PαS cells were isolated as described (Houlihan et al., 2012) (Fig. 11A). The "lineage population" eliminated by FACS from the freshly isolated cells consists of a pool of different cells of hematopoietic origin that either express CD45 (marker of hematopoietic cells), TER119 (marker of erythroid cells), CD11b (marker of macrophage and dendritic cells) or CD31 (marker of endothelial cells). In addition, the CD11b and CD31 markers were also included in the lineage marker cocktail to also eliminate macrophages and endothelial cells from the analysis of mesenchymal cells. Dead cells were gated-out using cell dyes (DAPI) to stain the cells and the PDGFRα and Sca1 double positive mesenchymal cells were isolated using FACS for analysis and culture. The fibroblast-like morphology of PαS cells was observed after 5 days in culture (Fig. 11B). CD146 is an important marker expressed by self-renewing osteoprogenitors in human bone marrow and constitutes ~6% of the non-hematopoietic cells in mouse bones (Sacchetti et al., 2007). However, only ~3.5% of PαS cells express CD146 (Fig. 11C). On the other hand, CD106 (vascular cell adhesion protein 1 or VCAM-1), another marker expressed by hMSCs (Mabuchi et al., 2013), is detected in ~90% of PDGFRα cells and by ~20% of all lineage-negative cells (Fig. 11D). PDGFRβ, another marker expressed by hMSCs, is expressed in ~90% of all PαS cells (Fig. 11E). PDGFRα was expressed in ~20% of all Lin⁻ cells whereas PDGFRβ was expressed in ~18% of all Lin⁻ cells. Hence, in mouse, PDGFRα appears to be a slightly better marker to isolate mesenchymal cell populations. In a recently published study (Pinho et al., 2013), the CD51 surface marker was used together with PDGFRα to prospectively identify the human MSCs corresponding to the Nestin[+] sphere-forming mesenchymal stem cells that were identified in mouse (Mendez-Ferrer et al., 2010; Frenette et al., 2013). Recently, CD51 was shown to be co-expressed with CD200 in a rare population of mouse skeletal stem cells (mSSCs; Chan et al., 2015). CD51 is expressed by ~95% of the PDGFRα[+] cell population and more than 90% of the Sca1^{+} positive cells also express CD51 (Fig. 11F), which means that PDGFRα and CD51 marks mostly the same cells and both can be used to identify the majority of the PαS cell population together with Sca1. Interestingly, FACS gating of the CD51^{+} cell population also shows that PαS and CD200^{+} cell populations (containing

skeletal progenitor cells; (Chan et al., 2015) are largely mutually exclusive with an overlap of only ~1% between the two populations (Fig. 11F).
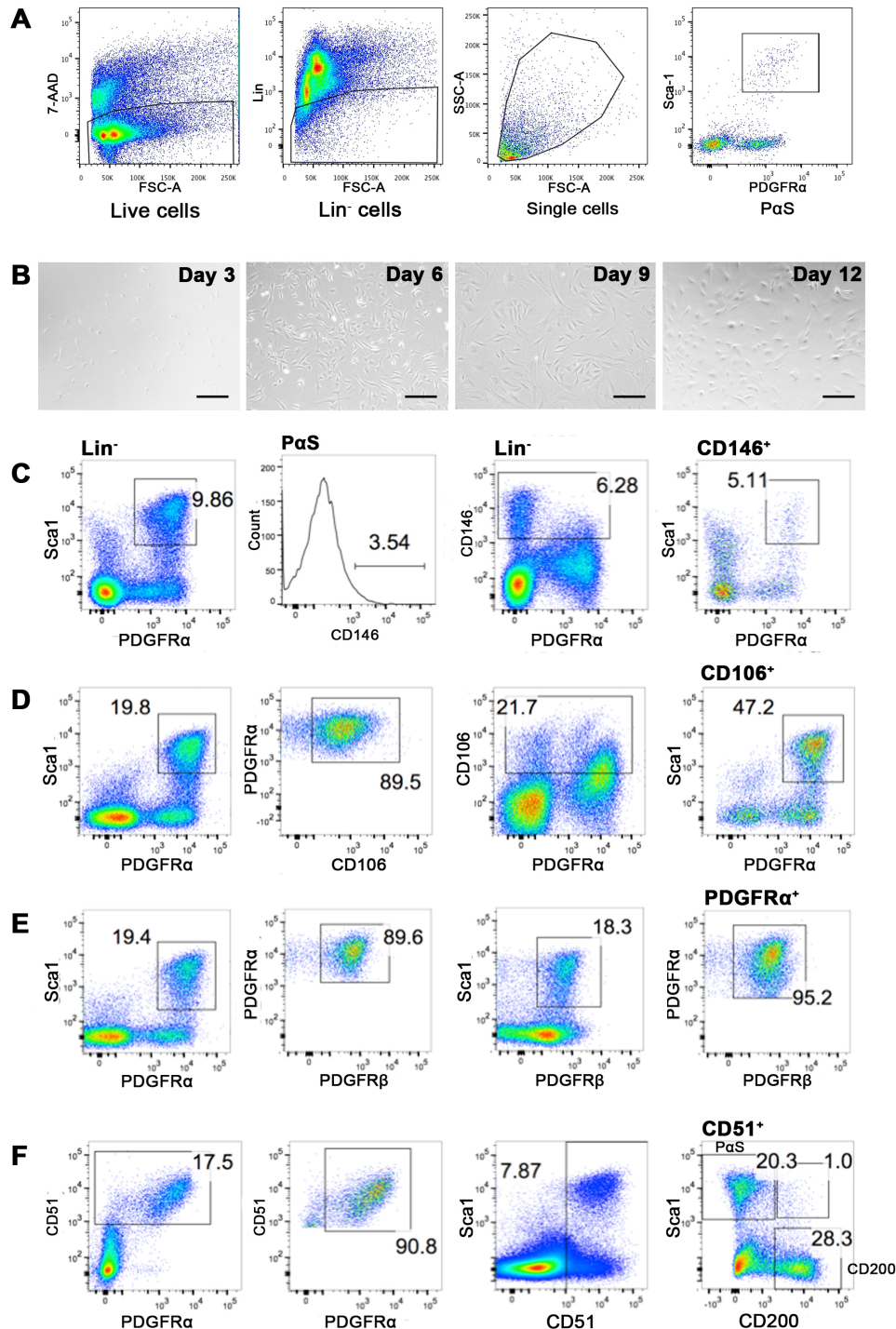
Fig. 11. FACS based identification and characterization of PαS cells. (A) 7-Aminoactinomycin D (7-AAD) cell dye allows electronic gating-out of dead cells. Sequentially, non-hematopoietic lineage (Lin⁻) cells were gated including a gate for single cells (based on forward (FSC-A) and side scatter (SSC-A) analysis. Finally, the population of Sca1⁺PDGFRα⁺ double positive cells are isolated as PαS cells. (B) Representative PαS cells cultured for 3, 6,

9 and 12 days. **(C)** Most PαS cells do not express the CD146 marker. **(D)** ~20% of all Lin⁻ cells and ~90% of all PDGFRα⁺ cells express the CD106 marker. **(E)** ~90% of all PαS cells express PDGFRβ. **(F)** CD51 is expressed in ~95% of all PDGFRα⁺ cells and ~90% of all Sca1⁺ cells. CD200⁺ cells and PαS cells are mutually exclusive, with a minimal overlap of ~1%. Numbers in gates represent the percentages of the gated populations. Scale bar = 100 µm. (n ≥3 independent experiments analyzed).

6.1.4 Comparative analysis of freshly isolated and cultured PαS cells

To date, a serum-free culture medium able to maintain the stemness of MSCs has not been defined. Therefore, the "CD signature" of freshly isolated PαS cells was compared with the one of PαS cells cultured for several passages in parallel to assessing their stemness in tri-lineage differentiation assays (Figs. 12, 13).
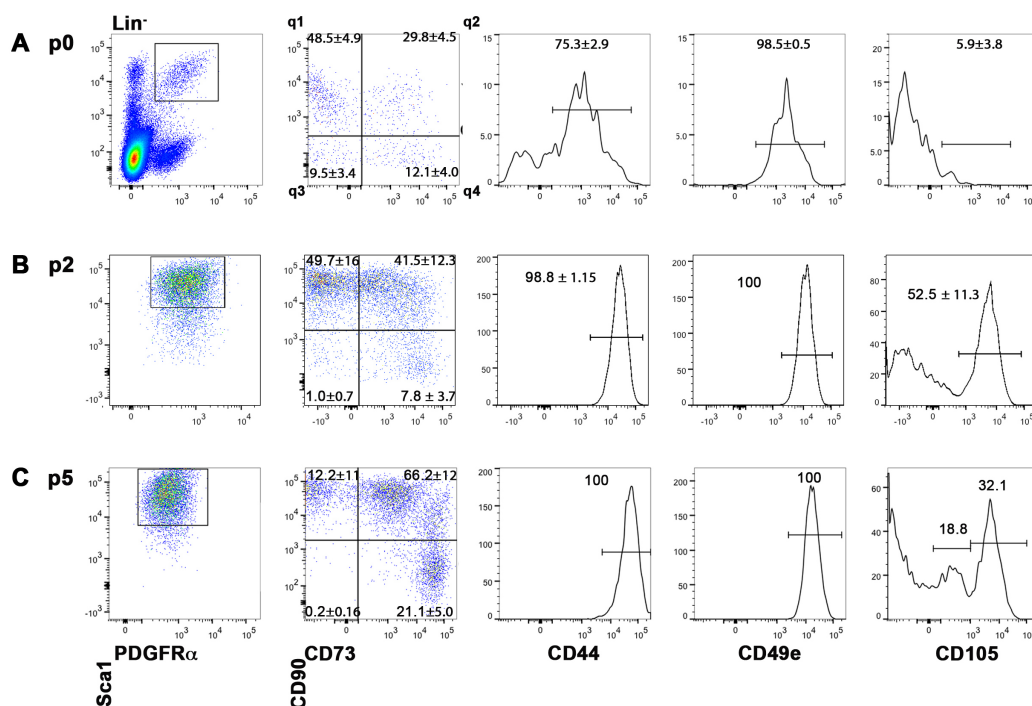
Fig. 12. FACS analysis of the CD signature of freshly isolated and cultured PαS cells using standard markers for MSC populations. (A) PαS cells freshly isolated from adult mice (passage p0) analyzed using a panel of standard markers of MSCs: CD90, CD73, CD44, CD49e and CD105 (panels from left to right). Note that analysis of the CD90 and CD73 markers allows division of PαS cells into 4 distinct subpopulations: **q1**= CD90⁺CD73⁻; **q2**= CD90⁺CD73⁺; **q3**= CD90⁻CD73⁻; **q4**= CD90⁻CD73⁺). **(B)** CD signature of PαS cells at passage 2 in culture (p2). The q3 subpopulation disappears in culture. A significant fraction of the PαS cell population (52 ± 11%) upregulates CD105 expression. **(C)** CD signature of PαS

cells at passage 5 (p5). At p5, CD105 expression is reduced in comparison to p2 in PαS cells. (n ≥3 independent experiments).

Several striking differences in the CD signature profile were revealed between freshly isolated PαS cells and cells cultured up to five passages. Most importantly, combined analysis of several mesenchymal markers revealed that the PαS cell population consists of at least four subpopulations with distinct CD signatures (Fig. 12A). The relevant markers are CD90.1 (Thy1), a cell surface marker originally identified in thymocytes that is also expressed by mesenchymal cells (Reif and Allen, 1963; Haeryfar and Hoskin, 2004; Dominici et al., 2006; Maleki et al., 2014) and CD73, which functions in extracellular adenosine generation whose expression correlates with enhanced chondrogenic potential (Campbell and Pei, 2012). The four PαS subpopulations defined by the two markers occur with different frequencies: most abundant are PαS$^+$CD90$^+$CD73$^-$ (**q1:** 48.5 ± 4.9%), followed by PαS$^+$CD90$^+$CD73$^+$ (**q2**: 29.8 ± 4.5%), while PαS$^+$CD90$^-$CD73$^-$ (**q3**: 9.5 ± 3.4%) and PαS$^+$CD90$^-$CD73$^+$ cells (**q4**: 12.1 ± 4.0%) are much less abundant (Fig. 12A, second panel).

During passaging in culture, the proportion of PαS cells expressing higher levels of CD90 and CD73 (CD90$^+$CD73$^+$ double positive subpopulation) increased (~29.8% at P0 to ~66% at P5). Concurrently, the frequency of the double negative subpopulation of PαS cells (**q3**) decreased (Fig. 12A, B). In addition, CD49e (integrin alpha-5, which is part of the α5β1 integrin complex) is expressed by all freshly isolated PαS cells. The expression of CD44 (a cell adhesion molecule) increased from 75% in freshly isolated PαS cells to all cells in culture. Similarly, the expression CD105 (endoglin), which bind to ligands of the TGF-β superfamily (Fonsatti, Altomonte et al. 2003) and marks bone derived mesenchymal progenitors (Chan et al., 2015) is also upregulated to varying extents in culture (Figs 12A-C).

Most importantly, the altered CD signature in culture correlated with the loss of stemness in the tri-lineage differentiation assays. In particular, chondrogenic and osteogenic differentiation potential was lost after two

passages, while the adipogenic differentiation potential was retained in more advanced passages (Fig. 13A-F). Taken together, these results show that the CD signature of PαS cells changes significantly when freshly isolated cells are cultured, owing to the loss of multi-lineage potential, which may result in heterogeneity or trigger differentiation under serum-based cell culture conditions. This analysis shows that the stemness potential of PαS cells is lost by in vitro expansion under culture conditions normally used to expand mesenchymal stromal cells.
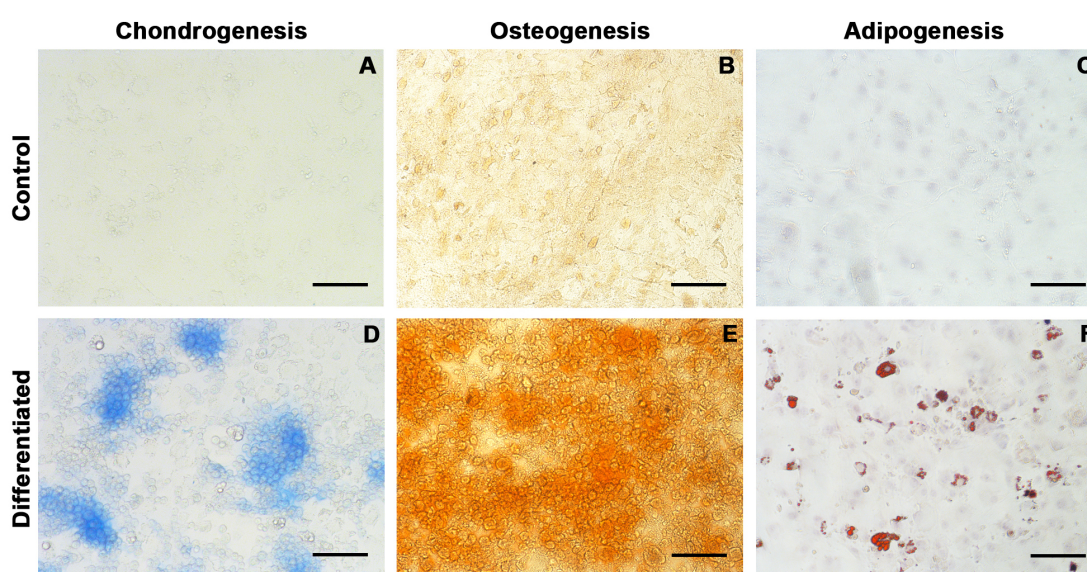
Fig. 13. Tri-lineage differentiation of PαS cells. (A, D) PαS cells from adult mice were differentiated in a chondrogenic cocktail for 7 days. Control PαS cells that were plated at high density in αMEM$^+$ medium do not initiate chondrogenesis (A). Alcian blue staining shows that the PαS cells condense and produce glycosaminoglycans (GAGs) in micromass/high-density cultures (D, up to passage p2). **(B, E)** PαS cells were differentiated in osteogenic medium for 3 weeks. Alizarin red S stains the calcium deposits produced during osteogenic mineralization (E, up to p2), while no osteogenesis is observed in controls (B). **(C, F)** Adipogenic differentiation of PαS cells for 10 days leads to formation of lipid droplets detected by Oil O Red (F, up to p6), while no adipogenesis is observed in controls (C). Scale bar = 100 μm. (n≥ 2 independent experiments).

6.1.5 Ontogenic analysis of PαS cells in Sox9-*GFP* mice revealed their appearance during mouse embryonic development

One of the major limitations to overcome in this study was that PαS cells, which are more abundant in the endosteum than in bone marrow, represent a very rare population (~10,000 cells per adult mouse; see also (Morikawa et al., 2009)). The low numbers of PαS cells in adult mouse precluded in-depth analysis and attempts to directed differentiation of MSCs into chondrocytes, since such experiments require larger numbers of mesenchymal progenitors. Besides, the results shown in Figs 12 and 13 establish that the tri-lineage potential of PαS cells is rapidly lost in culture. In order to determine if PαS cell might be more abundant at early postnatal stages and/or during embryonic and fetal development, an ontogenic analysis was performed using different stages of embryonic and adult limbs from mice expressing a Sox9-*GFP* reporter (Chan et al., 2011). The *SRY-box containing gene 9* (*Sox9*) is a master regulator of chondrogenesis and is one of the earliest markers expressed by osteo-chondrogenic progenitors (Akiyama et al., 2005). The enhanced GFP was knocked into the endogenous mouse *Sox9* locus such that the resulting bi-cistronic allele expresses both the SOX9 and EGFP proteins (Chan et al., 2011) (Fig. 14A, B). The GFP-positive cells can be easily tracked in the lineage negative populations during FACS isolation of PαS cells. When PαS cells were isolated from adult Sox9-*GFP* reporter mice, only a small fraction of these cells (~25%) co-expresses GFP (Fig. 14C). The majority of GFP-positive cells segregated with the other mesenchymal cells of non-hematopoietic origin. This result indicates that the PαS cells are mainly early progenitors not yet committed to either chondrogenic or osteogenic fates.
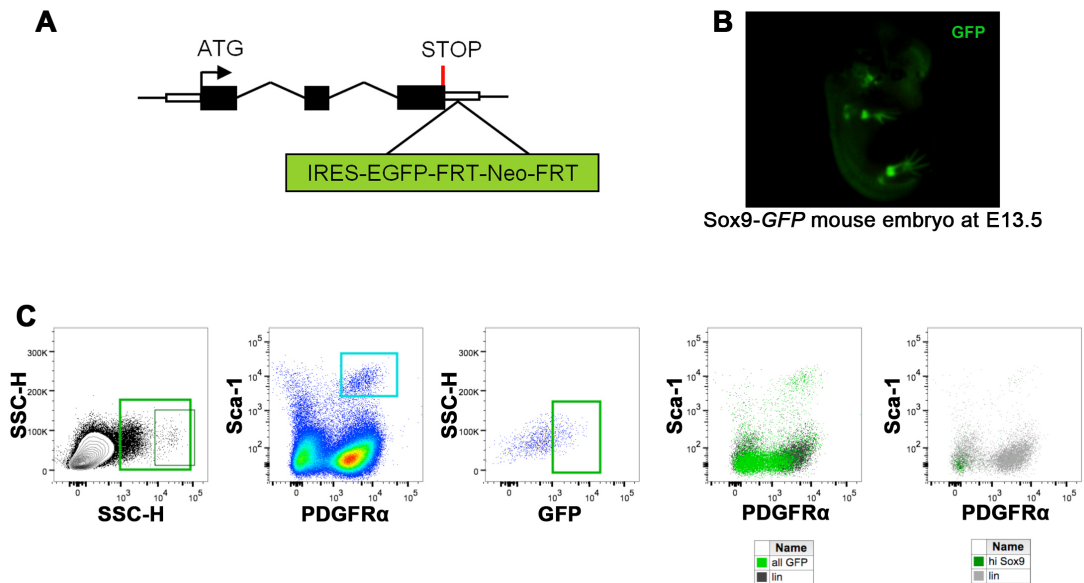
Fig. 14. Tracking Sox9-GFP expressing cells using a Sox9-*GFP* mouse reporter line. (A) Scheme showing the insertion of an enhanced GFP linked by IRES sequence *(IRES-EGFP-FRT-Neo-FRT cassette)* in the 3'UTR of the *Sox9* transcript. Black boxes- exons; solid black lines- intronic sequences; open boxes- UTRs (Chan et al., 2011). **(B)** Mouse embryo at embryonic stage E13.5 shows GFP-positive cells in limbs. **(C)** FACS of freshly isolated PαS cells shows that only ~25% of the PαS cell population expresses GFP. GFP-positive cells are mainly part of Sca1⁻PDGFRα⁻ cell population, which contains all strongly positive GFP cells. (n≥ 2 independent experiments).

In mouse embryonic limb buds, Sox9⁺ mesenchymal progenitors are present by embryonic days E9.25 - E9.5 (Akiyama et al., 2005). These cells are fated to chondrogenic and osteogenic lineage during subsequent limb development. Therefore, the Sox9-*GFP* reporter line allows direct comparison of adult PαS cells with embryonic LMPs (Sox9⁻ pool of cells) and osteochondro-progenitors (Sox9⁺ pool of cells). Embryonic limb buds at E11.5 were chosen as first developmental stage for ontogenic analysis (Fig. 15A). Cartilage in the developing limb is formed between E11.5 and E13.5 and at E12.5 – E13.5, genes that mark the onset of osteogenesis start to be expressed. Mineralization of osteoblastic cells is already evident by E14.5. Hence, this stage was analyzed to study a possible correlation of the appearance of PαS cells with fetal bone development. Hematopoietic cells migrate from the fetal liver into the forming bone marrow and this process continues from E15.5 until 2 weeks after birth in mice (see Appendix II) (reviewed by Dzierzak and Medvinsky, 2008). By perinatal day E18.5, the HSCs/HPCs have appeared in

the long bone marrow (reviewed by Mikkola and Orkin, 2006). Therefore, this time point was also chosen to study the abundance of PαS cells in fetal bones. As hormones such as estrogen regulate the stem cell niche during pregnancy and at birth (Nakada, et al., 2014; reviewed by Heo, et al., 2015), long bones isolated from mice at postnatal day 2 (P2) were also included in the ontogenic analysis. Further, mice at 2 and 4 weeks of age were included as adult mice (Fig. 15A). Since embryonic, fetal and adult mice were analyzed by FACS, lineage marker set was expanded to also include EpCAM to exclude ectodermal cells lineage, Flk-1 to exclude hemangioblasts (Craft et al., 2013), F4/80 to exclude macrophages and Gr-1 to exclude granulocyte as these cells are involved in marrow development during endochondral ossification (Chan et al., 2009).

FACS analysis of LMPs at E11.5 established that a most (~85%) of these cells express PDGFRα and about half of them (~45%) co-express Sox9-*GFP* (Fig. 15A). PαS cells are detected at a very low frequency (~0.9% of all Lin-negative LMPs), but they do not express the CD90 at E11.5 (Fig. 15 A). Interestingly, the appearance of PαS cells precedes the one of cells expressing *Osterix*, a master regulator of osteogenesis (Nakashima et al., 2002; Hosogane et al., 2010; Mizoguchi et al., 2014)). Analysis of fetal bones at E14.5 revealed that the PαS population (~1.5%) now also includes a significant fraction of CD90 positive (~25%) and negative cells (~75%), hence all 4 subpopulations have emerged (Fig. 15A). At E18.5, the abundance of PαS cell populations has increased significantly (~20%) and the maximum numbers appear immediately after birth (postnatal day 1-3) as the four PαS subpopulations make up to ~30% of all Lin negative cells (Fig. 15A, D). At this stage the CD90$^+$ subpopulations (including CD90$^+$CD73$^-$ and CD90$^+$CD73$^+$ cells) amounts to ~35% of total PαS cells, while the others are CD90$^-$ PαS cells (including both CD90$^-$CD73$^-$ and CD90$^+$CD73$^+$ subpopulations). In adult bones, the frequency of PαS population decreases to ~7% at 2 weeks and less than 1% at 4 weeks. The CD90$^+$ subpopulations increase to ~60% at 2 weeks and ~75% at 4 weeks of all PαS cells and was maintained at this high proportion in even older mice (Fig. 15A, E). Our ontogenic analysis also revealed that the fraction of the lineage negative cells decreased with

advancing prenatal and postnatal age in comparison to all cells isolated from limb buds and fetal/compact bones (Fig. 15B). This likely correlates with endochondral ossification, vascularization and the progression of bone marrow development, which results in increased presence of cells belonging to the hematopoietic lineage (Lin) (reviewed by Kronenberg, 2003; Chan et al., 2015); in the isolated cells. The fraction of *Sox9*-positive cells (corresponding to osteo-chondroprogenitors, chondroblasts and pre-hypertrophic chondrocytes) increases up to E12.5 and is maintained up to 2 weeks after birth, but then declines significantly in older mice (Fig. 15C). Maintenance of the Sox9$^+$ cell populations prior to birth correlates with cells differentiating into chondrocytes, while the osteoblast-producing cells are more prevalent after birth.

Taken together, these results show that CD90$^-$ PαS cells are first detected in limb buds at E11.5 concurrent with the appearance of the mesenchymal condensations that form the long bones and digits (Zeller et al., 2009). The CD90$^+$ subpopulations of PαS cells become apparent during endochondral ossification of the fetal long bones, the fraction of CD90$^+$ PαS cells gradually increases from ~25% (E14.5) to ~75% of all PαS cells in adult mice mouse (Fig. 15A, E, data not shown for mice after 4 weeks of age). This change in ratio likely reflects the in vivo functions of the four PαS subpopulations, which may fulfill specific functions and/or may assume different fates during progression of chondrogenic and osteogenic differentiation.
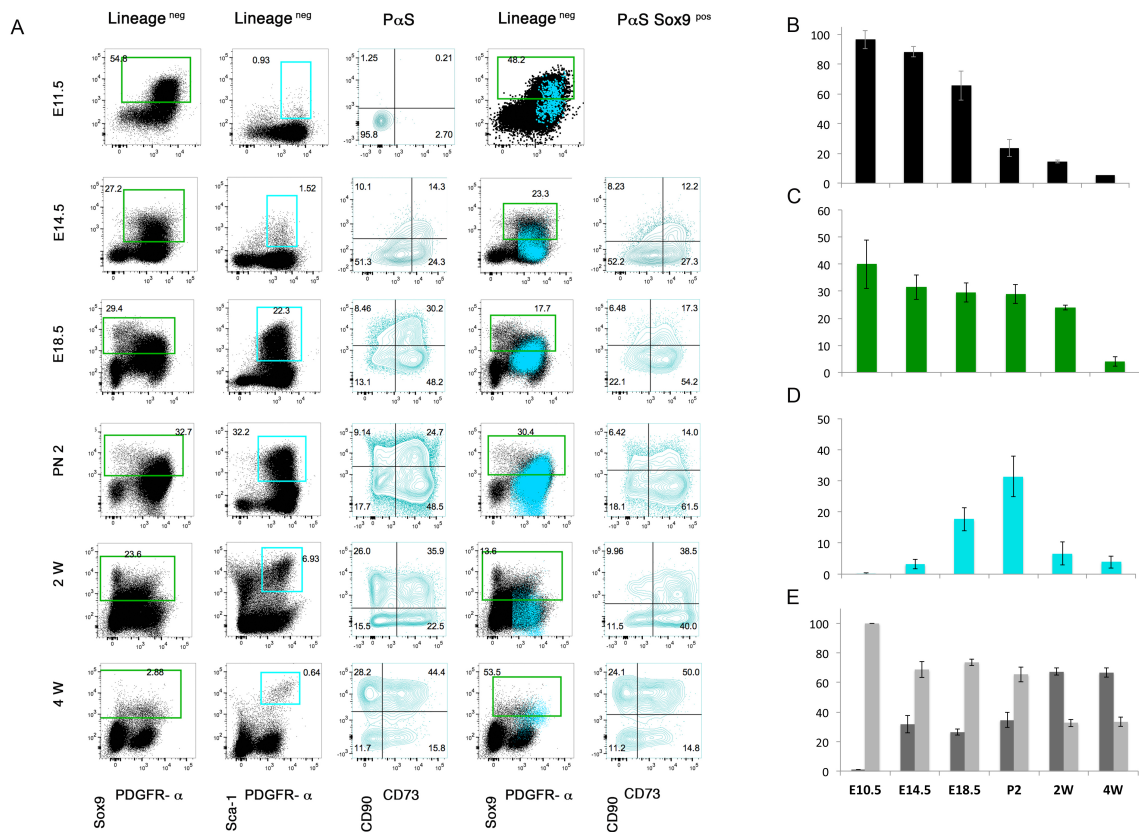
Fig. 15. FACS based ontogenic analysis of freshly isolated PαS cells during embryonic and fetal development and in adult mice. (A) PαS cells appear at around E11.5 (panels in 1st row). Maximum numbers of PαS cells were detected perinatally (E18.5) and immediately after birth (P2), while their numbers dropped as mice aged (panels in 2nd column). PαS⁺CD90⁻ subpopulations appear early (E11.5), while PαS CD90⁺ subpopulations arise during fetal bone formation (E14.5, ~25%) and become predominant in adults (4 weeks, ~75%; panels in 3rd column). **(B)** Graph showing a decrease in relative percentages of lineage negative (Lin⁻) cells from E11.5 onward. **(C)** The fraction of Sox9⁺ cells in Lin⁻ cells at the different stages. **(D)** The fraction of PαS cells in lineage negative population from E11.5 onward. **(E)** Relative abundance (in %) of PαS⁺CD90⁺ (light gray bars) and PαS⁺CD90⁻ (dark gray bars) subpopulations in the PαS cell fraction from E11.5 onward. (n≥ 3 independent experiments).

6.2 Stemness and multi-lineage differentiation potential of the four PαS subpopulations at postnatal day 2 (P2)

6.2.1 CFU-F efficiencies of the four PαS subpopulations

The maximum number PαS⁺ cells are detected in limb long bone around postnatal day 1-3 (P1-3; see before). Therefore, P2 was chosen to determine the CFU-F efficiencies of all four PαS subpopulations (q1-q4) individually in

comparison to a pool of PαS cells. Following in vitro expansion for 14 days, the CFU-F assay established that the colony forming potential of all four PαS subpopulations was robust and no significant differences between the pool and the different subpopulations were observed (Fig. 16A, B).
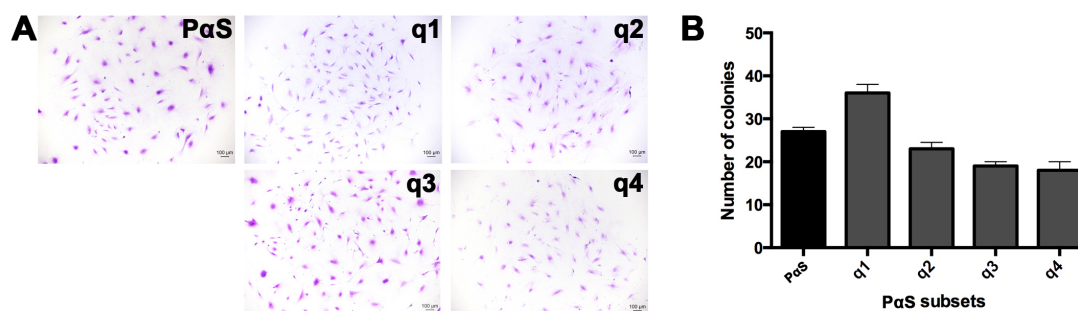
Fig. 16. CFU-F assay using PαS cells and the q1-q4 subpopulations isolated from postnatal day 2. (A) Representative staining of MSC colonies by toluidine blue. Colonies with more than 50 cells were counted after 14 days of culture. (**B**) Graph showing number of colonies formed by PαS cells and the four subpopulations per 1000 freshly isolated cells seeded in a 10 cm dish (n= 6 replicates from 3 independent sorting events).

6.2.2: The in vitro osteogenic and adipogenic differentiation potential of the four PαS subpopulations

To determine which of the four subpopulations (q1 – q4) harbors progenitors with osteogenic potential, their differentiation was induced in vitro and assessed by analyzing the expression of specific markers at the mRNA and protein level. Following an initial expansion for 5-7 days until which the CD signature of the four subpopulations is maintained in vitro (see Appendix III), cells were plated at confluency (20,000 cells per cm^2). For controls, cells from each subpopulation were plated at same density and cultured in expansion medium for the same time. Osteogenic differentiation was induced in a medium containing β-glycerophosphate, ascorbic acid, dexamethasone and BMP-2, and assessed after 21 days in culture. In order to quantify the relative fold change in transcription during the differentiation, the expression levels of *Osterix* (osteoblast marker) and *Osteocalcin* (mature osteocyte marker) were normalized to Ribosomal Protein L19 (*Rpl19*) following real-time qPCR amplification (Fig. 17A, B). In comparison to control cells, *Osterix* expression

is upregulated in all four PαS subpopulations. In particular, its normalized levels are highest in differentiated cells of the q3 subpopulation. Also, the expression in q4 cells is much higher than in q1 and q2 cells (Fig. 17A). In agreement to this, *Osteocalcin* expression is induced in differentiated q3 and q4 cells, whereas it is not expressed in q1/q2 differentiated subpopulations and controls. Mineralization during osteogenic differentiation was assessed by Alizarin Red S staining, which detects deposited calcium. Among the 4 PαS subpopulations, only q3 and q4 cells cultured in osteogenic differentiation medium showed mineralized Alizarin Red S positive areas (Fig. 17C). These results were also validated by immunohistochemistry, where Osterix detection was much more evident in q3 and q4 subpopulations than q1 and q2 cells and controls (Fig. 17D).

Taken together, these results show that the PαS$^+$CD90$^+$ subpopulations (q3/q4) are able to undergo osteogenic differentiation in contrast to the two PαS$^-$CD90$^-$ subpopulations (q1 and q2).
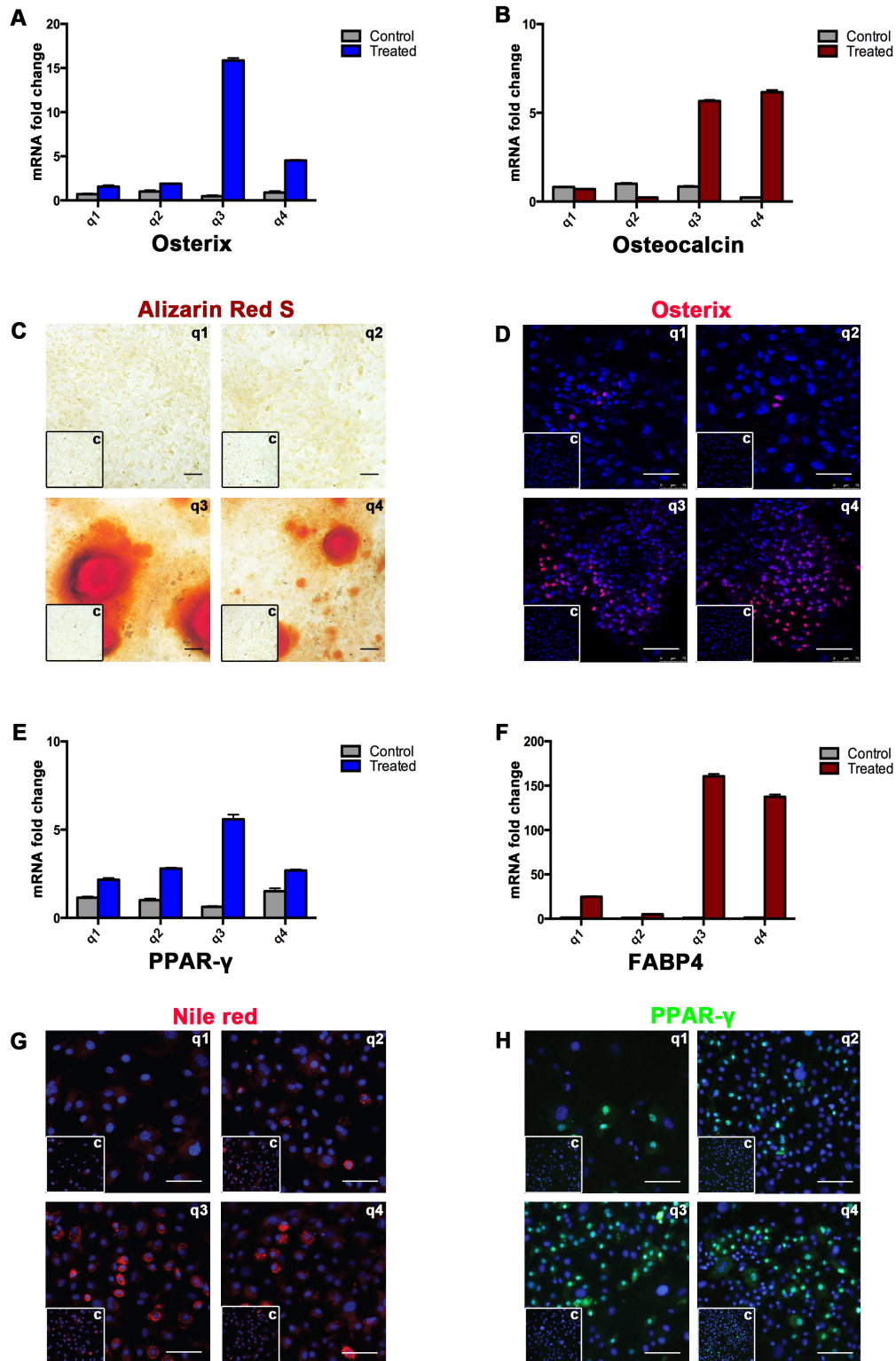
Fig. 17. In vitro osteogenic and adipogenic differentiation of PαS subpopulations from P2 mice. (A, B) Expression profile of *Osterix* and *Osteocalcin* after 21 days of osteogenic differentiation in q1-q4 subpopulations (normalized to *Rpl19 (ribosomal protein L19)* expression. **(C)** Alizarin Red S detects calcium deposition during osteogenesis. Insets represent the PαS subpopulations cultured in control medium. Scale bar = 100 μm. **(D)**

Immunodetection of Osterix (red) in q1-q4 subpopulations cultured in osteogenic differentiation medium and controls (insets). Nuclei are detected by Hoechst (blue). Scale bar = 100 µm. (n= 3 independent experiments). **(E, F)** Normalized expression profiles of *PPAR-γ* and *FABP4* after 5 days of adipogenic differentiation (**G**) Fluorescent staining using Nile red of the q1-q4 subpopulations to detect lipid droplets. Insets represent controls. Nuclei are detected by Hoechst (blue). Scale bar = 100 µm. (**H**) Immunodetection of PPAR-γ (green) in q1-q4 subpopulations cultured in adipogenic differentiation medium for 5 days and controls (insets). Nuclei are detected by Hoechst (blue). Scale bar = 100 µm. (n= 3 independent experiments).

To assess the potential of the four PαS subpopulations to undergo adipogenic differentiation, their differentiation was induced. For adipogenic differentiation, cells were induced by adding peroxisome proliferator-activated receptor *gamma (PPAR-γ)* ligand and BMP2 in a stepwise manner. For controls, cells from each subpopulation were again cultured in expansion medium. After 5 days of differentiation, the expression of *PPAR-γ* (marks pre-adipocytes) and fatty acid binding protein-4 (*FABP4*, a marker of adipocytes) were assessed by real-time qPCR. In comparison to controls, all four PαS subpopulations show increased *PPAR-γ* and *FABP4* expression (Fig. 17E, F). Among the 4 subpopulations, strongest induction of the pre-adipocyte differentiation marker *PPAR-γ* is seen in differentiating q3 cell subpopulations. *FABP4* expression is highest in q3 and q4 subpopulations, while levels are much lower in q1 and q2 subpopulations. The fluorescent dye Nile red was used to reveal lipid droplets in vacuoles (Fig. 17G). In agreement with molecular analysis, the differentiated q3 and q4 subpopulations contain most lipid droplets. These results were also validated by immunodetection of the PPAR-γ protein. Most PPAR-γ positive cells are detected in the differentiated q3 and q4 subpopulations (Fig. 17H). These results show that the PαS⁺CD90⁺ subpopulations undergo adipogenic differentiation, while the PαS⁺CD90⁻ subpopulations have only low adipogenic potential.

6.2.3 The molecular mechanisms that control the chondrogenic differentiation of mouse adult PαS cells

One of the key aspects of this study was to refine the conditions for directed

induction of chondrogenesis and track its progression at different time points in adult PαS cells with the aim to use the refined protocol to study chondrogenic differentiation of the P2 PαS subpopulations. Previous studies have established that TGFβs and BMPs play an important role in determining the fate of mesenchymal progenitors by regulating mesenchymal condensation and differentiation of chondrocytes. MSCs differentiate into chondrocytes in a chondrogenic cocktail that includes these growth factors, which is able to induce chondrogenesis with variable success (Pelttari et al., 2008; Scotti et al., 2010; Solchaga et al., 2011). Based on recent further refinements (Schmitt et al., 2003; Karamboulas et al., 2010), we decided to add TGFβ (TGFβ1 and TGF-β3) and BMP (BMP2 and BMP4) ligands as recombinant proteins to the differentiation medium in order to enhance chondrogenesis of adult PαS cells. The differentiation medium is a serum-reduced medium (to avoid serum-effects on chondrogenic differentiation) that is supplemented with ITS$^+$ premix (supplementation that contains insulin, human transferrin and selenous acid as essential components of the cell culture media), dexamethasone and ascorbic acid. The signaling ligands were added in different combinations: for protocol 1/Tp the chondrogenic medium contained TGFβs for the first 24 hours and was replaced by BMPs. For protocol 2/T+B, TGFβs and BMPs were added together for the entire period of chondrogenic differentiation.

In order to assess the efficiency of these chondrogenic differentiation conditions, adult PαS cells were expanded for 5-7 days in culture and plated at high density/ micromass to induce chondrogenesis in the two different chondrogenic media or expansion medium for control purposes. Flow cytometry, mRNA expression and immunohistochemistry approaches were used to assess the progression of chondrogenic differentiation:

a) Flow cytometry based approach: To track the Sox9-*GFP* expression, adult PαS cells from the Sox9-*GFP* reporter line were used to study the commitment of PαS cells to the osteochondrogenic progenitor and chondroblast lineages based on GFP expression. To study the progression of cell commitment by flow cytometry, it was important to determine the time

frame for in vitro cartilage differentiation. As chondrogenic differentiation is initiated by the two chondrogenic differentiation media, the expression of Sca1 is downregulated over time (Fig. 18A, panels from left to right). However, under 'Tp' conditions, the downregulation of Sca1 was less prominent in comparison to differentiating PαS cells under 'T+B' conditions. In particular, the majority of PαS cells downregulated the Sca1 expression in T+B differentiation medium after 10 days in culture. In contrast, Sca1 expression remains and *Sox9* is not activated in the controls (Fig. 18A, 1st row, panels from left to right and 4th row, panels from left to right). In differentiating PαS cells, *Sox9* is activated as early as 3 days of chondrogenesis under both conditions (Fig. 18A, histogram in 4th row). GFP levels are stable over prolonged culture in PαS cells cultured under 'Tp' conditions, while PαS cells cultured under 'T+B' conditions initially upregulate *Sox9* expression, but GFP levels are reduced again when culture is prolonged (Fig. 18A, histogram in 4th row). The massive deposition of extracellular matrix by the differentiating chondrocytes interfered with preparation of single suspension after 10 days of culture such that later time points could not be analysed by flow cytometry.
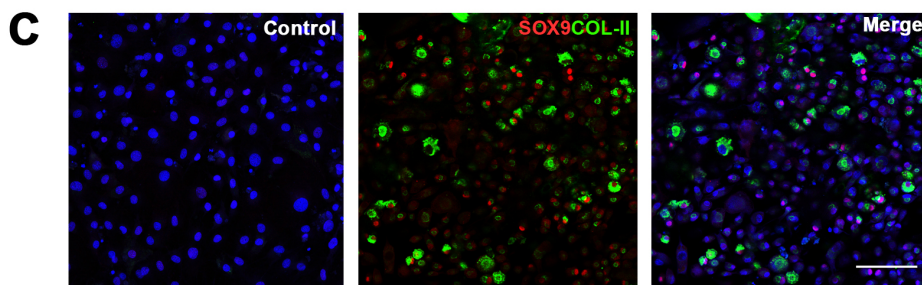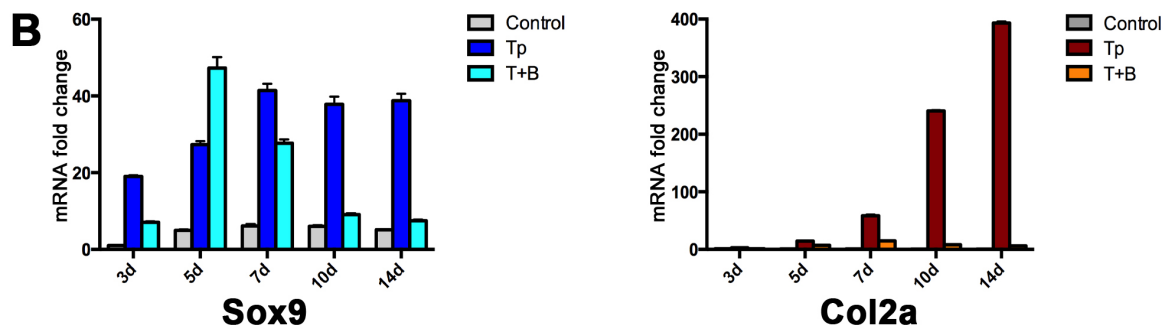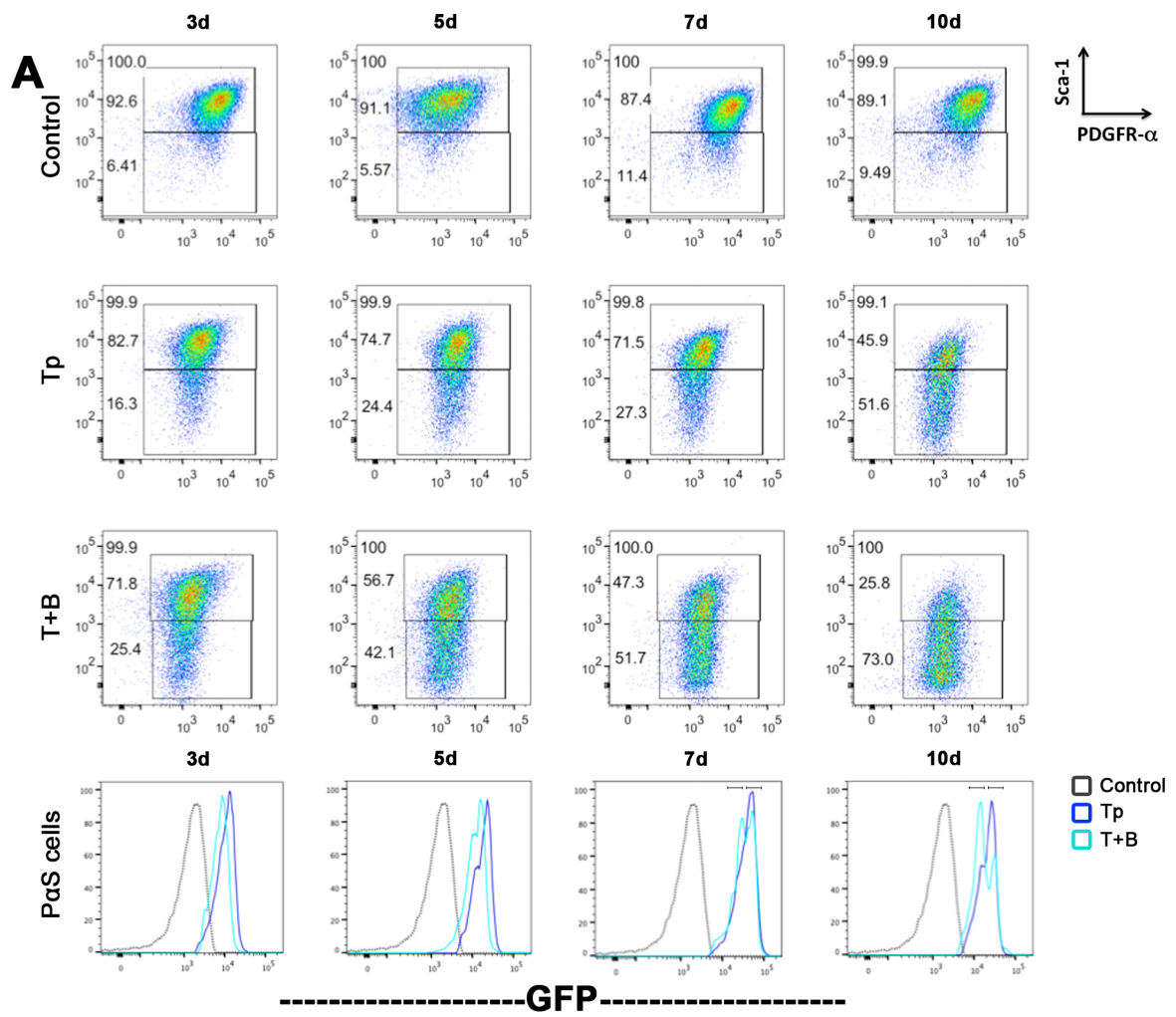
Fig. 18. Time-course of chondrogenic differentiation of adult PαS cells in culture.
(A) Dot plot representation of the flow cytometry analysis of PαS cells isolated from the Sox9-*GFP* reporter line in two different chondrogenic differentiation media (Tp, T+B). Control PαS cells were kept in expansion medium for the same duration of time. Panels in the first 3 rows detect the Sca1 and PDGFRα positive (PαS) cells during the 10 day culture period: control condition (1st row), 'Tp' conditions (2nd row) and 'T+B' conditions (3rd row). Panels in 4th row represent the histogram analysis of the Sox9-GFP expression in control versus differentiating cells at the different time-points (left to right). **(B)** RT-qPCR analysis of *Sox9* and *Col2a* expression (normalized with of *Rpl19* expression). **(C)** Immunofluorescence analysis of adult PαS chondrogenesis (cultured for 5 days under 'Tp' conditions) detects SOX9 (red) and COL-II (green). Control = PαS cells at high density in expansion medium. Nuclei are detected by Hoechst (blue). Scale bar = 100 μm. (n= 3 experiments from 3 independent sorting events).

b) Molecular approach: In order to validate the results obtained by flow cytometry approaches, *Sox9* and *Col2a* expression, which marks osteochondrogenic progenitors and chondrocytes was assessed by RT-qPCR over 2 weeks of differentiation (Fig. 18B). Consistent with the results from flow cytometric analysis of chondrogenic differentiation, *Sox9* expression is already induced at the 3rd day using the 'Tp' culture conditions, maintained over time and followed by robust activation of *Col2a*. Immunofluorescence to detect the SOX9 and type-II collagen (COL-II) proteins after 5 days of differentiation confirmed the chondrogenic differentiation of the adult PαS cells (Fig. 18C). In 'T+B' culture conditions, the initial increase in *Sox9* expression is followed by downregulation after 5 days and the change in *Col2a* expression remained negligible at all time points. This indicates that in 'T+B' culture conditions adult PαS cells does not give rise to stable chondrocytes. Importantly, in contrast to *Sox9* and *Col2a*, no *Col10a1* expression was detected in either of the culture conditions (see Appendix IV), which indicates that *in vitro* differentiated chondrocytes derived from adult PαS cells do not progress to hypertrophic stages.

Taken together, flow cytometry allows to assess chondrogenic differentiation by tracking the *Sox9*-GFP cells committed as osteo-chondroprogenitors during differentiation of PαS cells. This analysis reveals the specific time-points of chondrogenic differentiation *in vitro*. Moreover, the expression analysis shows that the step-wise implementation of TGFβs and BMPs ('Tp'

culture conditions) induce robust chondrogenic differentiation of PαS cells into chondrocytes. In contrast, adding TGFβs and BMPs simultaneously to the culture medium does not induce stable chondrocyte differentiation. The presence of the SOX9 and COL-II proteins at day 5 of differentiation under 'Tp' conditions confirmed the robustness of the protocol and faster cartilage generation in vitro. Therefore, the step-wise induction of chondrogenesis involving a TGFβ priming step ('Tp' conditions) was used for all subsequent chondrogenic differentiation of MSCs in culture.

6.2.4 In vitro chondrogenic differentiation potential of the four PαS subpopulations

The chondrogenic differentiation potential of the four PαS subpopulations was assessed at postnatal day P2. Cells of the four subpopulations were plated at high density/ micromass and their differentiation in vitro for 5 days and the expression of *Sox9* and *collagen type-II* assessed. For controls, cells from each subpopulation were plated at same density and cultured in expansion medium. Chondrogenic differentiation was induced in the 'Tp' culture conditions (stepwise addition of TGFβ and BMP ligands (Fig. 19). Analysis of transcript levels showed that *Sox9* gene expression was upregulated in all subpopulations in comparison to the controls. However, the normalized expression levels of *Sox9* and *Col2a* genes are much higher in the differentiated q3 and q4 subpopulations in comparison to the q1 and q2 subpopulations (Fig. 19B). The strongest chondrogenic differentiation is observed in q4 subpopulation. The highest levels of *Col2a* transcripts are observed in the differentiated q3 and q4 subpopulations. Immunofluorescence analysis confirmed that SOX9 and COL-II protein levels are highest in the differentiated q4 subpopulation followed by q3 subpopulation, while much lower levels of SOX9 and COL-II are observed in the q1, q2 subpopulations and all control populations (Fig. 19C). These results show that the PαS$^+$CD90$^-$ subpopulations (harboring the q3 and q4 cell) undergo chondrogenic differentiation with much higher efficiency than the PαS$^-$CD90$^-$ subpopulations (harboring the q1 and q2 cells).
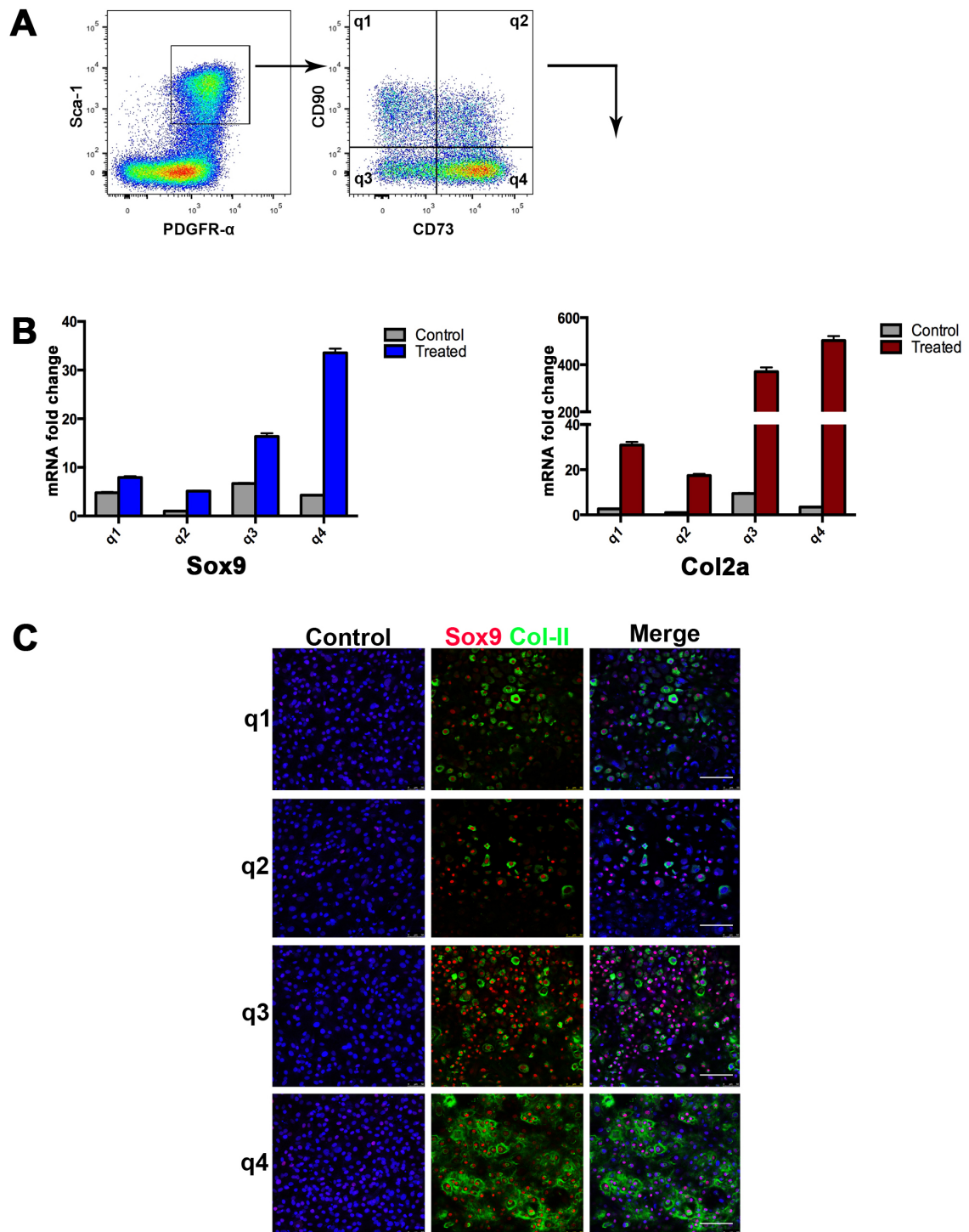
Fig. 19. In vitro chondrogenic differentiation of the four PαS subpopulations isolated from P2 mice. (A) Representative gating by flow cytometry shows isolation of the 4 PαS subpopulations. **(B)** Normalized *Sox9* and *Col2a* transcript levels in q1-q4 subpopulations after 5 days of chondrogenic differentiation. Controls are cells cultured in expansion medium for the same time. (**C**) Immunofluorescence detection of SOX9 (red) and COL-II (green) in the 4 PαS subpopulations after 5 days chondrogenic differentiation. Nuclei are detected by Hoechst (blue). Scale bar = 100 μm. Each analysis was performed using n= 3 experiments from 3 independent sorting events.

6.2.5 The chondrogenic differentiation potential of MSCs isolated from mice is robust in 3D scaffold cultures

It is important to culture MSCs differentiating into chondrocytes in an environment that is closer to the native state of the cells, which allows the production of their own extracellular matrix in the scaffold. The results described indicated that the tri-lineage differentiation potential of PαS$^+$CD90$^-$ cells (q3 and q4 subpopulations) is significantly higher than the one of PαS$^+$CD90$^+$ cells (q1 and q2 subpopulations). In order to assess the chondrogenic differentiation of these subpopulations in 3D culture, isolated PαS$^+$CD90$^+$, PαS$^+$CD90$^-$ and PαS cell populations were expanded for 7 days before seeding them in 3D scaffolds. These consisted of type-I collagen sponges seeded with 100,000 cells per 4mm diameter of scaffold. These 3D culture constructs were induced to undergo chondrogenic differentiation for another 7 days using the step-wise 'Tp' culture conditions. Controls were plated in the same set-up and cultured in expansion medium (no induction of chondrogenesis). Histological staining with Safranin O reveals the presence of glycosaminoglycans (GAGs) produced during the chondrocyte maturation and deposited as extracellular matrix (Fig. 20A). Most GAGs are produced by PαS$^+$CD90$^-$ cells, followed by PαS$^+$ and PαS$^+$CD90$^+$ cells. The levels of SOX9 and COL-II proteins (Fig. 20B) are in agreement with the data obtained by Safranin-O staining. These results show that the chondrogenic differentiation potential of PαS cells and its subpopulations is robust in 3D culture, with the chondrogenic differentiation potential being highest in PαS$^+$CD90$^-$ cells. Hence, the differences in the chondrocyte differentiation potential recapitulate the results obtained in two-dimensional high density/ micromass cultures. However, this 3D culture analysis also shows that PαS$^+$CD90$^+$ cells (q1 and q2 subpopulations) are able to undergo chondrogenic differentiation cartilage in contrast to 2D cultures. One possibility is that the q1 and q2 subpopulations together are able to trigger chondrogenesis in 3D culture, whereas separately they cannot trigger differentiation in 2D culture.
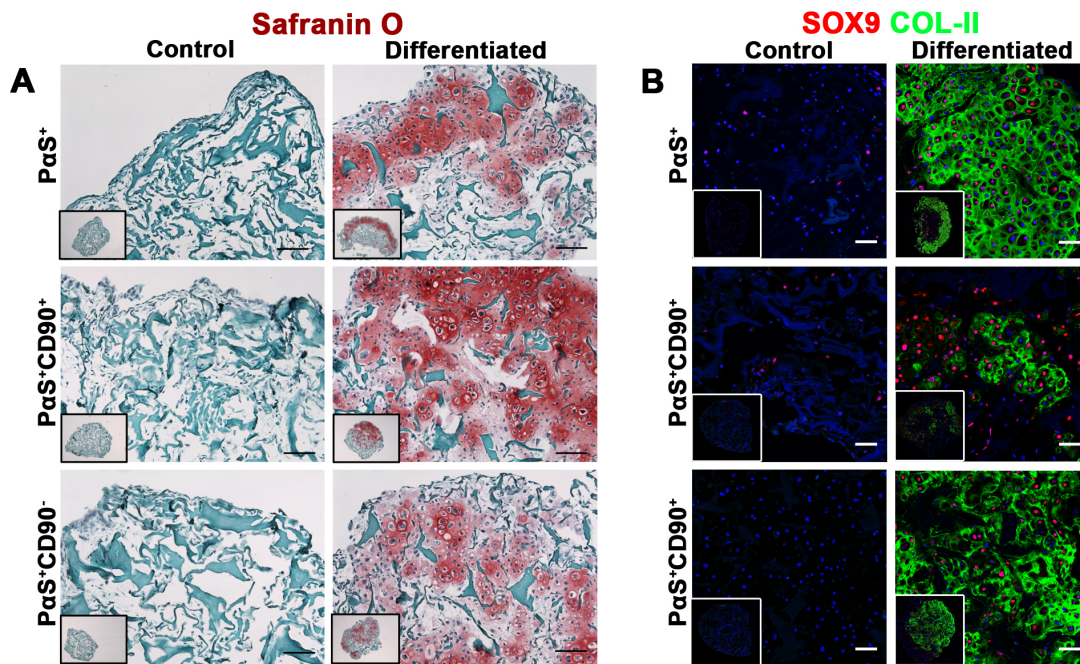
Fig. 20. In vitro chondrogenic differentiation of PαS subpopulations in collagen type-I sponge matrixes (3D scaffolds). (A) Histological sections stained by Safranin-O reveal the GAGs produced during 7 days of chondrogenic differentiation by PαS (upper panels), PαS$^+$CD90$^+$ (middle panels) and PαS$^+$CD90$^-$ cells (lower panels). No GAGs production was observed in control scaffolds. Scale bar = 100 μm. **(B)** Immunofluorescent detection of SOX9 (red) and COL-II (green) in PαS (upper panels), PαS$^+$CD90$^+$ (middle panels) and PαS$^+$CD90$^-$ cells (lower panels) after 7 days of chondrogenic differentiation. Nuclei are stained by Hoechst (blue). Scale bar = 100 μm. (n= 2 independent experiments).

These results reveal a very important finding that fully supports the results of the ontogenic analysis described in section 6.1.5. The PαS subpopulations with better tri-lineage differentiation capacity (q3 and q4) arise early during embryonic limb bud development. In addition, the q3 subpopulation is the one that most rapidly differentiates/disappears in culture. Another interesting finding of the 3D chondrogenic cultures is that PαS$^+$CD90$^+$ cells (q1 and q2 subpopulations) that performed poorly in 2D chondrogenic differentiation assays are able to undergo chondrogenic differentiation in collagen scaffolds.

6.3 Assessment of the in vivo chondrogenic and osteogenic potential of PαS cells isolated from postnatal day P2

Next, we assessed the in vivo differentiation potential of PαS cells and subpopulations with respect to generating cartilage and bone tissue via

endochondral ossification. The in vivo differentiation potential was assessed using subcutaneous implantation of the 3D scaffolds containing differentiated cartilage and expanded PαS cells and subpopulations (Fig. 20) in nude mice (Scotti et al., 2010).

6.3.1 Remodeling of implants from PαS, PαS$^+$CD90$^+$ and PαS$^+$CD90$^-$ cells

PαS cells, PαS$^+$CD90$^+$ and PαS$^+$CD90$^-$ cells differentiated into cartilage for 7 days in 3D scaffolds were implanted subcutaneously under the skin of nude mice together with matched constructs containing undifferentiated cells. Eight weeks later, the implants were initially analyzed by Hematoxylin/eosin and Safranin-O staining. This analysis showed that bone tissue has formed in the cartilage-differentiated constructs derived from PαS and PαS$^+$CD90$^+$ cells (Fig. 21A, B). The bony ossicles formed by PαS implants are overall smaller in comparison to their PαS$^+$CD90$^+$ counterparts, but bone marrow cells are observed in both types. In contrast, only rudimentary bone tissues are seen in PαS$^+$CD90$^-$ constructs (Fig. 21B). No bony ossicles form in any of the control constructs implanted (Fig. 21, insets). These results show that PαS and their subpopulations undergo remodeling from cartilage to bone following in vivo implantation of the in vitro differentiated 3D scaffolds. Remodeling of cartilage into bone is most prominent for PαS$^+$CD90$^+$ cells, while PαS$^+$CD90$^-$ cells appeared to only partially remodel into bone, suggesting that the two PαS subpopulations have a distinct in vivo potentials.
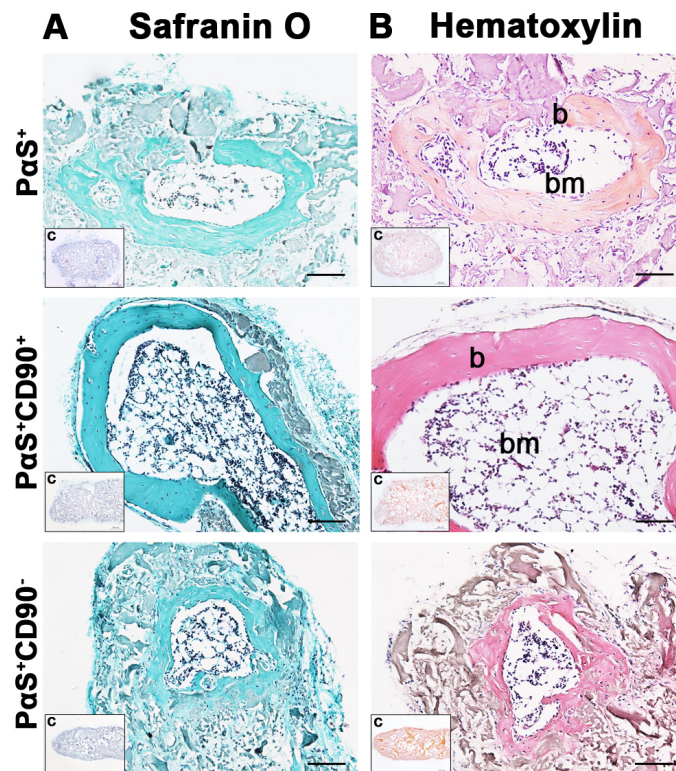
Fig. 21. Implants of cartilage templates derived from PαS, PαS⁺CD90⁺ and PαS⁺CD90⁻ cells at P2 undergo differential remodeling into bone in vivo. (A, B) Safranin O and Hematoxylin/eosin staining on histological sections of PαS (upper panels), PαS⁺CD90⁺ (middle panels) and PαS⁺CD90⁻ constructs (lower panels) after 8 weeks of subcutaneous engraftment in nude mice. Regions of bony tissue (b) and bone marrow (bm) are indicated. Insets show undifferentiated control implants (c). Safranin-O stained sections (A) were counterstained by acid fast green to stain the non-collagen sites in the scaffold. Scale bar = 200 μm. (n= 2 independent implants).

6.3.2 Sox9 remains expressed specifically in implants of PαS⁺CD90⁻ seeded scaffolds after eight weeks

In PαS and PαS⁺CD90⁺ explants that have undergone remodeling of cartilage into bone, no cells positive for nuclear SOX9 proteins are detected by immunofluorescence within the bony ossicle (Fig. 22). A few SOX9-positive cells are detected outside the bony ossicles formed by PαS⁺CD90⁺ cells. In contrast to PαS and PαS⁺CD90⁺ implants, larger regions of SOX9-positive cells are detected in the PαS⁺CD90⁻ implants that have undergone ossification to a lesser extent (Fig. 21 and Fig. 22F-F2). The small areas that by histology display characteristics of bony tissue were mostly devoid of SOX9-positive cells. These data indicate that although PαS and PαS⁺CD90⁺ constructs

differentiated into cartilage in vitro undergo remodeling upon engraftment, the PαS$^+$CD90$^-$ constructs tend to retain their cartilage-like features. The presence of significant numbers of SOX9 expressing cells with lower levels of remodeling into bone is indicative of either partial differentiation of chondrocytes into pre-hypertrophic chondrocytes or retention of mesenchymal features by PαS$^+$CD90$^-$ cells eight weeks after implantation of the differentiated cartilage into nude mice. However, no Col-II and Aggrecan expression was detected (data not shown).
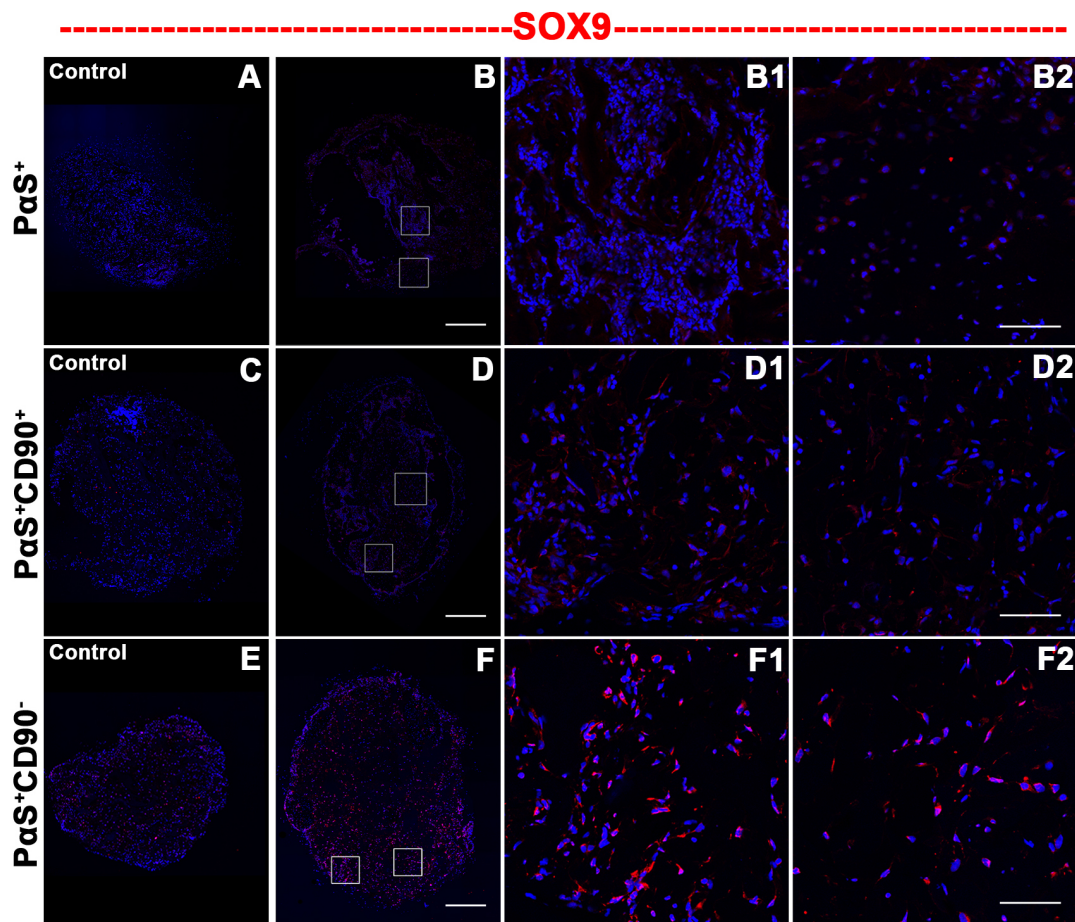
Fig. 22. SOX9 expression in the different implants after eight weeks in nude mice
(**A, C, E**) undifferentiated control implants. (**B, D, F**) Immunofluorescent detection of the SOX9 protein (red) in the in vivo differentiated (8 weeks) implants of PαS (B), PαS$^+$CD90$^+$ (D) and PαS$^+$CD90$^-$ (F) constructs. The two enlargements show the SOX9 positive cells in PαS (B1 and B2), PαS$^+$CD90$^+$ (D and D2) and PαS$^+$CD90$^-$ (F1 and F2) constructs. Abundant SOX9-positive cells remain only in the PαS$^+$CD90$^-$ constructs after 8 weeks of implantation (F1, F2). Nuclei are detected by Hoechst (blue). Scale bars = 500 μm (left panels, low magnification). Scale bars = 100 μm (high magnifications). n≥ 3 independent experiments per dataset shown.

6.3.3 Development of a bona-fide hematopoietic environment in the bony ossicles of the PαS and PαS$^+$CD90$^+$ constructs upon implantation

Immunofluorescent detection of Osterix antibody (OSX) revealed the presence of abundant osteoblasts in sites of bony tissue formation (Fig. 23B, with 2 representative insets enlarged as B1, B1', B2, B2'; and D, with 2 representative insets enlarged as D1, D1', D2, D2'). In addition, the forming bone tissue is vascularized by recruitment of endothelial cells as chondrocytes undergo the pre-hypertrophic to hypertrophic transition and ossification is initiated (Fujita et al., 2010; reviewed by Kronenberg, 2003). Indeed, OSX-positive osteoblasts were present throughout the bony ossicle in close proximity to CD31$^+$ endothelial cells. In contrast, significantly fewer OSX$^+$ osteoblasts and no CD31$^+$ endothelial cells were detected in PαS$^+$CD90$^-$ implants (Fig. 23F-F2'). This feature of the PαS$^+$CD90$^-$ constructs agrees with their retention of more cartilage-like feature after 8 weeks of implantation. The lack of endothelial cells suggests that these implants were likely not undergoing endochondral ossification at the time of analysis. Finally, only cartilage that had formed during the prior in vitro differentiation can be remodeled into bone after implantation, as no osteoblasts and endothelial cells were detected in control implants (Fig. 23A, C, E).

OSX CD31 ——————Merge

67
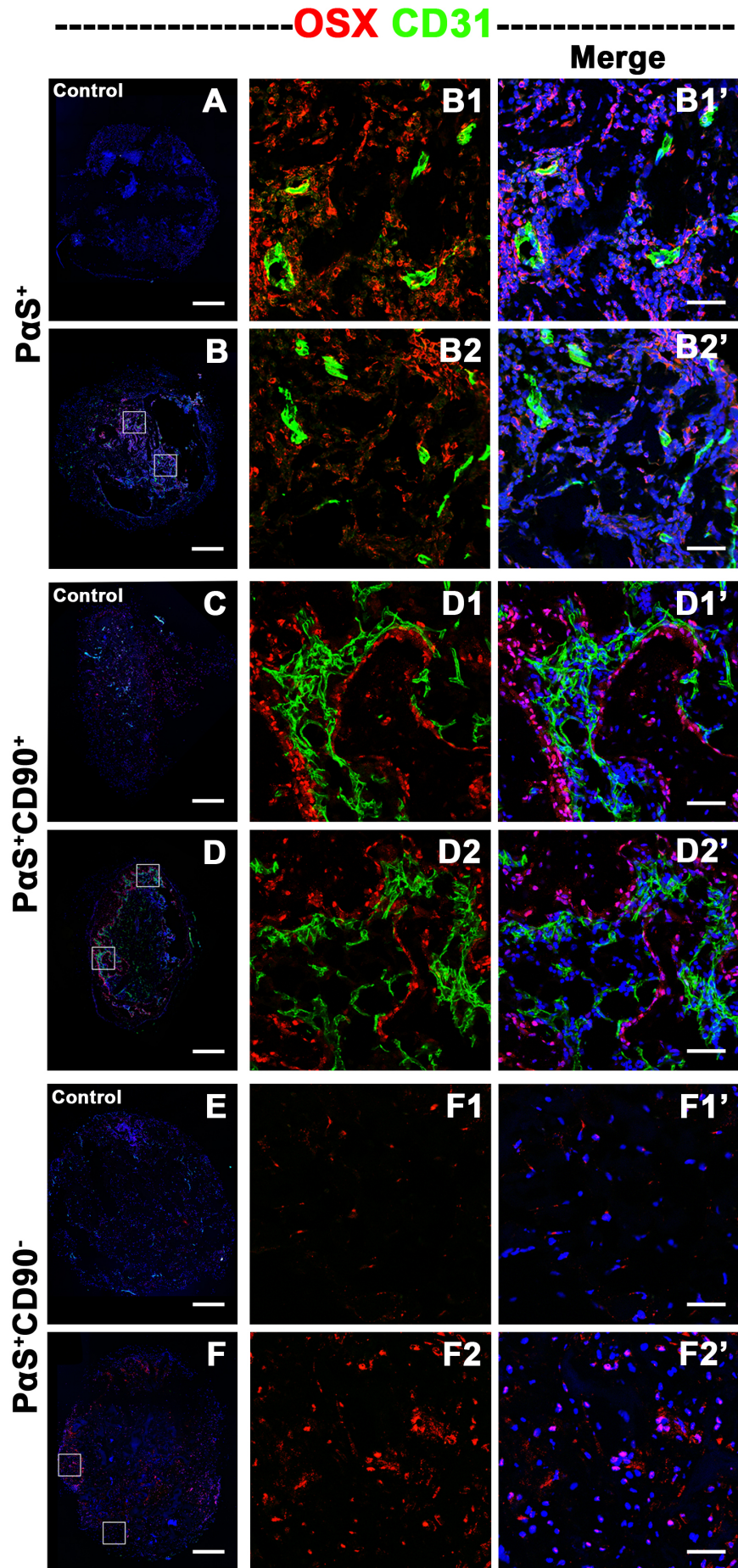
Fig. 23. PαS and PαS⁺CD90⁺ constructs remodeled into bone tissue in vivo attract endothelial cells. (**A, C, E**) Control implants. (**B, D, F**) Immunofluorescence detects OSX – positive osteoblasts (red) and CD31-positive endothelial cells (green) in implants of PαS (B), PαS⁺CD90⁺ (D) and PαS⁺CD90⁻ (F) cells. The enlargements show the presence of osteoblasts and endothelial cells in the PαS (B1, B1', B2 and B2'), PαS⁺CD90⁺ (D1, D1', D2 and D2') and PαS⁺CD90⁻ (F1, F1', F2 and F2') subpopulations. Endothelial cells have a typical elongated morphology and are always surrounded by the osteoblasts in the marrow forming regions. In the PαS⁺CD90⁻ subpopulation, very few OSX-positive osteoblasts (F2, F2') and no endothelial cells are detected. Nuclei are detected by Hoechst (blue). Scale bars on overview images = 500µm. Scale bars in enlargements =100 µm. (n≥ 3 independent experiments).

Histological analysis of the PαS and PαS⁺CD90⁺ implants revealed the bony ossicles with the enclosed bone marrow. The cells of the bone marrow in these implants could arise from HSCs specified as myeloid and lymphoid progenitors in the functionalized bone tissue during hematopoiesis. In particular, common myeloid progenitors (CMPs) give rise to erythrocytes, platelets, macrophages, neutrophils, eosinophils, basophils; whereas common lymphoid progenitors (CLPs) gives rise to natural killer cells, T-cell progenitors and B-cell progenitors that complete their differentiation program in the bone marrow. Dendritic cells are known to arise from both CMPs and CLPs (Miyamoto et al., 2002; Iwasaki and Akashi, 2007; Kondo, 2010; reviewed by Weissman and Shizuru, 2008). Macrophages present in the developing bone marrow are detected by F4/80 (also positive for CD45) in the long bones at postnatal day 2 in regions also containing Sca1-positive cells (Fig. 24A-D). Analysis of bone ossicles derived from implants of PαS⁺CD90⁺ cells shows that their bone marrow contains CD45-positive hematopoietic cells (CD45⁺) and F4/80-positive myeloid cells. (Fig. 24E-E1", E2-E2").
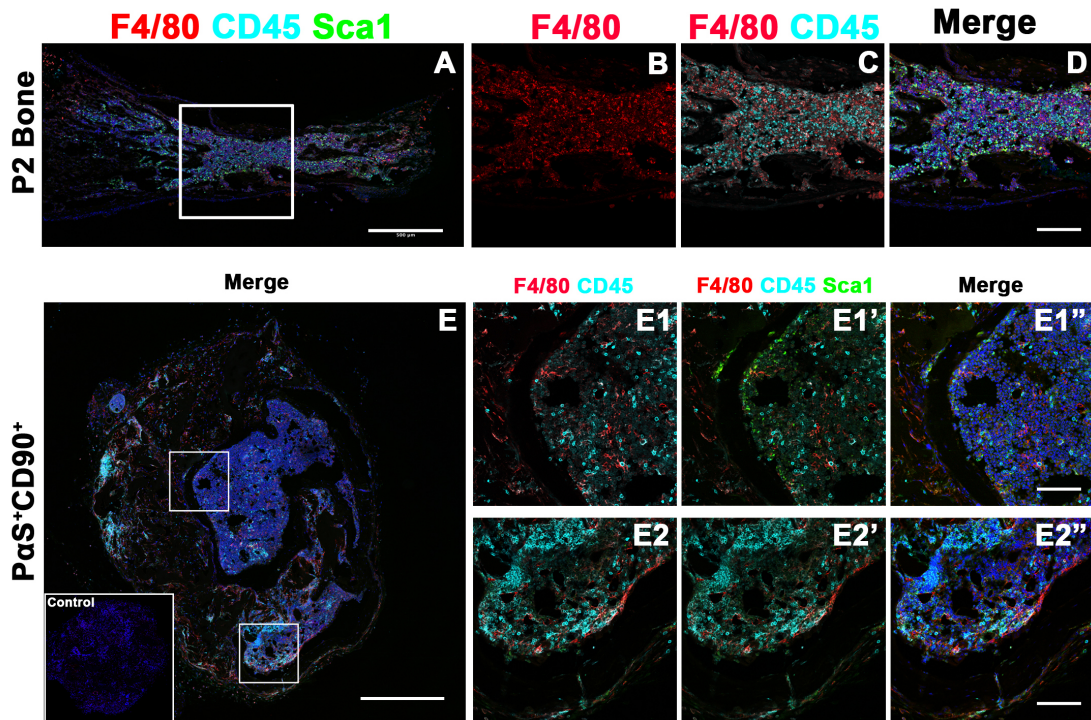
Fig. 24. Macrophages are observed at sites of hematopoiesis in remodeled bony tissue derived from the P2 cartilage implants (**A-D**) Immunofluorescence analysis of the distributions of the F4/80 (red), Sca1 (green) and CD45 (cyan) antigens in the bone marrow of long bones at postnatal day P2. **(E, E1-E1", E2-E2")** Immunofluorescence analysis of the distributions of the F4/80, CD45 and Sca1 antigens in two representative insets from the remodeled implants of PαS⁺CD90⁺ cells. This analysis reveals the presence of F4/80-positive macrophages in the marrow together with CD45 and Sca1-positive cells. Inset in panel E shows the undifferentiated control without macrophages. Nuclei are detected by Hoechst (blue). Scale bars in left panels = 500μm. Scale bars in right panels = 100μm. (n≥ 2 independent experiments).

B220, an isoform of CD45, is predominantly expressed by pre and mature B-cells and in plasmocytoid dendritic cells (Ferrero et al., 2002; Manilay and Zouali, 2014). In order to access whether the bone marrow in the bone ossicles derived from PαS and PαS⁺CD90⁺ cells contained lymphoid progenitors, the B220 antibody was used to detect B-cells at the sites of hematopoiesis. Indeed, B220-positive B-cells are present in the marrow of the bony ossicles in both types of implants (Fig. 25B-B2 and Fig. 25D-D2). In contrast, no B220-positive cells are present in implants derived from PαS⁺CD90⁻ cells (Fig. 25F- F2) and controls (Fig. 25A-A2, C-C2 and E-E2). Taken together, these results show that the implants derived from PαS and PαS⁺CD90⁺ cells support hematopoiesis and the development of myeloid and

lymphoid cells in the resulting bone ossicles, while this is not the case for PαS$^+$CD90$^-$ cells.
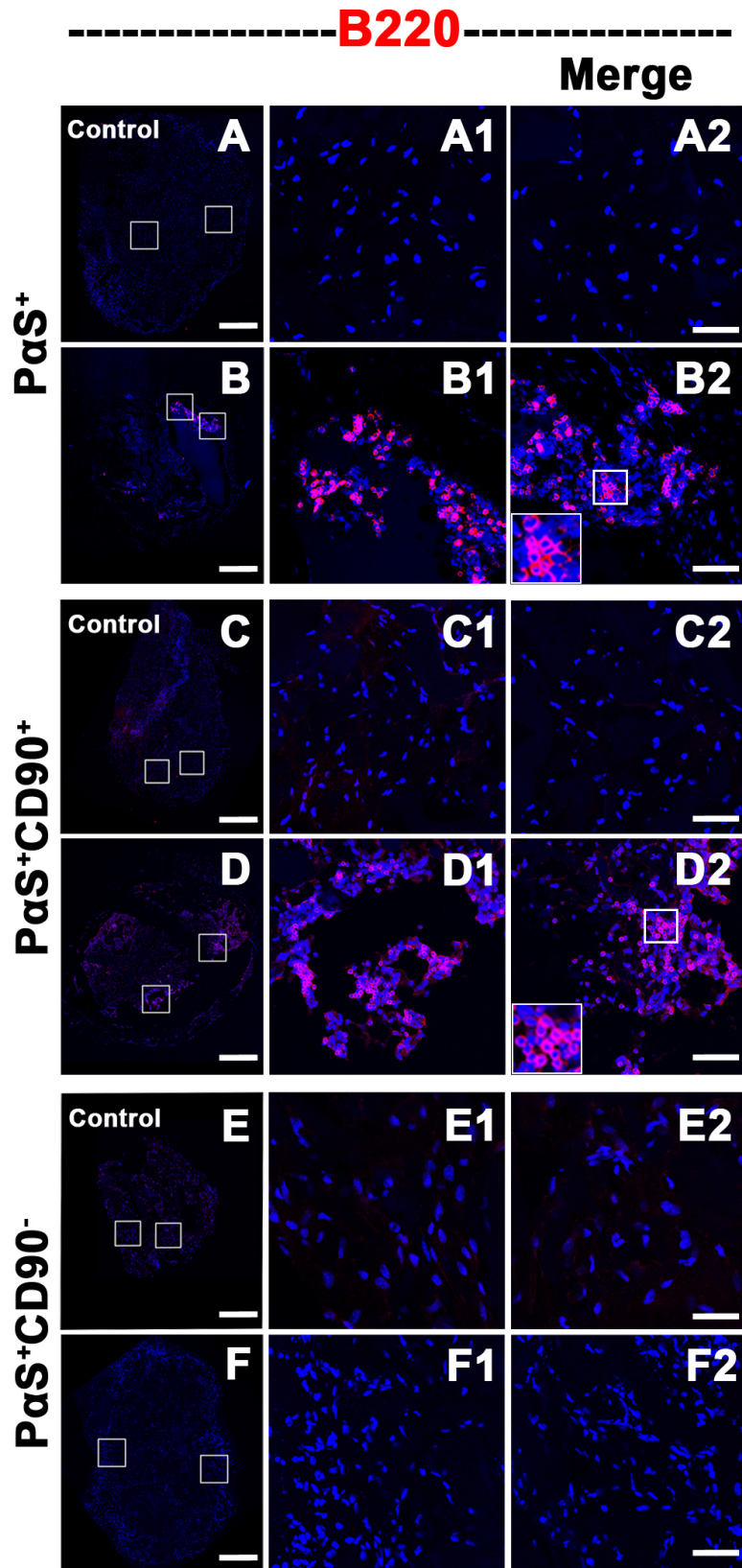
Fig. 25. Implants derived from PαS and PαS$^+$CD90$^+$ cells support B-cell development at sites of bone formation. (A, C, E) Controls do not contain B220-positive cells. **(B, D, F)** Sections of bone ossicles derived from PαS cells (B), PαS$^+$CD90$^+$ (D) and PαS$^+$CD90$^-$ (F) to detect B220-positive B-cells (red fluorescence). Middle and right panels: enlargements to show the presence of B220-positive cells. B220-positive cells are absent from implants derived from PαS$^+$CD90$^-$ cells. Nuclei are detected by Hoechst (blue). Scale bars left panels = 500µm. Scale bars right panels = 100µm (n≥ 3 independent experiments).

To determine whether the bone ossicles derived from PαS and PαS$^+$CD90$^+$ cells had recruited bona-fide hematopoietic progenitors, the potential expression of Sca1 was assessed. Hematopoietic progenitors express Sca1 and CD45 (Sca1$^+$CD45$^+$) in the lineage negative population, which consists of long- and short-term HSCs (Rebel et al., 1996; Ara et al., 2003). In implants derived from PαS and PαS$^+$CD90$^+$ cells, clusters of Sca1-positive cells are observed at the sites of hematopoiesis in contrast to controls (Fig. 25). Among these cells, rare hematopoietic progenitor cells (HPCs) expressing both CD45 and Sca1 antigens (CD45$^+$Sca1$^+$) are observed (Fig. 26B, B1-B1', B2-B2'; 25D, D1-D1', D2-D2'). In contrast, only few scattered CD45-positive, but no CD45$^+$Sca1$^+$ double positive cells are detected in implants derived from PαS$^+$CD90$^-$ cells (Fig 26F, F1-F1' and F2-F2').

CD45 Sca1 Merge

PαS⁺

PαS⁺CD90⁺

PαS⁺CD90⁻

72
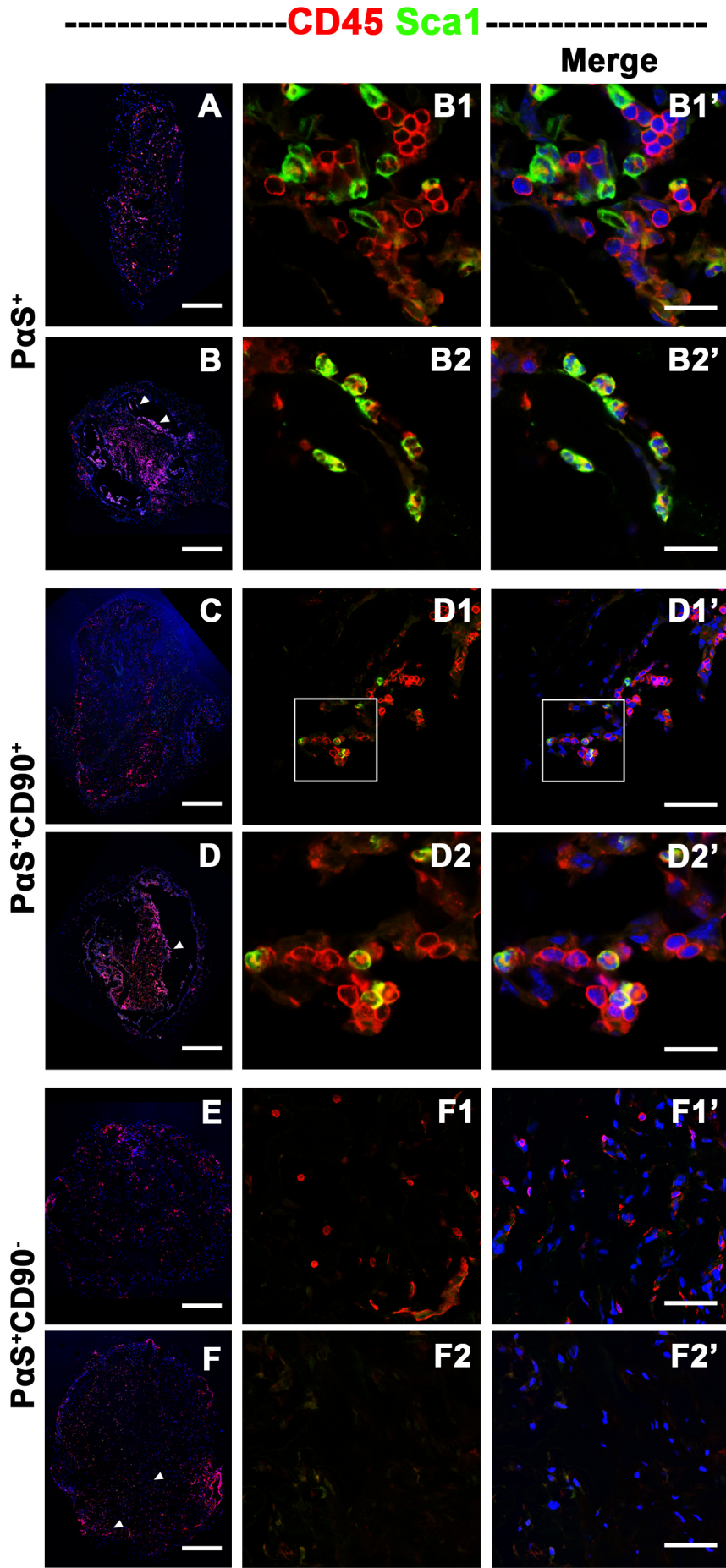
Fig. 26. Bone ossicles that develop from implants derived from PαS and PαS⁺CD90⁺ cells contain hematopoietic progenitors. (A, C, E) No CD45 and Sca1 double positive HPCs are observed in undifferentiated control implants. **(B, D, F)** Analysis of implants derived form PαS (B), PαS⁺CD90⁺ (D) and PαS⁺CD90⁻ (F) cells reveals CD45 (red) and Sca1 (green) positive cells. Solid arrowheads point to regions with HPC cells that co-express CD45 and Sca1 (HPCs). Representative regions showing these double positive HPCs are shown in the middle and right panels for the PαS (B) and PαS⁺CD90⁺ (D) derived implants. In contrast, HPCs are absent in remodeled PαS⁺CD90⁻ cells (panels F). The enlargements show the presence of few CD45 single positive cells. Nuclei are detected by Hoechst (blue). Scale bars left panel = 500µm. Scale bars in D1 = 500µm. Scale bar in composites (D1, D1', F1, F1', F2, F2') = 100µm. Scale bars in enlarged insets = 20µm. (n≥ 3 independent experiments).

Taken together, these results show that HPCs are present in the bone ossicles that had developed from cartilage implants derived from PαS and PαS⁺CD90⁺ cells isolated at postnatal day P2. The analysis of Osterix and CD31 expression showed that remodeling of cartilage implants derived from PαS and PαS⁺CD90⁺ cells into bone tissue results in vascularization and endothelial cell recruitment from the host must be one of the first steps in this process. The bone ossicles derived from PαS and PαS⁺CD90⁺ cells support hematopoiesis resulting in lymphoid and myeloid progenitors. The presence of Sca1⁺CD45⁺ HPCs at sites of hematopoiesis are indicative of the bone ossicles having developed the microenvironment required for hematopoiesis within the implant placed ectopically under the skin of a nude mouse. In contrast, remodeling of the implants derived from PαS⁺CD90⁻ cells is much more restricted. The continued presence of Sox9⁺ cells in the remaining areas of cartilage suggest that the PαS⁺CD90⁻ derived implants retain cartilage-like features and are likely unable to remodel into bone by endochondral ossification.

6.3.4 Analysis of bone ossicles derived from DsRed cells shows that the hematopoietic progenitors are host-derived

As MSCs can differentiate into endothelial cells (Starlinger et al., 2011) and as FACS of PαS cells may result in low-level contamination by hematopoietic cells, it was essential to determine if the CD31, B220 and CD45 expressing

cells are derived from the host (nude mouse) or implant. Therefore, PαS, PαS$^+$CD90$^+$ and PαS$^+$CD90$^-$ cells were isolated from mice expressing a DsRed transgene expressed in all cells under control of a CMV enhancer and chicken β-actin promoter (Vintersten et al., 2004). Analysis of bone ossicles indeed established that the majority of cells in the implants are DsRed positive (Fig. 27B, C). However, CD45-positive endothelial cells and the CD31 and B220-positive hematopoietic cells are all not expressing DsRed (Fig. 27D-L). These results establish that the endothelial and hematopoietic cells are derived from the host nude mice and must invade during the endochondral ossification.
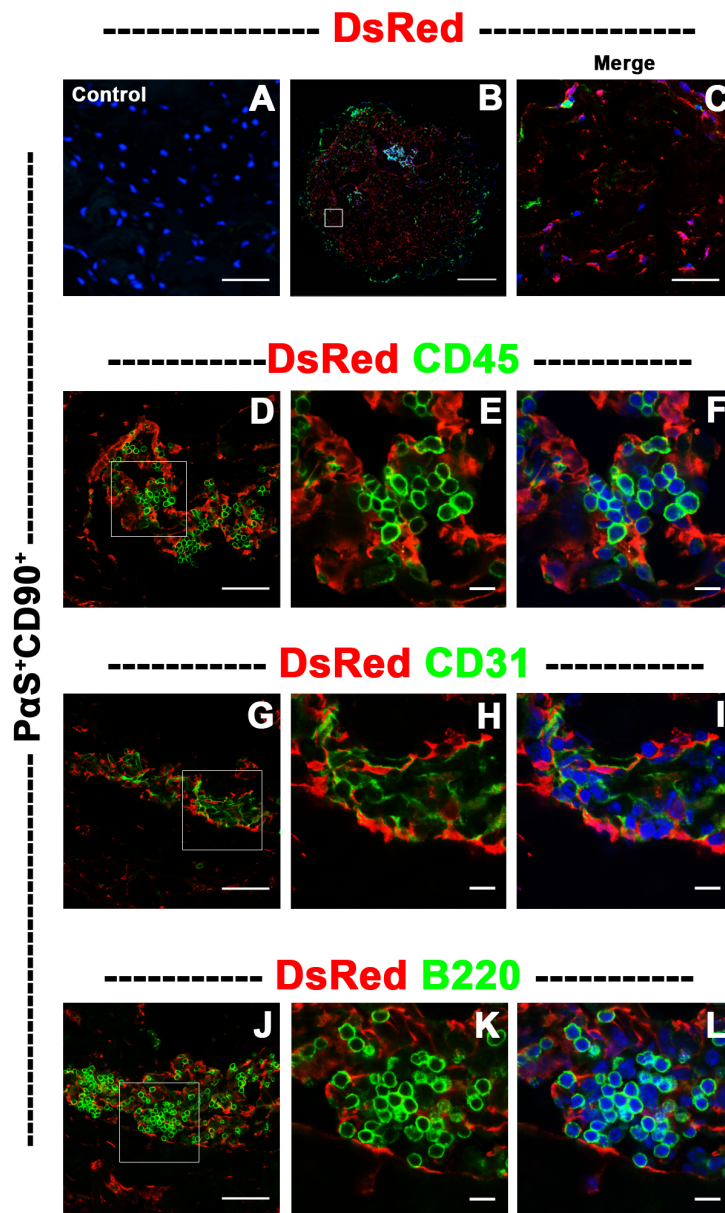
Fig. 27. Cells of hematopoietic origin are host derived in PαS⁺CD90⁻ bone ossicles. (A) Wild-type cells serve as background control for DsRed fluorescence **(B, C)** Detection DsRed (red) cells and CD45⁺ (cyan) hematopoietic cells in regions of cartilage **(D, E, F)** Detection of DsRed and CD45 at sites of hematopoiesis. **(G, H, I)** Detection of DsRed and CD31 positive (cyan) endothelial cells at sites of hematopoiesis. **(J, K, L)** Detection of DsRed and B220-positive (green) B-cells at sites of hematopoiesis. Nuclei are detected by Hoechst (blue). Scale bars on low power image (B) = 500μm. Scale bars on the panels on the left and C = 50μm. Scale bars for the enlargements from insets = 10μm (n≥ 2 independent experiments).

6.4 Assessment of the in vivo differentiation potential of PαS cells isolated from embryonic day E18.5

From ontogenic studies, it was concluded that CD90 is expressed in PαS cells that appear in limb long bones during fetal development (≥E14.5). Furthermore, this analysis also showed that the fraction of PαS⁺CD90⁺ cells among all PαS cells is similar at embryonic day E18.5 and postnatal day P2 in mice. Interestingly, the migration of HSCs/HPCs from the fetal liver to their definitive location in bone marrow starts at ~E17.5-18.5 and continues until ~2 weeks postnatally during establishment of bone marrow stem cell niches (reviewed by Mikkola and Orkin, 2006). In addition, E18.5 and P2 coincide with changes in hormonal regulation during pregnancy and shortly after birth (Nakada et al., 2014). Therefore, the migration of HSCs/HPCs and/or the hormonal regulation of the developing stem cell niches around birth may also influence the PαS cell populations and/or other skeletal progenitor cell-types. To assess whether prenatal and postnatal PαS cell populations differ in their in vivo differentiation potential, PαS cell populations isolated at E18.5 were also analyzed.

6.4.1 Remodeling of implants derived from perinatal PαS cell populations (E18.5)

After 8 weeks of subcutaneous engraftment in nude mice, implants derived from prenatal PαS cell populations differentiated in culture prior to implantation were analyzed by Safranin-O and H&E staining. This analysis reveals their reduced endochondral differentiation potential in comparison to implants derived from P2 PαS cell populations (Fig. 28 and see before). A

small bone ossicle formed only in implants with differentiated PαS⁺CD90⁺ cells, while no such ossicles were observed in implants of differentiated PαS and PαS⁺CD90⁻ cells (Fig. 28). Safranin-O staining did not reveal significant levels of GAGs in implants after 8 weeks for these latter two cell populations, which indicates that these cells did not undergo significant remodeling.
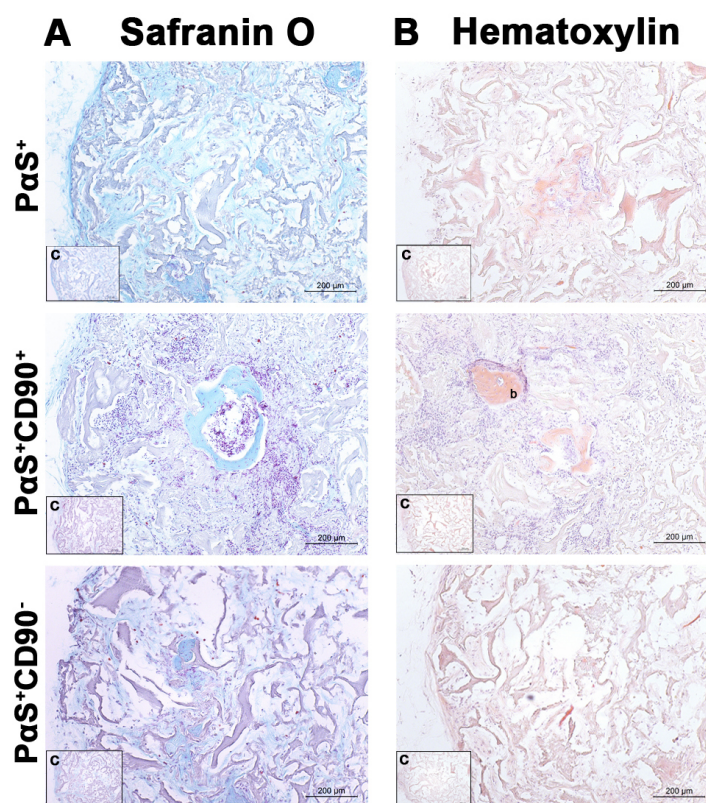
Fig. 28. Cartilage templates derived from perinatal (E18.5) PαS⁺CD90⁺ cells undergo some remodeling to form small bone ossicles, while this is not the case for PαS⁺CD90⁻ and PαS cells at E18.5. (A, B) Safranin-O and H&E staining of histological sections of Implants of the three cell populations after 8 weeks of subcutaneous engraftment in nude mice. H&E staining reveals a small region of bony tissue (b) in PαS⁺CD90⁺ derived implants. Insets show the undifferentiated control implants (c). Safranin-O stained histological sections were also counterstained by acid fast green to stain non-cartilaginous sites in the scaffold. Scale bar =200µm. (n =2 independent implants for each cell-type).

6.4.2 Perinatal PαS cells and their PαS⁺CD90⁺ and PαS⁺CD90⁻ subpopulations maintain SOX9 expression to a different extent

SOX9 positive cells were observed in the implants in which cells were differentiated into cartilage in vitro prior to implantation (Fig. 29B, D and F),

while only few scattered cells were detected in control implants that were kept undifferentiated in culture (Fig. 29A, C and E). In implants derived from PαS and PαS$^+$CD90$^+$ cells, SOX9 positive cells were detected predominantly in regions that appear to have remained as cartilage as judged by histological assessment, i.e. have not undergone remodeling into bony tissues (Fig. 29B2, D2). In cartilage implants derived from PαS$^+$CD90$^-$ cells, SOX9 positive cells are detected even more (Fig. 29F1, F2). The striking difference between these results and the SOX9 expression analysis at postnatal day P2 is that many more SOX9-positive cells are detected in implants derived from PαS$^+$CD90$^-$, but also PαS and PαS$^+$CD90$^-$ cells, at E18.5 than at P2. Hence, implants derived from PαS cells and mainly the PαS$^+$CD90$^-$ subpopulation preserves more cartilage-like features after 8 weeks if the cells are isolated just prior to birth (E18.5) rather than shortly after birth (P2). However, immunofluorescence analysis did not detect two typical marker proteins for chondrocytes, namely COL-II and Aggrecan in implants after 8 weeks in nude mice (data not shown).
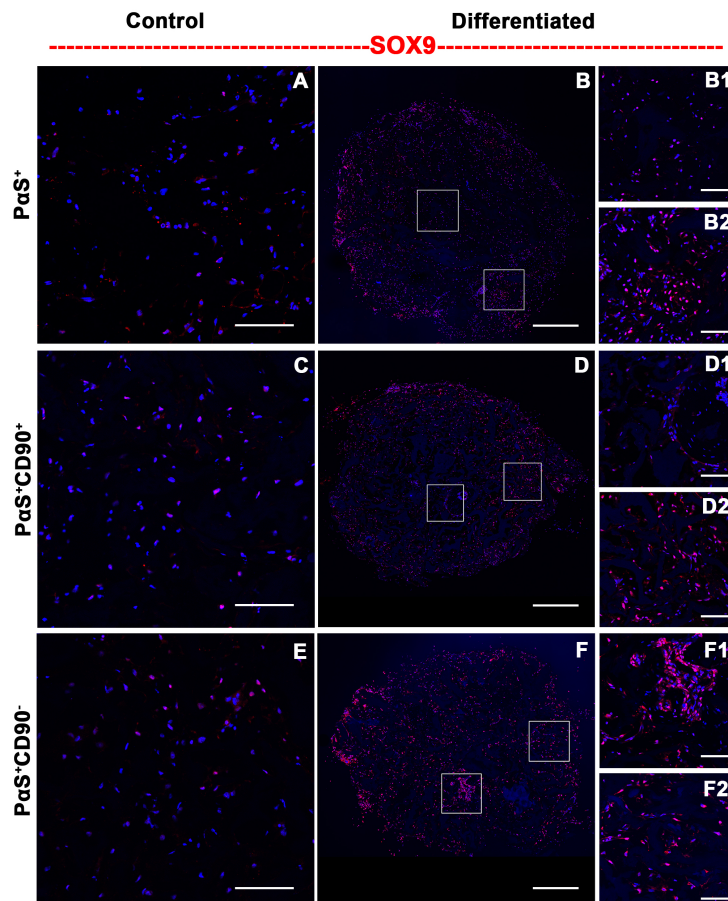
Fig. 29. Perinatal (E18.5) PαS cells maintain SOX9 expression after 8 weeks of implantation of cartilage templates into nude mice. (**A, C, E**) Undifferentiated control implants. (**B, D, F**) Immunofluorescence to detect SOX9-positive cells (red). The enlarged insets show the presence or absence of SOX9-positive cells (B1 and B2 in PαS cells; D1 and D2 in the PαS$^+$CD90$^+$ subpopulation; F1 and F2 in the PαS$^+$CD90$^-$ subpopulation). Nuclei are detected by Hoechst (blue). Scale bar in left panels = 100µm. Scale bar in middle panels = 500µm. Scale bar in right panels = 50µm (n≥ 3 independent experiments).

Further molecular analysis reveals that the small bone ossicles that form in implants derived from perinatal PαS$^+$CD90$^+$ cells are vascularized, contain bone marrow and sites of active hematopoiesis similar to the ossicles derived from cells isolated at postnatal day 2 (for details see Appendix VI and data not shown).

These results reveal differences in the differentiation potential of fetal (E18.5) and early postnatal (P2) PαS cells. The fractions of cells that continue to express SOX9 was much higher in embryonic than postnatal MSCs. SOX9 expressing cells were observed in all implants derived from embryonic PαS, PαS$^+$CD90$^+$ and PαS$^+$CD90$^-$ cells. The PαS and PαS$^+$CD90$^+$ cells have the ability to undergo remodeling and form bone by endochondral ossification. Importantly, the ontogenic analysis shows that PαS$^+$CD90$^-$ cells arise during embryonic development and the emergence of PαS$^+$CD90$^+$ cells coincides with the appearance of fetal bone around ~E14.0-14.5 in mouse embryos (Coskun et al., 2014). Despite the fact that PαS$^+$CD90$^-$ cells are most potent with respect to tri-lineage differentiation in culture, the in vivo analysis suggest that the different PαS subpopulations may have distinct differentiation potentials with respect to endochondral ossification (highest in the PαS$^+$CD90$^+$ subpopulation), which is possibly influenced by the microenvironment these cells encounter in vivo.

7. Discussion

Attempts to identify and characterize "mesenchymal stem cells" have been progressing over the last year from both humans and mice, but the ultimate proof of the existence of true mesenchymal stem cells is still lacking. In contrast to HSCs, which are by now well-established stem cells, the positive identification of true mesenchymal stem cells has thus far had several limitations. It has proved difficult to establish their stemness at the single cell level and their origin and niche in the living organism. That is why the term MSC is still used rather for mesenchymal stromal cells than mesenchymal stem cells. At the start of my PhD studies, I used classical approaches to isolate and expand mouse bone marrow stromal cells (MSCs) and in line with other investigators observed significant contamination of the preparation with hematopoietic cells. Several improved isolation approaches, which includes new markers have been recently developed to enrich MSCs from bone and the stromal compartment of bone marrow. But the main aim to use a single, homogeneous population of stem/progenitor cells, whose multi-lineage potential could be exploited to generate the desired tissues for regenerative tissue engineering has not been achieved. For my PhD research, I used the PαS cells that were previously identified as a rare MSC-like population in mouse bone fractions (Morikawa et al., 2009; Houlihan et al., 2012). PαS cells were used as candidate MSC population as based on the in vitro analysis they best fitted the criteria used to define MSCs.

7.1 PαS cells are a heterogeneous population

The previous studies identified adult mouse PαS cells from long bones using various surface markers (Morikawa et al., 2009; Houlihan et al., 2012). One of the potential problems of working with mouse PαS cells is that the Sca1 marker cannot be used to identify the human counterparts (Holmes and Stanford, 2007). Sca1 is a mouse glycosyl phosphatidylinositol-anchored cell surface protein (GPI-AP) belonging to the Lymphocyte antigen 6 (Ly6) gene family. A 500kb region of the *Ly6* locus was deleted in humans in comparison to the orthologous locus in rodents. Notably, the genes flanking the deleted

region are conserved between rodents and humans (Holmes and Stanford 2007). Several human homologs of the *Ly6* family do exist, which are closely related to the orthologous locus on mouse chromosome 8 (reviewed by Bamezai, 1995; Kamiura et al., 1992), but none of these genes are orthologous to the rodent Sca1 gene. As the human orthologue of Sca1 has not been identified, we considered it important to better define the CD-marker signature of mouse PαS cells with the ultimate goal to compare this signature with the potentially homologous hMSCs. Both CD51 and PDGFRβ are co-expressed by the vast majority (≥90%) of all PαS cells, which means that these markers for human MSCs can be used interchangeably for prospective isolation of MSCs. CD90 and CD73, which are expressed by human MSCs (Dominici et al., 2006), are expressed differentially by mouse PαS cells resulting in identification of four distinct subpopulations of PαS cells. This finding is corroborated by the fact that PαS cells isolated from long bones consist of heterogeneous mesenchymal stem and/or progenitor cells. We also evidenced additional PαS subpopulations based on the expression analysis of other CD markers. CD44, in combination with CD90 also defines four PαS subpopulation. However, we predominantly used the CD90 and CD73 markers to further characterize the PαS cells as CD73 correlates with chondrogenic lineage development in studies of human MSCs (Arufe et al., 2010; Campbell and Pei, 2012; Ode et al., 2013). Furthermore, CD146 is expressed by a very small fraction of PαS cells, which underscores the differences of these cells from self-renewing osteoprogenitors in the human bone marrow (Sacchetti et al., 2007). We also show that the vast majority of PαS cells do not express CD200 (only ~1% co-expressing cells), which was recently used to identify a skeletal stem cell population (Chan et al., 2015). These data also indicate that the PαS and CD200 populations have distinct developmental origins. Interestingly, PαS cells up-regulate CD105 during early passages in culture. This marker has been used to isolate human and also mouse MSCs and CD105 expression has been correlated with increased osteogenic potential (Chan et al., 2009). In addition CD105 is implicated in angiogenesis (Li et al., 1999; Duff et al., 2003) by mediating the chemokine response in endothelial cells and stimulating their migration (Young et al., 2012). The involvement of CD105 in angiogenesis is in agreement with the

increased osteogenic potential of mouse MSCs expressing this marker. In particular, PαS cells are able to undergo osteogenic differentiation only during early passages in culture, when CD105 expression is upregulated in most cells. However, it is important to mention that the observed difference in CD signature could be a consequence of the mechanical stress during isolation and/or due to removing the PαS cells from their in vivo niche, which could result in phenotypic variations within the isolated PαS cell population. Nonetheless, these phenotypic differences underscore the complexity of PαS cells and MSCs in mice and humans that may reflect differences in their cell fates and/or differentiation status. Indeed, the changes in the CD signature of PαS cells observed during prolonged culture also affect their multi-lineage differentiation potential. The chondrogenic and osteogenic differentiation potential is reduced upon prolonged culture, while the adipogenic differentiation persisted in these cells. These observations are consistent with previously published results (Mabuchi et al., 2013) and corroborate the notion that MSCs in serum-based cultures commit to specific lineage(s). The increased adipogenic potential at higher passages correlates with the fact that during aging MSCs contribute progressively more to adipogenesis in the bone marrow (Zhou et al., 2014). Moreover, my analysis showed that the PαS$^+$CD90$^-$CD73$^-$ subpopulation (q3), which is the rarest and possibly most immature of the four subpopulations, disappears first when PαS cells are expanded in culture. Either the q3 subpopulation gets eliminated by cell death or, if these cells would represent the most immature and stem cell like cells, they could give rise to more differentiated cells in culture (thereby contributing e.g. to the other 3 subpopulations as q1: PαS$^+$CD90$^+$CD73$^-$, q2: PαS$^+$CD90$^+$CD73$^+$ or q4: PαS$^+$CD90$^-$CD73$^+$). BrdU incorporation showed that q3 subpopulation proliferates most in culture, which indicates that these cells survive and expand rapidly (see Appendix I). This rapid proliferation at the expense of 'stemness' in culture could explain the observed changes with respect to the tri-lineage differentiation potential. Currently, we attempt to establish culture conditions that will allow more long-term expansion of PαS cells without them undergoing lineage commitment using different combinations of signaling molecules known to maintain progenitor/stem cells in a proliferative and undifferentiated state.

7.2 PαS cells arise around embryonic day E11.5 and increase in numbers during perinatal development

The loss of multi-lineage potential of PαS cells during late passages precluded their expansion in culture for more than a few days. Besides, in adult mice, PαS cells are rather a rare population in long bones, which poses another bottleneck in scaling of experiments. This observation, together with the aim to identify the time point when PαS cells arise during embryonic/fetal development prompted an ontogenic analysis. Using the Sox9-*GFP* reporter line, we were able to show that PαS cells arise in parallel to specification of the Sox9-positive osteo-chondroprogenitors (OCPs) in mouse limb buds. The analysis revealed PαS cells in limb buds at E11.5, which coincides with the onset of digit condensation and chondrogenic differentiation in the distal limb bud mesenchyme (reviewed by Zeller et al. 2009). At this stage the fraction of PαS cells is very low and about half of them also express Sox9 indicating that this PαS subpopulation is likely specified as OCPs. These results indicate that PαS cells contribute to embryonic limb bud development. Interestingly, these early PαS cells neither express CD90 nor CD73, i.e. likely correspond to the rare q3 subpopulation detected in adult long bones. This supports the hypothesis that the q3 subpopulation is first and likely most immature of the PαS subpopulations. CD90 is activated only at later stages, as PαS$^+$CD90$^+$ cells are identified only at embryonic day E14.5, which coincides with mineralization of the extracellular matrix (ECM) by osteoblastic cells (Mizoguchi et al., 2014). Therefore, the PαS$^+$CD90$^+$ subpopulation (~25% of all PαS cells) may be functionally required for osteogenesis during skeletal development as has been proposed by previous studies in MSCs (Chung et al., 2013, Yamamoto et al., 2014). Unexpectedly, PαS cells are becoming much more abundant by E18.5 and their numbers increased until postnatal day P2. It is important to note that the migration of HSCs/HPCs from fetal liver to bone marrow starts at E18.5, which results in establishment of the stem cell niche in the bone marrow. Several studies provide evidence for an interaction of MSCs and HSCs/HPCs in formation of the stem cell niche in the bone marrow (Chan et al., 2009; Mendez-Ferrer et al., 2010; Greenbaum et al.,

2013). The increase in PαS cells may provide a suitable microenvironment for HSCs/HPCs during the niche formation in the fetal bone. Of note, the above studies also highlighted that the interactions of stromal populations/MSCs with hematopoietic progenitors helps to retain the HSCs/HPCs in the bone marrow niche. These activities are most prominent during endochondral ossification as vascularization and the development of sinusoids in the marrow progresses.

As fetal development progresses, osteogenesis becomes dominant over chondrogenesis in limbs. Interestingly, comparative ontogenic analysis of PαS cells at E18.5 and P2 revealed an increase in the fraction of PαS$^+$CD90$^+$ cells. Taken together, these observations suggest that the two subsets of PαS cells might have been assigned different fates, whereby the PαS$^+$CD90$^+$ cells could contribute to osteogenesis, while the PαS$^+$CD90$^-$ cells retain chondrogenic potential. Other skeletal progenitors have also been shown to contribute either to chondrogenic or to osteogenic lineages (Chan et al., 2009; Park et al., 2012; Mizoguchi et al., 2014). Two weeks after birth, a striking drop in the number of PαS cells isolated from long bones bone is observed. This decrease in PαS cells is paralleled by an increase of the PαS$^+$CD90$^+$ subpopulation up to ~75% of total PαS cells. This continuous increase in PαS$^+$CD90$^+$ subpopulation may correlate to the fact that bone growth and ossification increases and dominates over chondrogenesis in development.

These studies point to the importance of studying the fates of the different PαS subpopulations in situ during embryonic and fetal long bone development in more detail. However, Sca1 not only marks PαS cells but also HSCs and endothelial cells in the bone marrow (Luna et al., 2004; Bradfute et al., 2005), which precluded a single cell analysis by immunofluorescence to identify PαS cells in their bone marrow niche. Therefore, fate-mapping studies using more sophisticated approaches are needed to provide insights into the locations and possible functions of the PαS cells during cartilage and bone development.

7.3 Tri-lineage differentiation potential of the four PαS subpopulations

The "MSC characteristics" were inherent in all subpopulations of PαS cells from postnatal P2 mice. However, the trilineage differentiation could be induced much more efficiently in the q3 and q4 subpopulations (PαS$^+$CD90$^-$ subset), compared to q1 and q2 subpopulations (PαS$^+$CD90$^+$ subset), which may correlate to higher stemness potential in this subset. Interestingly, induction of osteogenic differentiation in P2 PαS subpopulations was possible only after adding BMP4 to the osteogenic cocktail, as against adult PαS cells that do not require BMPs for osteogenic differential, was striking. BMPs are important mediators of osteogenesis during skeletal development. In vitro and genetic analysis has revealed the distinct functions of BMP ligands BMP2, BMP4 and BMP7 (Bandyopadhyay et al., 2006). In this study, it was shown that absence of BMP2 and BMP4 causes severe limb deformation due to impairment in the development of bony tissue. Thus, need of BMPs to trigger in vitro osteogenic differentiation in P2 PαS subpopulations is in agreement with its distinct role in regulating osteogenesis. BMPs and their receptors are known to be already expressed in early embryonic stages and regulate digit condensation. During mouse limb bud development, antagonists of BMP signaling, such as Gremlin 1 and Noggin modulate BMP activity in spatio-temporally controlled manner (Merino et al., 1999; Nifuji and Noda, 1999; Zuniga; et al., 1999; Ohyama et al., 2001; Wijgerde et al., 2005). In addition, it has been shown that TGFβs are secreted by the pre-chondrogenic mesenchyme and seem to determine the chondrogenic fates of mesenchymal cells during mouse limb bud development, (Lorda-Diez et al. 2009; Karamboulas et al., 2010). TGFβs and BMPs are both required for inducing chondrogenic differentiation of MSCs. I was able to show that this process is more efficient if adult PαS cells are first primed with TGFβs and subsequently treated with BMPs to differentiate into chondrocytes. In fact, time-course analysis of chondrogenic differentiation of adult PαS cells showed an early commitment to the osteo-chondrogenic lineage by upregulation of *Sox9* expression, followed by robust differentiation into chondrocytes as revealed by sustained upregulation of *Col2a1* expression. On the other hand, a

simultaneous exposure of PαS cells to both TGFβs and BMPs had an opposing effect as observed in previous studies (Karamboulas et al., 2010). PαS cells treated sequentially with TGFβs and BMPs generated stable cartilage that did not undergo hypertrophy, which highlights the effectiveness of PαS cells to generate cartilage in contrast to the MSC populations used in other studies (Tian et al., 2007; Hui et al., 2008; Kim and Im, 2009). I was able to show that the q3/q4 PαS subpopulation display the best chondrogenic potential both in 2D and 3D culture systems and also produce significantly more ECM than the q1 and q2 subpopulations. Together with tri-lineage differentiation analysis, these results showed that the PαS$^+$CD90$^-$ subpopulation (q3/q4) has a better multi-lineage differentiation potential than the PαS$^+$CD90$^+$ subpopulation (q1/q2).

7.4 Differential bone remodeling potential of PαS subpopulations

My analysis showed that the cartilage templates derived from PαS and PαS$^+$CD90$^+$ but not PαS$^+$CD90$^-$ cells are efficiently remodeled into bone. This highlights the differences in the in vivo differentiation potential of these two main subpopulations of PαS cells. The efficient remodeling of these cartilage templates into bone suggest that the factors required to form hypertrophic cartilage and bone could be provided by blood vessels at the ectopic site during the process of vascularization, as no hypertrophic chondrocytes were seen by in vitro differentiation. Further analysis shows that remodeling had occurred to varying extents in all implants, but the PαS$^+$CD90$^-$ subpopulation retained its "cartilage-like" phenotype or a pre-chondrogenic status to a much larger extent than PαS and PαS$^+$CD90$^+$ cells. These results also suggested that while PαS$^+$CD90$^-$ subset may have the capability to generate more stable cartilage in vivo, possibly due to the fact that the cells are not receptive to paracrine signals that induce angiogenesis and endochondral ossification, which results in maintenance of cartilage-like features following implantation. Recently, antagonizing VEGF signaling has been shown to significantly promote cartilage tissue generation in vivo from skeletal stem cells in mice (mSSCs; Chan et al., 2015). In contrast, implantation of mSSCs without blocking the VEGF pathway resulted in differentiation towards the

endochondral route. In another study, a subpopulation of Flk⁻PDGFRα⁺ mouse ESCs was used to generate chondrogenic mesoderm (Craft et al., 2013). Upon exposure of these cells to BMP and FGFs resulted in formation of hypertrophic chondrocytes. In contrast, exposure to GDF5 in combination with blocking the Hedgehog and BMP signaling pathways resulted in chondrocytes with features of articular cartilage (Craft et al., 2013). In addition, human ES and pluripotent cells (hESC and hPCs) have been differentiated into to stable cartilage, by exposing them first to BMP4 and FGFs together with other factors and subsequently to TGFβ3 in a temporally controlled manner (Craft et al., 2015). Hence, similar pathways might be required to induce chondrogenic differentiation of both ESCs and MSCs, which suggest that they might also play a role in determining PαS cells to generate stable cartilage.

7.5 PαS and PαS⁺CD90⁺ cartilage implants promote host-derived hematopoiesis during bone marrow formation

Angiogenesis, which is initiated with formation of the pre-hypertrophic cartilage, also results in recruitment of hematopoietic cells to the forming bone marrow together with several mesenchymal stromal populations. During endochondral ossification, the hypertrophic chondrocytes produce extracellular matrix and secrete angiogenic molecules like VEGF and transferrin, which stimulate endothelial cell migration towards the hypertrophic cartilage (Gerber et al. 1999; Carlevaro et al., 2000). Osteoclasts eliminate the apoptotic hypertrophic chondrocytes and the void is filled by osteoblasts. In mouse, fate-mapping studies have shown that bone marrow development involves complex interactions among several stromal cell populations such as Nestin-, CAR-, LepR-, and Cxcl12- positive cells (Mendez-Ferrer et al., 2010; Greenbaum et al., 2013; Zhou et al., 2014). In addition, different cells committed to osteogenic lineage such as Mx1- and Osterix- positive cells and *Gremlin1*-expressing osteochondroreticular (OCR) stem cells contribute to osteoblast formation during endochondral ossification (Park et al., 2012; Mizoguchi et al., 2014; Worthley et al., 2015). These cells in the bone marrow stroma express HSC maintenance factors and function in the stem cell niche

that regulates and maintains HSCs in the bone marrow. Indeed, the process of endochondral ossification has been linked to development of the hematopoietic stem cell niche (Chan et al., 2009).

As Osterix-positive osteoblasts are detected in the remodeled bone tissue formed by PαS and PαS$^+$CD90$^+$ derived cartilage implants, they should function to attract endothelial cells in order to continue towards endochondral route (my results and Fujita et al., 2010). Indeed, I was able to show that CD31-positive endothelial cells expressing CD31 are present in the bone ossicle, which indicates that vascular invasion had occurred. By genetic marking with DsRed, I was able to show that the endothelial cells are host-derived, but this only occurred in the cartilage implants that underwent significant remodeling of cartilage into bone.

Another important step during hematopoiesis in the developing bone marrow is the migration and differentiation of common myeloid progenitors (CMP) and common lymphoid progenitors (CLP) due to lineage-specific differentiation of HSCs. Host-derived macrophages, which represent one of the differentiated cell-types derived form CMPs, were abundantly detected in the remodeled bone formed by PαS$^+$CD90$^+$ derived cartilage templates. Moreover, the presence of host-derived B-cells and precursors confirmed the establishment of lymphoid lineages within the remodeled bone. As no such host-derived cells were detected in the poorly or not remodeled cartilage templates derived from PαS$^+$CD90$^-$ cells, one can conclude that development of a proper hematopoietic environment depends on the PαS$^+$CD90$^+$ subpopulation. A recent study has shown that conditional deletion of osteoprogenitors results in reduced numbers of B-lymphoid progenitors (Greenbaum et al., 2013), which may explain their absence from PαS$^+$CD90$^-$ derived implants that mostly lack osteoblasts. Most importantly, my studies show that PαS$^+$CD90$^+$ derived implants provide an environment supportive of initiating HSCs/HPCs niche formation during endochondral ossification. In fact, I was able to detect few CD45$^+$Sca1$^+$ double positive cells, which represent rare hematopoietic progenitor cells (HPCs) within bony ossicles formed by PαS and PαS$^+$CD90$^+$ derived implants. As expected, these hematopoietic progenitors are also host-

derived, which confirms that the fully functional hematopoiesis is entirely host-derived. Hematopoiesis is a continuous process during bone development and maintenance of hematopoietic cells as a consequence of reconstituting a hematopoietic microenvironment by stromal populations within an ossicle model has been shown before (Song et al., 2010), but it has not been shown that this can be achieved by the PαS⁺CD90⁺ subpopulation of PαS cells.

Taken together, these findings also suggested striking differences between the in vitro and in vivo functions of PαS cells and their subpopulations. While "stem" like features in terms of multipotency are more prominent in the PαS⁺CD90⁻ subpopulation during in vitro differentiation, the remodeling by endochondral ossification that is supportive for host-derived hematopoiesis is a dominant feature of the cartilage implants derived from PαS⁺CD90⁺ cells in vivo. Such differences in the in vitro and in vivo properties of MSCs have been observed before and my results indicate that the complex in vivo roles of MSCs may be mediated by specific subpopulations. Moreover, these subpopulations may interact in a differential functional manner with hematopoietic cells and other stromal components. Furthermore, the PαS⁺CD90⁺ derived cartilage template, which remodels efficiently into bone and attract host-derived hematopoiesis, correlates well with the previously observed role of CD90 in enhancing osteogenesis (Chung et al., 2013; Yamamoto et al., 2014). In agreement, PαS⁺CD90⁺ cells emerge later than PαS⁺CD90⁻ cells during mouse embryonic limb buds development. The fact that PαS⁺CD90⁻ cells are already present at stages during which cartilage formation is pre-dominant may explain why these cells retain their cartilage-like phenotypes better upon engraftment in vivo than PαS⁺CD90⁺ cells, which remodel efficiently. Hence, correlating the ontogenic appearance of these different cell populations with their phenotype following engraftment of cartilage templates appears to provide insights into their normal roles during endochondral ossification and in attracting endothelial and hematopoietic stem cells.

In addition, cartilage templates derived from E18.5 PαS cells, i.e. isolated from mouse fetuses prior to birth has less potential to undergo endochondral

ossification. Consistent with the observation in the cells from P2 mice, the prenatal PαS$^+$CD90$^-$ subset appeared to play major role in chondrogenesis, while the fate choice of PαS$^+$CD90$^+$ subset towards endochondral route could have just been started in prenatal stages.

7.6. Scheme describing the origin of the PαS subpopulations and their potential different fates during limb skeletal development

The results I have obtained during my PhD research can be summarized in a scheme that shows development of PαS cells, emergence of the most relevant subpopulations and their eventual fates during endochondral ossification (Fig. 30A). PαS cells arise from the pool of Sox9$^-$ and Sox9$^+$ limb bud mesenchymal progenitors around embryonic day E11.0. PαS cells express CD73 early in development, followed by the activation of CD90 expression in a fraction of them, which allows discrimination of two major subpopulations at the time the endochondral ossification of the limb skeletal bones advances (~E14.5: PαS$^+$CD90$^+$ make up ~25% and PαS$^+$CD90$^-$ cells ~75% of all PαS cells). Following the transition from embryonic to fetal development in mice at ~E14.5, HSCs begin to migrate from the fetal liver to the developing bone marrow and hematopoiesis is initiated. Together with angiogenesis, these events may influence the in vivo choices of PαS cells, which coincide with a significant burst in proliferation of both subpopulations that are most abundant just at the time of birth. While endochondral ossification leads to extensive hematopoiesis, late fetal, i.e. perinatal development is also influenced by changes in hormonal regulation, which may also affect the differentiation potential of PαS cells, in particular their osteogenic and chondrogenic differentiation potential. After birth, osteogenesis becomes dominant over chondrogenesis and we observe a significant drop in numbers of PαS cells, while the PαS$^+$CD90$^+$ subpopulation becomes predominant (making up ~75% of all PαS cells).
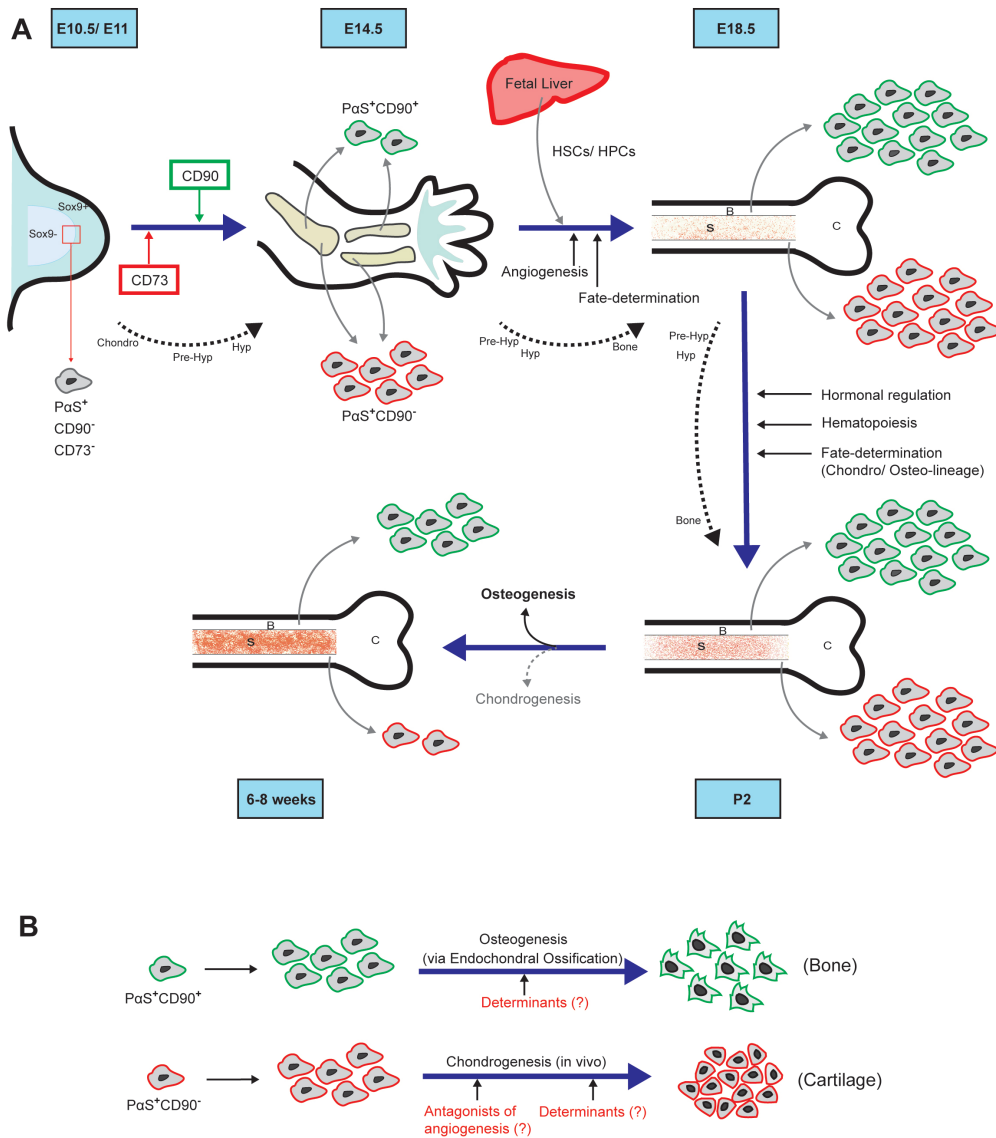
Fig. 30. Scheme showing the ontogenic development of PαS cells and possible regulators of the two main subpopulations during endochondral ossification.

(A) Mouse limb bud at ~E10.5-E11.0. PαS$^+$CD73$^-$CD90$^-$ cells are first detected. CD73 is activated prior to CD90. Chondrogenesis (Chondro) lead to pre-hypertrophic (Pre-Hyp) and hypertrophic (Hyp) stages. By E14.5, the PαS$^+$CD90$^+$ and PαS$^+$CD90$^-$ subpopulations are present in the developing fetal bones. Pre-hypertrophic and hypertrophic stages lead to bone (B) formation concurrent with migration of HSCs/HPCs from the fetal liver to the developing bone marrow stroma (S). Cartilage (C) remains in the epiphyseal region of the developing long bones. From ~E18.5 to P2, PαS cells are abundant and bone formation is regulated by hormonal changes during birth. Osteogenesis (bold) is pre-dominant over chondrogenesis (grey) from early postnatal to adult stages, which is paralleled by a significant drop in PαS cells (with PαS$^+$CD90$^+$ cells being the most prominent subpopulation). **(B)** Scheme shows the mechanism by which PαS$^+$CD90$^+$ cells initiate endochondral ossification under the influence of unknown determinants (in red). PαS$^+$CD90$^-$ cells rather retain cartilage-like features, which may depend on antagonists of angiogenesis and other unknown determinants.

Thus, identifying and studying the morpho-regulatory signals and determinants is a key step to understand the in vivo specification and functions of the different PαS subpopulations. Treating mice with specific angiogenic antagonists, for example, could be an interesting approach to study the specific differentiation and functions of PαS$^+$CD90$^-$ cells (Fig. 30B). Several studies that have shown the interactions between HSCs and MSCs, including the stromal cells in bone marrow and osteoprogenitors regulate the activity of the stem cell niche (Mendez-Ferrer et al., 2010; Greenbaum et al., 2013; Mizoguchi et al., 2014). Therefore it will be important to explore if these interactions also regulate the fate choices of PαS cells. Besides, hormonal regulation of fate determination and functions of MSCs at the time of birth cannot be ruled out. Estrogen (E2), for example, regulates the cell cycle activity of HSCs in the developing bone marrow (Nakada et al., 2014; reviewed by Heo et al., 2015). In summary, while my study has identified the developmental profile, in vitro multi-lineage and in vivo endochondral differentiation potential of the different PαS subpopulations, it need to be determined which molecular signals and hormone receptors regulate the fate choice of the different PαS subpopulations and their potential usefulness as a developmental paradigm for cartilage and bone engineering.

8. Conclusions and Outlook

The major aims of this thesis were to characterize the mouse PαS cells as MSC cells for models of chondrogenic differentiation in vitro by mimicking the molecular signals that are active in vivo. Moreover, in vivo functionality of the cartilage templates generated from PαS cells and its subsets were assessed. My study also contributes to a better understanding of developmental origin of mouse MSCs, in particular the four newly identified PαS subpopulations. Ontogenic analysis of limb bud mesenchymal cells and developing long bones revealed the sequential emergence of the two main subsets of PαS cells (PαS$^+$CD90$^+$ and PαS$^+$CD90$^-$ cells) and provided evidence for their distinct chondrogenic and osteogenic differentiation potential during progression of limb skeletal development. Using flow cytometry, molecular analysis and immunohistochemistry based approaches allowed me to determine the tri-lineage potential of the different PαS subpopulations in culture. This showed that the in vitro tri-lineage differentiation potential of PαS$^+$CD90$^-$CD73$^-$ and PαS$^+$CD90$^-$CD73$^+$ subpopulations is much higher in comparison to the PαS$^+$CD90$^+$CD73$^-$ and PαS$^+$CD90$^+$CD73$^+$ subpopulations. By mimicking the molecular pathways that control chondrogenesis in vivo, it was possible to generate robust cartilage template in an efficient manner in vitro.

Engraftment of cartilage templates into nude mice revealed striking differences between bone-forming potential of the two main PαS subpopulations. PαS$^+$CD90$^+$ cell derived cartilage implants display features resembling growth plate-like cartilage and are able to remodel into bone undergoing endochondral ossification. Interestingly, the resulting bone ossicles are vascularized and their sites of active hematopoiesis are both a consequence of recruiting host-derived endothelial and hematopoietic stem/progenitor cells. In contrast, cartilage implants derived from PαS$^+$CD90$^-$ cells are only partially remodeled, fails to initiate endochondral ossification process and hematopoiesis; and the majority of cells in the implant continue to express the Sox9 transcription factor, normally marking osteo-chondrogenic progenitors and early chondrocytes.

These differences were even exaggerated upon implantation of cartilage templates derived from PαS cells from prenatal stage. These observations support the hypothesis that was suggested by my ontogenic studies, namely that the differentiation potential of implants derived from PαS cells likely mimic their normal in vivo potential, which changes during progression of limb bud and skeletal bone development. Therefore, it would be most interesting and telling to use genetic fate-mapping approaches to track PαS cells in vivo during development and combine this approach with manipulation of the pathways that control angiogenesis to see if the PαS cells and/or specific subpopulations can generate stable cartilage in vivo.

9. Materials and Methods

9.1 Mice husbandry and animal experimentation

9.1.1 Ethics statement

All experiments with mice were performed in strict accordance with Swiss law, the 3R principles and the Basel Declaration. It includes licensing for animal experimentation through completion of the LTK-1 course and fulfillment of the yearly continuing animal education courses. The severity of experiments with mice is classified as grade 0 (implying minimal suffering) for most experiments with exception of the engraftment in nude mice (grade 2).

9.1.2 Mouse strains

For this study, the following mouse strains were used:

C57BL/6 (wild type), NMRI (wild type), Sox9-*GFP* reporter strain (Chan et al. 2011), CMV-Cre transgenic strain (Schwenk et al., 1995), β-Actin-GFP transgenic strain (Okabe et al., 1997), CD-1 nude mice (Charles River Laboratories). All mouse strains were bred in the in-house mice facility and the last phalange were cut within the first 10 days postnatally to genotype and mark the mice. CD-1 nude mice were kept at the Department of Research at Universitätspital Basel and the engraftments were done by the group of Prof. Ivan Martin.

9.2 Cell preparation and culture

Cells were grown in their respective media at 37^0C and with 5% CO_2, under normal oxygen and humidity conditions in sterile tissue culture incubators.

Cell preparation buffer

DPBS: Dulbecco's Phosphate Buffered-saline, pH 7.4 (Gibco #14190-94)
HBSS: Hank's balanced salt solution (Gibco #14175-053)

HBSS$^+$: 2% FBS Hyclone (Thermo fisher Scientific #1030-9433), 10 mM HEPES (Gibco #15630-056) and Penicillin-streptomycin (1000 units, Gibco #15070063) were added to HBSS.

Cell culture media compositions

DMEM: Dulbecco's Modified Eagle's Medium (high glucose 4.5g/l, Gibco #41966-029).

DMEM$^+$: 10% FBS (Hyclone), 10mM Glutamax and Penicillin-streptomycin (1000 units) were added to the DMEM

DMEM/F-12: Advanced Dulbecco's Modified Eagle's Medium pre-mixed 1:1 with F-12 medium (high glucose- 4.5g/l, Gibco #21331-020).

DMEM/F-12$^+$: 10% FBS (Hyclone), 10mM Glutamax and Penicillin-streptomycin (1000 units) were added to the DMEM/F-12.

α-MEM: alpha-Minimum Essential Medium (Gibco #22561-021),

α-MEM$^+$: 10% FBS (Hyclone), 10mM Glutamax and Penicillin-streptomycin (1000 units) were added to the α-MEM medium.

Cell freezing medium: 50% α-MEM$^+$, 40% FBS (Hyclone), 10% Dimethyl Sulfoxide/DMSO (Sigma #D8418)

Chondrogenic medium (per ml):

Opti-MEM (Gibco #51985-026), 10µl ITS$^+$ premix (contains human recombinant insulin 0.6mg/ml, human transferrin 0.6mg/ml, selenous acid 0.6µg/ml, BSA 125mg/ml, linoleic acid 0.5mg/ml, BD #7341315), 10^{-6}M Dexamethasone (Sigma #D4902), 100µM Sodium L-Ascorbate (Sigma #A4034).

Osteogenic medium cocktail (per ml)

1. DMEM$^+$, 1mg/ml β-Glycerophosphate (Calbiochem #35675), 10^{-7}M Dexamethasone and 100µM L-Ascorbate, 1mM Sodium Pyruvate (Sigma #S8636).

2. Pre-prepared osteogenic medium premix: Lonza Kit # PT-3002

Adipogenic medium cocktail (per ml)

1. For adult MSCs:

Induction medium: DMEM$^+$, 1mM Sodium Pyruvate, 100µM Indomethacin (Sigma #I7378), 500µM IBMX (3-isobutyl-1-methylxanthine, Sigma #I5879), 10µg/ml Insulin (Actrapid) 10^{-6}M Dexamethasone and 100µM L-Ascorbate.

Maintenance medium: DMEM$^+$, 1mM Sodium Pyruvate 10µg/ml Insulin (Actrapid) 10^{-6}M Dexamethasone and 100µM L-Ascorbate.

2. For P2 MSCs:

Induction medium: DMEM$^+$, 50ng/ml bone morphogenetic protein-2 (BMP2, Sigma #B355).

Maintenance medium: 2µM Rosiglitazone (71740 Cayman), 1µM Dexamethasone (Sigma #D4902), 5µg/ml Insulin (Sigma #I9278) and 50ng/ml BMP2 along with DMSO control.

9.2.1 Isolation of MSC populations from compact long bones

Method adapted from previously published protocol (Houlihan et al., 2012). Long limb bones (tibias and femurs) from 4-8 weeks old mice were harvested and freed from adherent muscle tissues using scalpel and dissection scissors. To flush the bone marrow, the epiphysis of bones were cut and long bones were spun down at 13,000 rpm (Heraeus Biofuge pico) for 1 minute in a punctured 500µl eppendorf tube that is placed in a 1.5 ml eppendorf tube. Bones were then washed three times with ice-cold PBS, crushed and cut into small pieces in a sterile mortar and pestle that contained HBSS$^+$. A fine, paste-like bone mass was prepared using sterile scalpels, replacing the HBSS$^+$ at intervals to get rid of remnant bone marrow and adherent connective tissues. Long bones from 4-5 adult mice were pooled and digested using 2mg/ml (0.19 U/mg) collagenase D (Roche #110882001) in a total of 20ml of DMEM high glucose medium (pre-warmed to 37^0C) in a 50ml falcon tube incubated for 1 hour at 37^0C on a shaker at 1100 rpm. After incubation, an equal amount of cold α-MEM$^+$ was added to stop the collagenase activity.

The cell suspension was filtered through 70µm cell strainer (Falcon #352350) into a 50ml Falcon tube kept on ice or at 4^0C from now on. The digested bones were collected again in the sterile mortar in 5ml HBSS$^+$, tapped gently using the pestle for ~50 times to homogenize and release the cells from the bone. This homogenization step was repeated 6 times to harvest the maximum amount of cells. Each time the cell suspension was collected and filtered through 70µm cell strainer in the 50ml Falcon tube on ice. Finally, the cell suspension was spun in a centrifuge (pre-cooled to 4^0C) at 1300 rpm for 10 minutes. The supernatant was aspirated and cell pellets were re-suspended by gentle tapping until they were fully dispersed. Red blood cells were lysed by adding 1ml of ice-cold sterile H_2O for 6 seconds, followed immediately by addition of 1ml 2x PBS containing 4% FBS and an excess of HBSS$^+$. The cell suspension was again filtered through a 70µm sterile cell strainer. After recentrifugation, the supernatant was aspirated and cell pellets re-suspended in 1-2 ml HBSS$^+$ and filtered through a 50µm sterile cell strainer (Partek CellTrics #04-0042-2317). The filtered cell suspension was stained with specific antibodies for flow cytometry-based analysis or sorting (see 9.2.3; 9.8.1).

For isolation of MSC populations from embryonic and early postnatal days, same protocol was used with the following few modifications:

Collagenase digestion step: The duration of incubation of cells with 2mg/ml collagenase D at 37^0C was modified as in Table 9.1:

Mice stage	Time (minutes)
E10.5 – E12.5	10
E13.0 – E14.5	15
E15.5 – E18.5	20
P1– P3	30

Table 9.1 Duration of collagenase digestion for various stages of mice.

The embryonic limb buds were gently pipetted (every 3-5 minutes) during the collagenase digestion until a single cell suspension was obtained.

<u>Red blood cell lysis</u>: For bones of embryonic and early postnatal day 2 (P2), the H_2O-lysis step was omitted and red blood cell were removed by extensive PBS/ HBSS$^+$ washing and re-centrifugation.

9.2.2 Isolation of embryonic limb bud cells from mice

Pregnant mice at specific day of gestation were euthanized in a CO_2 inhalation chamber (99.5% at 49.5 bar) and embryos collected in a petri dish filled with ice-cold PBS. Embryos were harvested quickly and the head was cut before dissecting limb bud using a Leica L2 stereomicroscope. Fore- and hindlimb buds were harvested into HBSS$^+$ using bent dissection forceps.

To prepare single cells, the limb buds were incubated in 2% trypsin/PBS at 4^0C for 25 minutes, followed by addition of excess serum (Hyclone FBS) to stop the trypsin activity. The limb bud ectoderm was removed using soft pipettes and a sharp dissection needle. The limb buds were transferred to a 15 ml falcon tube, containing cell culture medium (DMEM-F12) with 10% FBS Hyclone, 10mM Glutamax and Penicillin-streptomycin (1000 units) at 4^0C under the tissue culture hood and a single cell suspension was prepared by gentle pipetting. The mesenchymal cell suspension was centrifuged at 1200 rpm for 5 minutes, filtered using a 70µm cell strainer and re-suspended in cell culture media at e.g. 10^6 cells/ml for analysis or culture.

Cell suspensions to be processed for flow cytometer analysis or sorting were incubated in DMEM high glucose medium with 2mg/ml collagenase D at 37^0C for duration as mentioned in table 9.1. During the incubation time, limb buds were gently pipetted every 5 minutes until a single cell suspension was achieved. Ice-cold HBSS$^+$ was added to stop the collagenase activity, followed by centrifugation at 1200 rpm for 5 minutes. Cell pellet was resuspended in 1ml HBSS$^+$ and filtered through 50µm sterile cell strainer. Cells were then incubated with antibodies (Table 9.9.2) for flow cytometry analysis on a BD FACS Canto II (excitation lasers of 405nm: violet; 488nm: blue and 633nm: red wavelengths) or sorting on a BD FACS Aria III^{TM}

(excitation lasers of 405nm: violet; 488nm: blue; 561nm: yellow-green and 633nm: red wavelengths).

9.2.3 Cell sorting and seeding

Compensations (to avoid "spillover" of the fluorescent emission spectra of the different chromophores to other channels) were set up for the BD cell sorter and/or analyzer for each panel of antibodies using the BD FACSDiva™ 8.0 program (Table 8.9.2). Analysis of the cell populations of interest was done using the FlowJo vX.0.6 program. Fluorescent dyes, either 0.25µg/ml of 7-AAD (7-Aminoactinomycin D, Biolegend #420404) or 1µg/ml of DAPI (4',6-diamidino-2-Phenylindole, Sigma #D952) were added to electronically gate out dead cells from the analysis. Populations were defined by examining FSC-A vs SSC-A on a dot plot to identify and gate the singlet cells. Different cell populations were electronically gated and sorted directly into the appropriate cell culture medium. Cell re-analysis was always done and the sorting enrichment was always between 90-97%. Sorted cells were either plated into tissue culture dishes (Falcon) by seeding them at a density of ~5000 cells per cm^2 or processed for RNA isolation. The culture medium was replaced every day to every 3rd day of cell culture depending on the type of assay and cells.

9.3 Cell culture and storage

9.3.1 MSCs culture and freezing

Cell culture: Cells seeded at 5000 cells/ cm^2 were cultured in α-MEM$^+$ medium in tissue culture dishes (Falcon) at in 37^{0}C and 5% CO_2 in HeraCell 240 incubator. The culture media was changed every 72 hours. Upon reaching confluency, MSCs were split 1:3 as follows: cells were detached in 0.05% Trypsin EDTA (Gibco #25300054) for 90 seconds at 37 °C. The resulting single cell suspension was collected in 10ml pre-warmed α-MEM$^+$ medium in a 15ml Falcon tube and centrifuged at 1200 rpm for 5 minutes. Cell pellets were re-suspended in 1ml of α-MEM$^+$ medium and seeded in new tissue culture dishes accordingly. MSCs were kept in culture for up to 4 passages.

Cell freezing: Cells were detached in 0.05% Trypsin EDTA for 90 seconds at 37^0C. The resulting single cell suspension was collected in 10ml pre-warmed α-MEM$^+$ medium in a 15ml Falcon tube and centrifuged at 1200 rpm for 5 minutes. Supernatant was discarded and the tube was gently tapped at the bottom to loosen the pellet. To this, 1ml of cold (4^0C) cell freezing medium was added gently (up to 1×10^6 cells per ml) and the cell suspension was kept in cryo-tubes at -80^0C for short-term or -196^0C for long-term storage.

9.3.2 Limb bud mesenchymal cell culture

Single cell suspension of limb buds were prepared from appropriate embryonic stages (see before) and then centrifuged at 1200 rpm for 10 min in pre-warmed cell culture medium in a falcon tube. The supernatant medium was aspirated. Limb bud mesenchymal cell pellets were re-suspended in 1ml of cell culture medium and seeded in new tissue culture dishes at the density of $5 \times 10^5 - 8 \times 10^5$ cells/ cm^2. Limb bud mesenchymal cells were not passaged or freezed, i.e. always used fresh for analysis.

9.3.3 Colony forming unit fibroblastic (CFU-F) assays

Freshly sorted MSCs were plated at a density of 1000 cells per 10cm petri dish and grown in α-MEM$^+$ medium (37^0C, 5% CO_2). Media was changed every 72 hours and cells were cultured for 14 days. The fibroblast-like colonies that had formed were fixed with 4% PFA. Then the plates were washed with PBS and stained with Toluidine Blue (1 mg/ml, pH 2.3) for 10 minutes and washed again in PBS. Colonies of more than 50 cells were counted and the CFU-F efficiency was calculated as a measure of the clonogenicity of MSCs. The CFU-F efficiency was calculated as total number of colonies per total number of cells plated and multiplied by 100%.

9.4 In vitro cell differentiation assays

9.4.1 Chondrogenic differentiation of MSCs

MSCs were plated at high-density or as micromass cultures in 96-well plastic plates or 96-well glassbottom microplates (Falcon #353219; for immunofluorescence) at 10^5 cells/well. After overnight in α-MEM$^+$ medium, cells were cultured in different chondrogenic differentiation media. To the media cocktail, the appropriate combination of 10ng/ml recombinant human (rh) ligands such as TGF-βs (TGF-β1, R&D #240-B and TGF-β3, R&D #243-B3) and BMPs (BMP-2, R&D #355-BM and BMP-4, R&D #314-BP) were added to define the conditions to induce chondrogenesis in culture. The chondrogenic differentiation medium was changed every 48 hours. For control purposes MSCs were cultured in α-MEM$^+$ (expansion medium). All rh ligands and additional supplements were kept frozen in small aliquots and added freshly to the differentiation medium at the time of changing the media.

9.4.2 Chondrogenic differentiation of MSCs on Collagen type-I matrixes

12-well tissue culture plates were coated with 2% agarose (Invitrogen #16520-050). Sterile Collagen type-I sponge matrixes were prepared to a size of 4 mm diameter and thickness and placed in coated wells using 1 µl of PBS to keep it stable on the surface. MSCs were pelleted and re-suspended in α-MEM$^+$ medium at high density (~20,000 cells/µl) and 5 µl of cell suspension was carefully pipetted on top of the Collagen type-I matrix. The cells were allowed to settle by incubating them for 45 minutes in the tissue culture incubator. Then 1ml of pre-warmed α-MEM$^+$ medium was added and cultured overnight. The following day, the expansion medium was replaced by the appropriate differentiation medium supplemented with growth factors to induce chondrogenesis and cells were cultured as described before.

9.4.3 Chondrogenic differentiation of limb bud mesenchymal cells

Single cell suspensions of embryonic limb cells were prepared in DMEM-F12$^+$ and plated in 96-well plate at high density of 2.5-5 x10^5 cells/well. Cells were incubated and media was changed every day. Limb bud mesenchymal

cells adhere to the tissue culture plates and undergo spontaneous mesenchymal condensation to initiate chondrogenesis.

9.4.4 Osteogenic differentiation of MSCs

MSCs were plated in 48-well tissue culture plates at a density of ~20,000 cells/well. After overnight culture in α-MEM$^+$ medium, the cells were cultured in the osteogenic differentiation medium. For MSCs from adult mice, pre-prepared osteogenic medium from Lonza was used. The differentiation medium was changed every 48 hours and osteogenic differentiation was analysed after 14-21 days. To study the osteogenic differentiation potential of MSCs from postnatal day P2 mice, the DMEM$^+$-based osteogenic medium was used and 10 ng/ml BMP4 added each time the medium was changed. As a control for both assays, MSCs at same density were cultured for same time in α-MEM$^+$ medium.

9.4.5 Adipogenic differentiation of MSCs

MSCs were plated in 48-well plates at ~20,000 cells/well. After overnight culture in α-MEM$^+$ medium, MSCs from adult mice were cultured in the differentiation medium consisting of an insulin-based induction medium for 72 hours followed by expansion medium for 24 hours. This 96-hour cycle was repeated 3 times followed by 7 days of culture in maintenance medium. As control, MSCs were cultured at same density and duration in α-MEM$^+$ medium. MSCs from postnatal P2 mice were seeded into 8 well μ-slide (Ibidi #80826) for immunofluorescence or into 48-well plates for RNA extraction at ~20,000 cells/well. After overnight culture, the α-MEM$^+$ medium was replaced with DMEM$^+$ containing BMP2 (B3555 Sigma) at concentration of 50ng/ml. After 72 hours, the medium was changed to DMEM$^+$ containing 2μM Rosiglitazone, 1μM Dexamethasone, 5μg/ml insulin and BMP2 along. After an additional 48 hours, cells were either harvested (day 5) for analysis or the culture was continued by repeating the treatment with the different media for another cycle and harvesting the cells for analysis at 10 days of differentiation. Control cells were grown in α-MEM$^+$ medium supplemented with an equal concentration of DMSO as the differentiation medium.

9.5 Engraftment of cartilage templates derived from differentiated MSCs into nude mice

In vivo experiments using nude mice (CD-1 nude/nude) involved engraftment of expanded MSCs and cartilage templates derived from MSCs seeded into collagen type-I scaffold and having undergone chondrogenic differentiation.

9.5.1 Subcutaneous implantation into nude mice

This procedure was performed by Dr. Atanas Todorov and Alexander Haumer, together with technical assistance of Dr. Andrea Barbero in the group of Prof. Ivan Martin at the University Hospital of Basel.

MSC derived-cartilage templates and controls were implanted into anesthetized adult nude mice. Two small incisions on the epidermis and dermis (approx. 10mm) were made on the center back of the shoulder and waist under sterile conditions. The seeded and differentiated Collagen type-I matrixes were placed through the incisions in the subcutaneous pockets (up to 4 constructs per mice). Incisions were then stapled and mice monitored until they wake-up under the warming red light source. After transferring the operated mice to their cages, they received the analgesic Buprenorphine (2mg/Kg) every 12 hours for the first 48 hours. After the surgery, the health of all mice was monitored every day for the duration of the experiment to detect possible wound infections or other complications. In no case wound infections or other complications were observed. Staples were removed after wound healing was complete (1 - 2 weeks) and the implants remained up to 8 weeks prior to analysis.

9.5.2 Analysis of the nude mouse implants

After euthanizing the experimental nude mice, the implants were resected by removing most of the host tissue and blood vessels surrounding them. The constructs were washed in PBS, cleaned further and fixed in 4% PFA in PBS overnight at 4^0C. The calcified constructs were incubated in decalcification

buffer (7% w/v EDTA, 10% w/v sucrose in PBS) for 24-48 hours at 37^0C on a rotator before processing them for histology and/or analysis by immunofluorescence.

9.6 Histology

9.6.1 Cryo-embedding

Fixed tissue samples or cell constructs were rinsed 2x in PBS and passed through a graded series of sucrose/PBS (w/v) at 4^0C: 10% sucrose, 20% sucrose, 30% sucrose; each incubation step ranging from 30 minutes to 1 hour; i.e. samples had to be equilibrated completely at each step. Then, the samples were transferred to an embedding mold (Sakura Tissue-Tek 4565) and the 30% sucrose was carefully removed. Optimum Cutting Temperature (OCT) embedding medium was mixed with 30% sucrose at 50:50 (v/v) was carefully added to the samples in the embedding molds. These were then frozen using 2-methylbutane by dry ice and the frozen blocks stored at -80^0C until cryosectioning.

9.6.2 Paraffin embedding

Fixed tissues samples or cell constructs were rinsed 3x in PBS and dehydrated in a graded series of ice-cold EtOH: 25% EtOH, 50% EtOH, 75% EtOH, 100% EtOH (2 times); each incubation step ranging from 5 minutes to 30 minutes depending on the type of tissue. Then the samples were cleared in Xylene for 2x 30 minutes at room temperature, followed by 30 minutes incubation in 50:50 (v/v) Xylene/paraffin wax at 60^0C. Samples were then treated with freshly melted paraffin for ≥3x at 60^0C for 1 hour. Then they were embedded in fresh paraffin (60^0C) using a stereomicroscope for positioning the tissue in the embedding cassettes (Kaltek #2882). The blocks were cooled to solidify the paraffin, after which they were stored at 4^0C.

9.6.3 Sectioning of embedded samples for fluorescent microscopy

Sectioning of OCT embedded samples was performed using Microm HM 500 OM Cryostat (-20°C). The sectioning blade was cooled down to -22^0C and

frozen blocks were transferred from -80^{0}C storage to the cryostat chamber. The thickness of sections ranged from 8µm-30µm. Sections were mounted on Superfrost Plus slides (Thermo Scientific) and stored at -80^{0}C.

Paraffin embedded samples were sectioned using Microm HM 355 microtome, the sectioning blade was cooled down to 10^{0}C and a water bath at 40^{0}C was used to stretch the sections on the glass slides. 7µm-10µm sections were cut and mounted on Superfrost Plus slides (Thermo Scientific), which were stored at room temperature.

9.6.4 Alcian Blue staining

Alcian blue staining was performed on chondrocytes to detect the glycosaminoglycans (GAGs) produced during chondrocyte differentiation. The medium was carefully aspirated from differentiated cells, which were then fixed for 30 minutes in 4% PFA in PBS. After aspirating the 4% PFA and 3x washing in double-distilled H$_2$O (ddH$_2$O; 5 minutes each), the Alcian blue staining (1%, prepared with 3% acetic acid solution in ddH$_2$O, pH = 1.0; Sigma #A3157) was done overnight at room temperature. The dye was washed using ddH$_2$O and samples were analyzed and documented using a Leica DMI-4000 microscope.

9.6.5 Alizarin Red-S staining

Alizarin Red-S staining was performed to detect the calcium deposits produced by differentiated osteoblasts. The medium was carefully aspirated and cells were fixed for 30 minutes in 70% EtOH at 4^{0}C. After aspirating the 70% EtOH and 3x washing in ddH$_2$O for 5 minutes each, the Alizarin Red-S staining (2mg/ml, prepared in ddH$_2$O, pH = 4.1 - 4.3; Sigma #A5533) was done for 1 hour at room temperature. The dye was washed off in ddH$_2$O and samples documented using a Leica DMI-4000 microscope.

9.6.6 Oil Red-O staining

Oil Red-O staining was performed to detect the lipid droplets in differentiated adipocytes. The medium was aspirated and cells were fixed for 30 minutes in 4% PFA in PBS at RT. After washing, cells were treated with 60% isopropanol for 5 minutes at room temperature. Then the isopropanol was substituted by Oil Red-O solution. The stock solution is prepared at 3mg/ml in 99% isopropanol and is stable for (~1 year; Fisher #M312512), the working solution prepared by mixing 3 parts of the stock solution with 2 parts of de-ionized H_2O and leaving them for 10 minutes at room temperature. Cells are incubated with prepared working solution for 5 minutes at room temperature. The Oil Red O solution was washed off in tap water. Cells are then counterstained by Hematoxylin solution (Sigma #H3136) for 1 minute at room temperature. Then they are rinsed again with tap water to remove the excess Hematoxylin. Samples were documented using a Leica DMI-4000 microscope.

9.6.7 Safranin-O staining

Safranin-O staining was performed to detect the presence of sulfated glycosaminoglycans (GAGs), produced by chondrocytes and in chondrogenic tissues. The medium was carefully aspirated and samples fixed for 30 minutes in 4% PFA in PBS. PFA was removed and specimens were washed in tap water for 5 minute followed by staining in 0.02% fast green (Sigma #F7252) for 4 minutes at room temperature. Cells were then dipped 3x in 1% acetic acid solution. Then, the Safranin-O staining (0.1% prepared in ddH_2O; Sigma #HT904) was done for 6 minutes at room temperature. Samples were thhen dehydrated by dipping them in a series of 95% EtOH to 100% EtOH (10 dips each), followed by washing them for 2x 1 minute in Xylene. The samples on slides were mounted in Eukitt (Fluka #03989) and documented using the Leica DMI-4000 microscope.

9.6.8 Hematoxylin/ Eosin (H&E) staining

Fixed specimens were washed extensively in tap water for 5 minutes. Hematoxylin staining was done by incubating the sections 3x in the filtered solution of Hematoxylin series (90 seconds each), followed by washing in tap

water for 2 minutes. Further staining was performed using filtered 0.10% Eosin Y/EtOH (Sigma #E4382). Cells were dehydrated in a series of 95% EtOH to 100% EtOH, 5 minutes each followed by 2x washing in Xylene for 5 minutes each time. Samples on slides were then mounted in Eukitt (Fluka) and documented using the Leica DMI-4000 microscope.

9.7 Molecular Biology

9.7.1 DNA extraction for genotyping of mice strains

Tail or ear clips from mice were placed in 400µl of tail buffer (10 mM Tris HCl pH 8.0, 50 mM EDTA, 100 mM NaCl, 0.5% SDS) including 40µl Proteinase K (1µg/ml) (Merck #24568) and incubated overnight in thermostat at 55^0C with rotation at 750 rpm. The following day, tail buffer was added to a total volume of 750µl and samples mixed on a rotator for 2 minutes. 250µl of 6M NaCl was added to the sample and mixed on a rotator for 2 minutes, followed by centrifugation at 13,000 rpm for 10 minutes. 75µl of clear supernatant was collected in fresh eppendorf tube, to which 500µl of isopropanol was added, mixed and spun down at 13,000 rpm for 5 minutes at room temperature. The supernatant was removed and the DNA pellets were washed with 70% ethanol and re-centrifuged. Pellets were then air-dried and re-suspended in 100-500µl of TE buffer (10 mM Tris HCl pH 8.0, 100µM EDTA). The re-suspended samples were incubated in Thermostat mixer at 55^0C for 10 minutes to dissolve the DNA and then stored at 4^0C.

9.7.2 RNA extraction using TRI-Reagent solution

Tissue samples or cells (embryonic limb bud cells or sorted MSCs) in monolayer or high-density culture were detached by controlled trypsin digestion (see before) and transferred into 1ml Tri-Reagent solution (Sigma #T9424) in eppendorf tubes. Samples were then homogenized by passing them several times through syringe with a 21G needle. For small amounts of cells, 10µl of 0.5% LPA (Linear Polyacrylamide) were added per 1ml of Tri-Reagent to act as carrier for precipitation of small amounts of RNA. Homogenates were left to rest for 10 minutes at room temperature, then 200µl

of chloroform (Sigma #372978) was added and the samples were vigorously shaken for 15 seconds. Samples were again incubated for 15 minutes at room temperature and then spun at 12,000 rpm in a 4^0C pre-cooled centrifuge to separate the phenol-chloroform from the aqueous phase. The aqueous phase was collected carefully into a fresh RNAse-free eppendorf tube and 0.5ml of isopropanol (Merck) was added. Samples were incubated for 10 minutes at room temperature to precipitate the RNA and then centrifuged at 12000g and at 4^0C for 10 minutes. The supernatant was removed and the RNA pellets washed with 75% EtOH, followed by re-centrifugation at 7500g at 4^0C for 5 minutes. The RNA pellets were then air-dried quickly and dissolved in DEPC (Diethylpyrocarbonate)-treated water in 20µl -50µl; depending on the amount of RNA. The samples were then incubated for 10 minutes at 55^0C to dissolve the RNA pellet and the RNA concentration quantified using the Nanodrop 2000C machine (Thermo Scientific).

9.7.3 DNase treatment of RNA samples

Samples with up to 2 µg of total RNA were treated as follows: 2µl of 10x DNase TURBO buffer (Ambion #4022G) and 1.5µl of TURBO DNase (2U/µl, Ambion #AM2238) were added and gently mixed. DEPC-treated water was added to a final volume of 20µl per sample. The samples were then incubated for 15 minutes at room temperature, followed by addition of 1µl of EDTA (25 mM) per sample and 15 minutes incubation at 65^0C. Then, samples were transferred to ice and stored at -20^0C.

9.7.4 cDNA synthesis

For cDNA synthesis, 10pg-5µg RNA were mixed with: 1µl of oligo dT_{12-18} (500ng); 1µl of dNTP mix (10mM each of dATP, dGTP, dCTP and dTTP at neutral pH); sterile H_2O to a total volume of 13 µl. The reaction mixture was heated at 65^0C for 5min and incubated on ice for ≥1 minute. Then the following reagents were added to this reaction mixture: 4 µl of 5x first strand buffer, 1µl of 0.1M DTT, 1µl of RNaseOUT^{TM} 40U/µl, 1µl of Superscript^{TM} III reverse transcriptase (200U/µl; reagents from the Invitrogen kit). The mixture was then incubated for 1 hour at 50^0C, followed by heat inactivation for 15

minutes at 70^0C. The cDNA samples were stored at -20^0C.

9.7.5 Real-time quantitative PCR (RT-qPCR)

The Bio-Rad CFX96 Real-Time PCR system was used in together with iQ SYBR Green Supermix (Bio-RAD). RT-qPCR was used to quantify the gene expression levels in cells and tissues. 0.3µM of specific primers (Table 9.9.1) were diluted in EB buffer (10 mM Tris-HCl, pH 8.5) and used for PCR amplification. The reaction mixture also contained 50% SYBR Green and DNA template and the total volume of 20µl was prepared using milli-Q H_2O. Gene expression levels were quantified from cDNA templates analyzed in biological duplicate or triplicate replicates. Primers to amplify housekeeping genes (Table 9.9.1) were used as endogenous controls and to normalize gene expression levels between different samples. The C_q values of the transcripts of interest were normalized in relation to the C_q values of these controls and normalized fold expression levels ($2^{-\Delta\Delta Cq}$) of target transcripts were calculated with mean standard deviation, relative to the mean value of control sample.

9.8 Immunofluorescence (IF) analysis

9.8.1 Live cell staining for flow cytometry

Suspensions were prepared in $HBSS^+$ from freshly isolated cells (see before) or by collagenase treatment (2 mg/ml) of monolayer cultures. Monolayer cultures were washed with PBS prior to addition of 2 mg/ml Collagenase D and incubation at 37^0C for 10 minutes. Cells were then detached by flicking the dishes few times or using sterile cell scrappers (Sarstedt #83.1830). Collagenase was inhibited by addition of serum, followed by washing and centrifugation with $HBSS^+$. Cells were resuspended in $HBSS^+$ and filtered through a 70µm strainer, followed by incubation with primary antibodies (Table 9.9.2) for 20 minutes at 4^0C. Cells were then spun at 2,400 rpm for 4 minutes and pellets were re-suspended in $HBSS^+$. Since lineage markers are labeled with biotin, a second incubation with streptavidin conjugated to different chromophores was done for 5 minutes at 4^0C (Table 9.9.2). Cells

were spun down and re-suspended in HBSS$^+$ again before flow cytometric sorting or analysis.

9.8.2 Immunofluorescence analysis of monolayer cell cultures

Cells were cultured as monolayers or high-density micromasses in 96-well glass bottomed optical tissue culture microplates (Falcon #353219). Then, cells were washed 2x in PBS prior to fixation in 4% PFA in PBS for 30 minutes at room temperature. After fixation and washing in PBS, antigen retrieval was performed for specific antibodies by incubating the cells in 250 µg/ml of pepsin (Sigma #P6887) at 37^{0}C for 10 minutes. Following two washes in PBS for 5 minutes each, cells were incubated in permeabilization buffer (PBS with 0.3% Triton-X100) for 20 minutes at room temperature. Following permeabilization, the blocking step was performed using permeabilization buffer with 10% of either goat or donkey serum for 1 hour at room temperature. The incubation with primary antibodies (Table 9.9.2) was done overnight at 4^{0}C. The following day, cells were washed 3x in PBT for 5 minutes each and incubated with secondary antibodies (Table 9.9.2) for 1 hour at room temperature. Following 3 washes with PBT for 5 minutes each, nuclei were counterstained with 1 mg/ml of Hoechst-33258 in PBS for 5 minutes. Cells were washed again 3x in PBT and stored in PBS at 4^{0}C until image acquisition.

9.8.3 IHC on frozen sections

Frozen tissue sections were left at RT for 10 minutes, followed by washing step for three times in PBS (5 minutes each). Slides were marked with hydrophobic border around the tissue section, using Dako pen (Dako #S2002). Antigen retrieval for specific antibodies was performed enzymatically by incubating the plates in 250 µg/ml of pepsin for 10 minutes at 37^{0}C. Steps of blocking, antibody staining and nuclear staining was performed as in section 9.8.2, after which the tissue was washed in PBS and mounted using Mowiol 4-88 (Calbiochem #475904) and covered with a glass cover slip. Mounted slides were dried overnight at RT and stored until image acquisition.

9.8.4 Immunofluorescence analysis using paraffin embedded tissue sections

Slides with tissue sections were de-paraffinized by incubating them 2x in Xylene (10 minutes each), followed by 2x 100% EtOH (10 minutes each) at room temperature. Sections were then rehydrated in a reverse EtOH series- 70% EtOH/H_2O, 50% EtOH/H_2O, 30% EtOH/H_2O (5 minutes each) and rinsed 2x in H_2O and PBS each. Antigen retrieval on sections for specific antibodies was done by autoclaving at 120^0C in 10mM sodium citrate buffer (pH 6.0) with 0.05% Tween-20 for 6 min. Blocking steps, incubation with primary and secondary antibodies and counterstaining of nuclei was done as described in the previous section. Finally the slides were washed in PBS and mounted in Mowiol 4-88 and covered by a glass coverslip. Mounted slides were dried overnight at room temperature and stored at 4^0C.

9.8.5 BrdU labeling of proliferating cells

In order to label the proliferating limb bud cells in mouse embryos with BrdU, 1 mg of BrdU (BD Pharmingen BrdU kit #552598, dissolved in 1X DPBS) was administered twice to the pregnant female by intraperitoneal injection (IP), 4 and 2 hours prior to euthanasia and embryo isolation. Limb buds from the correct embryonic stages were collected for fixation and further analysis by immunofluorescence. For negative controls, mice were injected (IP) with 1x DPBS and limb buds from same stages were collected.

Cultured cells were labeled by adding 10 µM of BrdU to the culture medium. Treatment was done for 30 minutes and then cells were either fixed for immunofluorescence analysis or detached for flow cytometry (see before). First, cells were incubated with cell-surface markers using the appropriate fluorescent antibodies (Table 9.9.2) for 15 minutes at 4^0C. Then cells were washed in HBSS$^+$, fixed, permeabilized and BrdU positive cells were detected by immunofluorescence using the BD Pharmingen^{TM} BrdU Flow kit according to the manufacturers instruction manual.

9.8.6 BrdU detection by immunofluorescence on tissue sections

4% PFA-fixed cells in 96-well glass bottomed optical tissue culture plates or tissue cryo-sections on slides were rinsed 2x with PBS and permeabilized in 0.3% Tween-20 in PBS for 20 min at room temperature. DNA denaturation was performed in 1N HCl for 10 min and 2N HCl for 10min at room temperature. Then the samples were incubated at 37°C for 20min and neutralized with 0.1 M pH 8.6 Borate Buffer for 15min at room temperature. Next, samples were blocked in 10% goat serum and 0.3% Triton-100 in PBS for 1 hour, followed by incubation with anti-BrdU antibody (Bio-Rad clone BU1/75). The samples were then washed 3x in PBS, followed by incubation in secondary antibody for 1 hour at room temperature. After 3 washes in PBS, nuclei were detected with 1 mg/ml of Hoechst-33258 in PBS for 5 min, followed by 3 washes in PBS. Slides were mounted using Mowiol and stored at 4^0C in the dark. Immunofluorescence images were obtained using a Leica Sp5 confocal microscope and processed using Photoshop CS5 for Macintosh.

9.9 Tables

9.9.1 List of primers

Genotyping PCR			
Locus	**Forward primer**	**Reverse primer**	**Allele**
CMVCre	5' GCCTGCATTACCGGTCGATGCAACGA 3'	5' GTGGCAGATGGCGCGGCAACACCATT 3'	Tg
TmCre	5' CTCTAGAGCCTCTGCTAACC 3'	5' CCTGGCGATCCCTGAACATGTCC 3'	Tg
DsRed	5' GGTGATGTCCAGCTTGGAGT 3'	5' CCCCGTAATGCAGAAGAAGA 3'	Tg
β-actin-GFP	5' CATGAAGCAGCACGACTTCT 3'	5' GCTTGTCGGCCATGATATAG 3'	Tg
Sox9-GFP	5' CCTACGGCGTGCAGTGCTTCA GC 3'	5' CGGCGAGCTGCACGCTGCCGT CC 3'	Tg

qPCR primers			
Locus	**Forward primer**	**Reverse primer**	**Size**
Sox9	5' CAAGTGTGTGTGCCGTGGATAG 3'	5' CCAGCCACAGCAGTGAGTAAGA 3'	89
Col2a1	5' AGTGGAAGAGCGGAGACTACTG 3'	5' TTGGGGTAGACGCAAGTCTC 3'	106
Col10a1	5' GCTAATGTTCTTGACCCTGGT 3'	5' TGTTCTCCTCTTACTGGAATCC 3'	150
Osterix	5' CCTCGCTCTCCTATTGCA 3'	5' GCAAAGGCCTGAGAGGAGTT 3'	70
Osteocalcin	5' TGTGACGAGCTATCAGACCAGT 3'	5' GCTGTGACATCCATACTTGCAG 3'	177
PPAR-γ	5' GCTGTGAAGTTCAATGCACTGG 3'	5' GCAGTAGCTGCACGTGCTCTG 3'	250
FABP4	5' GATGCCTTTGTGGGAACCT 3'	5' CTGTCGTCTGCGGTGATTT 3'	230
RPL19	5' ACCCTGGCCCGACGG 3'	5' TACCCTTTCCTCTTCCCTATGCC 3'	53

9.9.2 List of primary and secondary Antibodies

Primary Antibodies					
Antigen and Host		**Distributor/ clone**	**Dilutions**	**Usage**	**Comment**
Anti-BrdU	rat	Bio-Rad clone BU1/75 (ICR1)	1:1000	IHC	Monoclonal
Anti-BrdU	mouse	eBioscience clone BU20A	1:200	FACS	Monoclonal
B220	mouse	Biolegend clone RA3-6B2	1:1000	IHC	Fluorophore conjugated
CD105	mouse	Biolegend clone MJ7/18	1:500	FACS	Fluorophore conjugated
CD117/ c-kit	mouse	Biolegend clone 2B8	1:250	FACS	Fluorophore conjugated
CD11b	mouse	BD Biosciences	1:1000	FACS	Biotinylated

		clone M1/70			
CD200	mouse	Biolegend clone OX-90	1:1000	FACS	Fluorophore conjugated
CD3	mouse	Biolegend clone 145-2C11	1:250	FACS	Biotinylated
CD31	mouse	eBioscience clone 390	1:1000; 1:250	FACS	Biotinylated
CD31	mouse	Biolegend clone MEC13.3	1:250	IHC	Fluorophore conjugated
CD34	mouse	Biolegend clone MEC14.7	1:250	FACS	Fluorophore conjugated
CD44	mouse	Biolegend clone IM7	1:5000	FACS	Fluorophore conjugated
CD45	mouse	BD Pharmingen clone 30-F11	1:500	FACS	Biotinylated
CD45	mouse	Biolegend clone 30-F11	1:250	IHC	Fluorophore conjugated
CD49e	mouse	eBioscience clone eBioHMa5-1	1:1000	FACS	Fluorophore conjugated
CD51	mouse	Biolegend clone RMV-7	1:1000	FACS	Fluorophore conjugated
CD73	mouse	eBioscience clone eBioTY/11.8	1:1000	FACS	Fluorophore conjugated
CD90	mouse	eBioscience clone 53-2.1	1:2000	FACS	Fluorophore conjugated
COL-II	mouse	Thermo Scientific clone 2B1.5	1:300	IHC	Monoclonal
COL-X	rabbit	Abcam Cat. #ab58632	1:300	IHC	Polyclonal
Ep-CAM	mouse	Biolegend clone G8.8	1:1000	FACS	Biotinylated
F4/80	mouse	Biolegend clone BM8	1:1000	FACS; IHC	Biotinylated
Flk-1	mouse	Biolegend clone 89B3A5	1:1000	FACS	Biotinylated
Gr-1	mouse	Biolegend clone RB6-8C5	1:1000	FACS	Biotinylated
OSTERIX	rabbit	Abcam Cat. #ab94744	1:2000	IHC	Polyclonal

PDGFR-α	mouse	Biolegend clone APA5	1:250; 1:1000	FACS; IHC	Fluorophore conjugated
PDGFR-β	mouse	eBioscience clone APB5	1:250	FACS	Fluorophore conjugated
PPAR-γ	rabbit	Cell Signaling Cat. # 2443	1:1000	IHC	Monoclonal
Sca-1	mouse	Biolegend clone D7	1:10000; 1:200	FACS; IHC	Fluorophore conjugated
SOX9	rabbit	Millipore Cat. # AB5535	1:5000	IHC	Polyclonal
Streptavidin		Biolegend	1:1000	FACS	Affinity to Biotin
TER119	mouse	Biolegend	1:200	FACS	Biotinylated

Secondary Antibodies			
Antigen	**Manufacturer**	**Dilution**	**Usage**
Donkey α Rat IgG (H+L) Alexa Fluor® 555	Invitrogen, A21209	1:500	IHC
Goat α Mouse IgG (H+L) Alexa Fluor® 488 F(ab')2	Invitrogen, A-11017	1:500	IHC
Goat α Mouse IgG (H+L) Alexa Fluor® 594 F(ab')2	Invitrogen, A-11020	1:500	IHC
Goat α Rabbit Alexa Fluor® 555	Invitrogen, A21428	1:500	IHC
Goat α Rabbit IgG (H+L) Alexa Fluor® 594	Invitrogen, A11037	1:500	IHC
Goat α Rabbit IgG (H+L) Alexa Fluor® 594	Invitrogen, A-11070	1:500	IHC
Goat α Rat Alexa Fluor® 555	Invitrogen, A21434	1:500	IHC
Ms X Fluorescein Alexa Fluor® 488	Millipore MAB045X	1:500	IHC
Rabbit α Goat IgG (H+L) Alexa Fluor® 594	Invitrogen, A-11080	1:500	IHC

9.9.3 List of additional reagents

Product	Manufacturer/ Reference
100% Acetic acid	Merck #100063
2-Propanol	Merck #109634
36.5% formaldehyde	Sigma #252549
Agarose (PCR)	Biozym #335010
Bovine Serum Albumin (BSA)	Sigma, #A3059
Bromophenol Blue	Sigma #B5525
Chloroform	Sigma #372978
EDTA	Sigma #E5134
Entellan	Merck #HX825968
Eukitt	Fluka #03989
iQ™ SYBR® Green Supermix	Bio-Rad #170-8882
Oligo(dT)12-18	Invitrogen #18418-012
Paraplast for embedding (Paraffin)	Sigma #P3558
RNaseOUT™ Ribonuclease Inhibitor	Invitrogen #10777-019
SuperScript™ III Reverse Transcriptase	Invitrogen #18080-044
Toluidine Blue	Sigma X4126
Xylene	Applichem #A2476

10. Acknowledgements

11. Bibliography

Akiyama, H., J. E. Kim, K. Nakashima, G. Balmes, N. Iwai, J. M. Deng, Z. Zhang, J. F. Martin, R. R. Behringer, T. Nakamura and B. de Crombrugghe (2005). "Osteo-chondroprogenitor cells are derived from Sox9 expressing precursors." Proc Natl Acad Sci U S A **102**(41): 14665-14670.

Amano, K., M. Densmore, R. Nishimura and B. Lanske (2014). "Indian hedgehog signaling regulates transcription and expression of collagen type X via Runx2/Smads interactions." J Biol Chem **289**(36): 24898-24910.

Ara, T., K. Tokoyoda, T. Sugiyama, T. Egawa, K. Kawabata and T. Nagasawa (2003). "Long-term hematopoietic stem cells require stromal cell-derived factor-1 for colonizing bone marrow during ontogeny." Immunity **19**(2): 257-267.

Arufe, M. C., A. De la Fuente, I. Fuentes, F. J. de Toro and F. J. Blanco (2010). "Chondrogenic potential of subpopulations of cells expressing mesenchymal stem cell markers derived from human synovial membranes." J Cell Biochem **111**(4): 834-845.

Balk, M. L., J. Bray, C. Day, M. Epperly, J. Greenberger, C. H. Evans and C. Niyibizi (1997). "Effect of rhBMP-2 on the osteogenic potential of bone marrow stromal cells from an osteogenesis imperfecta mouse (oim)." Bone **21**(1): 7-15.

Bamezai, A., Palliser, D., Berezovskaya, A., McGrew, J., Higgins, K., Lacy, E., Rock, K. L. (1995). "Regulated expression of Ly-6A.2 is important for T cell development." J Immunol **154**(9): 4233-4239.

Bandyopadhyay, A., K. Tsuji, K. Cox, B. D. Harfe, V. Rosen and C. J. Tabin (2006). "Genetic analysis of the roles of BMP2, BMP4, and BMP7 in limb patterning and skeletogenesis." PLoS Genet **2**(12): e216.

Barna, M. and L. Niswander (2007). "Visualization of cartilage formation: insight into cellular properties of skeletal progenitors and chondrodysplasia syndromes." Dev Cell **12**(6): 931-941.

Baur, S. T., J. J. Mai and S. M. Dymecki (2000). "Combinatorial signaling through BMP receptor IB and GDF5: shaping of the distal mouse limb and the genetics of distal limb diversity." Development **127**(3): 605-619.

Benazet, J. D., E. Pignatti, A. Nugent, E. Unal, F. Laurent and R. Zeller (2012). "Smad4 is required to induce digit ray primordia and to initiate the aggregation and differentiation of chondrogenic progenitors in mouse limb buds." Development **139**(22): 4250-4260.

Bianco, P., X. Cao, P. S. Frenette, J. J. Mao, P. G. Robey, P. J. Simmons and C. Y. Wang (2013). "The meaning, the sense and the significance: translating the science of mesenchymal stem cells into medicine." Nat Med **19**(1): 35-42.

Bianco, P., P. G. Robey and P. J. Simmons (2008). "Mesenchymal stem cells: revisiting history, concepts, and assays." Cell Stem Cell **2**(4): 313-319.

Bitgood, M. J. and A. P. McMahon (1995). "Hedgehog and Bmp genes are coexpressed at many diverse sites of cell-cell interaction in the mouse embryo." Dev Biol **172**(1): 126-138.

Boiret, N., C. Rapatel, R. Veyrat-Masson, L. Guillouard, J. J. Guerin, P. Pigeon, S. Descamps, S. Boisgard and M. G. Berger (2005). "Characterization of nonexpanded mesenchymal progenitor cells from normal adult human bone marrow." Exp Hematol **33**(2): 219-225.

Boland, G. M., G. Perkins, D. J. Hall and R. S. Tuan (2004). "Wnt 3a promotes proliferation and suppresses osteogenic differentiation of adult human mesenchymal stem cells." J Cell Biochem **93**(6): 1210-1230.

Bradfute, S. B., T. A. Graubert and M. A. Goodell (2005). "Roles of Sca-1 in hematopoietic stem/progenitor cell function." Exp Hematol **33**(7): 836-843.

Campbell, D. D. and M. Pei (2012). "Surface markers for chondrogenic determination: a highlight of synovium-derived stem cells." Cells **1**(4): 1107-1120.

Canalis, E., K. Parker and S. Zanotti (2012). "Gremlin1 is required for skeletal development and postnatal skeletal homeostasis." J Cell Physiol **227**(1): 269-277.

Caplan, A. I. (1991). "Mesenchymal stem cells." J Orthop Res **9**(5): 641-650.

Carlevaro, M. F., S. Cermelli, R. Cancedda and F. Descalzi Cancedda (2000). "Vascular endothelial growth factor (VEGF) in cartilage neovascularization and chondrocyte differentiation: auto-paracrine role during endochondral bone formation." J Cell Sci **113 (Pt 1)**: 59-69.

Caron, M. M., P. J. Emans, D. A. Surtel, A. Cremers, J. W. Voncken, T. J. Welting and L. W. van Rhijn (2012). "Activation of NF-kappaB/p65 facilitates early chondrogenic differentiation during endochondral ossification." PLoS One **7**(3): e33467.

Centola, M., B. Tonnarelli, S. Scharen, N. Glaser, A. Barbero and I. Martin (2013). "Priming 3D cultures of human mesenchymal stromal cells toward cartilage formation via developmental pathways." Stem Cells Dev **22**(21): 2849-2858.

Chan, C. K., C. C. Chen, C. A. Luppen, J. B. Kim, A. T. DeBoer, K. Wei, J. A. Helms, C. J. Kuo, D. L. Kraft and I. L. Weissman (2009). "Endochondral

ossification is required for haematopoietic stem-cell niche formation." Nature **457**(7228): 490-494.

Chan, C. K., E. Y. Seo, J. Y. Chen, D. Lo, A. McArdle, R. Sinha, R. Tevlin, J. Seita, J. Vincent-Tompkins, T. Wearda, W. J. Lu, K. Senarath-Yapa, M. T. Chung, O. Marecic, M. Tran, K. S. Yan, R. Upton, G. G. Walmsley, A. S. Lee, D. Sahoo, C. J. Kuo, I. L. Weissman and M. T. Longaker (2015). "Identification and specification of the mouse skeletal stem cell." Cell **160**(1-2): 285-298.

Chan, H. Y., S. V, X. Xing, P. Kraus, S. P. Yap, P. Ng, S. L. Lim and T. Lufkin (2011). "Comparison of IRES and F2A-based locus-specific multicistronic expression in stable mouse lines." PLoS One **6**(12): e28885.

Chen, P. M., M. L. Yen, K. J. Liu, H. K. Sytwu and B. L. Yen (2011). "Immunomodulatory properties of human adult and fetal multipotent mesenchymal stem cells." J Biomed Sci **18**: 49.

Chimal-Monroy, J., J. Rodriguez-Leon, J. A. Montero, Y. Ganan, D. Macias, R. Merino and J. M. Hurle (2003). "Analysis of the molecular cascade responsible for mesodermal limb chondrogenesis: Sox genes and BMP signaling." Dev Biol **257**(2): 292-301.

Christensen, J. L., D. E. Wright, A. J. Wagers and I. L. Weissman (2004). "Circulation and chemotaxis of fetal hematopoietic stem cells." PLoS Biol **2**(3): E75.

Chung, M. T., C. Liu, J. S. Hyun, D. D. Lo, D. T. Montoro, M. Hasegawa, S. Li, M. Sorkin, R. Rennert, M. Keeney, F. Yang, N. Quarto, M. T. Longaker and D. C. Wan (2013). "CD90 (Thy-1)-positive selection enhances osteogenic capacity of human adipose-derived stromal cells." Tissue Eng Part A **19**(7-8): 989-997.

Colter, D. C., I. Sekiya and D. J. Prockop (2001). "Identification of a subpopulation of rapidly self-renewing and multipotential adult stem cells in colonies of human marrow stromal cells." Proc Natl Acad Sci U S A **98**(14): 7841-7845.

Coskun, S., H. Chao, H. Vasavada, K. Heydari, N. Gonzales, X. Zhou, B. de Crombrugghe and K. K. Hirschi (2014). "Development of the fetal bone marrow niche and regulation of HSC quiescence and homing ability by emerging osteolineage cells." Cell Rep **9**(2): 581-590.

Craft, A. M., N. Ahmed, J. S. Rockel, G. S. Baht, B. A. Alman, R. A. Kandel, A. E. Grigoriadis and G. M. Keller (2013). "Specification of chondrocytes and cartilage tissues from embryonic stem cells." Development **140**(12): 2597-2610.

Craft, A. M., J. S. Rockel, Y. Nartiss, R. A. Kandel, B. A. Alman and G. M. Keller (2015). "Generation of articular chondrocytes from human pluripotent stem cells." Nat Biotechnol **33**(6): 638-645.

Crisan, M., S. Yap, L. Casteilla, C. W. Chen, M. Corselli, T. S. Park, G. Andriolo, B. Sun, B. Zheng, L. Zhang, C. Norotte, P. N. Teng, J. Traas, R. Schugar, B. M. Deasy, S. Badylak, H. J. Buhring, J. P. Giacobino, L. Lazzari, J. Huard and B. Peault (2008). "A perivascular origin for mesenchymal stem cells in multiple human organs." Cell Stem Cell **3**(3): 301-313.

Delorme, B., J. Ringe, N. Gallay, Y. Le Vern, D. Kerboeuf, C. Jorgensen, P. Rosset, L. Sensebe, P. Layrolle, T. Haupl and P. Charbord (2008). "Specific plasma membrane protein phenotype of culture-amplified and native human bone marrow mesenchymal stem cells." Blood **111**(5): 2631-2635.

Deng, C., A. Wynshaw-Boris, F. Zhou, A. Kuo and P. Leder (1996). "Fibroblast growth factor receptor 3 is a negative regulator of bone growth." Cell **84**(6): 911-921.

Derynck, R. and Y. E. Zhang (2003). "Smad-dependent and Smad-independent pathways in TGF-beta family signalling." Nature **425**(6958): 577-584.

Diefenderfer, D. L., A. M. Osyczka, G. C. Reilly and P. S. Leboy (2003). "BMP responsiveness in human mesenchymal stem cells." Connect Tissue Res **44 Suppl 1**: 305-311.

Ding, L. and S. J. Morrison (2013). "Haematopoietic stem cells and early lymphoid progenitors occupy distinct bone marrow niches." Nature **495**(7440): 231-235.

Dominici, M., K. Le Blanc, I. Mueller, I. Slaper-Cortenbach, F. Marini, D. Krause, R. Deans, A. Keating, D. Prockop and E. Horwitz (2006). "Minimal criteria for defining multipotent mesenchymal stromal cells. The International Society for Cellular Therapy position statement." Cytotherapy **8**(4): 315-317.

Duff, S. E., C. Li, J. M. Garland and S. Kumar (2003). "CD105 is important for angiogenesis: evidence and potential applications." FASEB J **17**(9): 984-992.

Dzierzak, E. and A. Medvinsky (2008). "The discovery of a source of adult hematopoietic cells in the embryo." Development **135**(14): 2343-2346.

Erices, A., P. Conget and J. J. Minguell (2000). "Mesenchymal progenitor cells in human umbilical cord blood." Br J Haematol **109**(1): 235-242.

Eswarakumar, V. P. and J. Schlessinger (2007). "Skeletal overgrowth is mediated by deficiency in a specific isoform of fibroblast growth factor receptor 3." Proc Natl Acad Sci U S A **104**(10): 3937-3942.

Farrell, E., S. K. Both, K. I. Odorfer, W. Koevoet, N. Kops, F. J. O'Brien, R. J. Baatenburg de Jong, J. A. Verhaar, V. Cuijpers, J. Jansen, R. G. Erben and G. J. van Osch (2011). "In-vivo generation of bone via endochondral ossification by in-vitro chondrogenic priming of adult human and rat mesenchymal stem cells." BMC Musculoskelet Disord **12**: 31.

Feng, X. H. and R. Derynck (2005). "Specificity and versatility in tgf-beta signaling through Smads." Annu Rev Cell Dev Biol **21**: 659-693.

Ferrero, I., W. Held, A. Wilson, F. Tacchini-Cottier, F. Radtke and H. R. MacDonald (2002). "Mouse CD11c(+) B220(+) Gr1(+) plasmacytoid dendritic cells develop independently of the T-cell lineage." Blood **100**(8): 2852-2857.

Fonsatti, E., M. Altomonte, P. Arslan and M. Maio (2003). "Endoglin (CD105): a target for anti-angiogenetic cancer therapy." Curr Drug Targets **4**(4): 291-296.

Foster, L. J., P. A. Zeemann, C. Li, M. Mann, O. N. Jensen and M. Kassem (2005). "Differential expression profiling of membrane proteins by quantitative proteomics in a human mesenchymal stem cell line undergoing osteoblast differentiation." Stem Cells **23**(9): 1367-1377.

Frenette, P. S., S. Pinho, D. Lucas and C. Scheiermann (2013). "Mesenchymal stem cell: keystone of the hematopoietic stem cell niche and a stepping-stone for regenerative medicine." Annu Rev Immunol **31**: 285-316.

Friedenstein, A. J., R. K. Chailakhjan and K. S. Lalykina (1970). "The development of fibroblast colonies in monolayer cultures of guinea-pig bone marrow and spleen cells." Cell Tissue Kinet **3**(4): 393-403.

Friedenstein, A. J., N. V. Latzinik, F. Gorskaya Yu, E. A. Luria and I. L. Moskvina (1992). "Bone marrow stromal colony formation requires stimulation by haemopoietic cells." Bone Miner **18**(3): 199-213.

Friedenstein, A. J., K. V. Petrakova, A. I. Kurolesova and G. P. Frolova (1968). "Heterotopic of bone marrow. Analysis of precursor cells for osteogenic and hematopoietic tissues." Transplantation **6**(2): 230-247.

Fujita, A., M. Migita, T. Ueda, R. Ogawa, Y. Fukunaga and T. Shimada (2010). "Hematopoiesis in regenerated bone marrow within hydroxyapatite scaffold." Pediatr Res **68**(1): 35-40.

Gang, E. J., D. Bosnakovski, C. A. Figueiredo, J. W. Visser and R. C. Perlingeiro (2007). "SSEA-4 identifies mesenchymal stem cells from bone marrow." Blood **109**(4): 1743-1751.

Gerber, H. P., T. H. Vu, A. M. Ryan, J. Kowalski, Z. Werb and N. Ferrara (1999). "VEGF couples hypertrophic cartilage remodeling, ossification and angiogenesis during endochondral bone formation." Nat Med **5**(6): 623-628.

Gothard, D., J. I. Dawson and R. O. Oreffo (2013). "Assessing the potential of colony morphology for dissecting the CFU-F population from human bone marrow stromal cells." Cell Tissue Res 352(2): 237-247.

Greenbaum, A., Y. M. Hsu, R. B. Day, L. G. Schuettpelz, M. J. Christopher, J. N. Borgerding, T. Nagasawa and D. C. Link (2013). "CXCL12 in early mesenchymal progenitors is required for haematopoietic stem-cell maintenance." Nature 495(7440): 227-230.

Grigoriadis, A. E., J. N. Heersche and J. E. Aubin (1988). "Differentiation of muscle, fat, cartilage, and bone from progenitor cells present in a bone-derived clonal cell population: effect of dexamethasone." J Cell Biol 106(6): 2139-2151.

Gronthos, S., J. Brahim, W. Li, L. W. Fisher, N. Cherman, A. Boyde, P. DenBesten, P. G. Robey and S. Shi (2002). "Stem cell properties of human dental pulp stem cells." J Dent Res 81(8): 531-535.

Haeryfar, S. M. and D. W. Hoskin (2004). "Thy-1: more than a mouse pan-T cell marker." J Immunol 173(6): 3581-3588.

Hagmann, S., B. Moradi, S. Frank, T. Dreher, P. W. Kammerer, W. Richter and T. Gotterbarm (2013). "Different culture media affect growth characteristics, surface marker distribution and chondrogenic differentiation of human bone marrow-derived mesenchymal stromal cells." BMC Musculoskelet Disord 14: 223.

Hammarstedt, A., C. X. Andersson, V. Rotter Sopasakis and U. Smith (2005). "The effect of PPARgamma ligands on the adipose tissue in insulin resistance." Prostaglandins Leukot Essent Fatty Acids 73(1): 65-75.

Heo, H. R., L. Chen, B. An, K. S. Kim, J. Ji and S. H. Hong (2015). "Hormonal regulation of hematopoietic stem cells and their niche: a focus on estrogen." Int J Stem Cells 8(1): 18-23.

Hilton, M. J., X. Tu, J. Cook, H. Hu and F. Long (2005). "Ihh controls cartilage development by antagonizing Gli3, but requires additional effectors to regulate osteoblast and vascular development." Development 132(19): 4339-4351.

Holmes, C. and W. L. Stanford (2007). "Concise review: stem cell antigen-1: expression, function, and enigma." Stem Cells 25(6): 1339-1347.

Hosogane, N., Z. Huang, B. A. Rawlins, X. Liu, O. Boachie-Adjei, A. L. Boskey and W. Zhu (2010). "Stromal derived factor-1 regulates bone morphogenetic protein 2-induced osteogenic differentiation of primary mesenchymal stem cells." Int J Biochem Cell Biol 42(7): 1132-1141.

Houlihan, D. D., Y. Mabuchi, S. Morikawa, K. Niibe, D. Araki, S. Suzuki, H. Okano and Y. Matsuzaki (2012). "Isolation of mouse mesenchymal stem cells

on the basis of expression of Sca-1 and PDGFR-alpha." Nat Protoc **7**(12): 2103-2111.

Hui, T. Y., K. M. Cheung, W. L. Cheung, D. Chan and B. P. Chan (2008). "In vitro chondrogenic differentiation of human mesenchymal stem cells in collagen microspheres: influence of cell seeding density and collagen concentration." Biomaterials **29**(22): 3201-3212.

Ichinose, S., K. Yamagata, I. Sekiya, T. Muneta and M. Tagami (2005). "Detailed examination of cartilage formation and endochondral ossification using human mesenchymal stem cells." Clin Exp Pharmacol Physiol **32**(7): 561-570.

Ikeda, T., H. Kawaguchi, S. Kamekura, N. Ogata, Y. Mori, K. Nakamura, S. Ikegawa and U. I. Chung (2005). "Distinct roles of Sox5, Sox6, and Sox9 in different stages of chondrogenic differentiation." J Bone Miner Metab **23**(5): 337-340.

Ito, T., R. Sawada, Y. Fujiwara, Y. Seyama and T. Tsuchiya (2007). "FGF-2 suppresses cellular senescence of human mesenchymal stem cells by down-regulation of TGF-beta2." Biochem Biophys Res Commun **359**(1): 108-114.

Iwasaki, H., Akashi, K. (2007). "Myeloid lineage commitment from the hematopoietic stem cell." Immunity **26**(6): 726-740.

Jacob, A. L., C. Smith, J. Partanen and D. M. Ornitz (2006). "Fibroblast growth factor receptor 1 signaling in the osteo-chondrogenic cell lineage regulates sequential steps of osteoblast maturation." Dev Biol **296**(2): 315-328.

James, A. W. (2013). "Review of Signaling Pathways Governing MSC Osteogenic and Adipogenic Differentiation." Scientifica (Cairo) **2013**: 684736.

Kamiura, S., Nolan, C. M., Meruelo, D. (1992). "Long-range physical map of the Ly-6 complex: mapping the Ly-6 multigene family by field-inversion and two-dimensional gel electrophoresis." Genomics **12**(1): 89-105.

Karamboulas, K., H. J. Dranse and T. M. Underhill (2010). "Regulation of BMP-dependent chondrogenesis in early limb mesenchyme by TGFbeta signals." J Cell Sci **123**(Pt 12): 2068-2076.

Keating, A. (2012). "Mesenchymal stromal cells: new directions." Cell Stem Cell **10**(6): 709-716.

Kember, N. F. and H. A. Sissons (1976). "Quantitative histology of the human growth plate." J Bone Joint Surg Br **58-B**(4): 426-435.

Kim, H. J. and G. I. Im (2009). "Chondrogenic differentiation of adipose tissue-derived mesenchymal stem cells: greater doses of growth factor are necessary." J Orthop Res **27**(5): 612-619.

Kindblom, J. M., O. Nilsson, T. Hurme, C. Ohlsson and L. Savendahl (2002). "Expression and localization of Indian hedgehog (Ihh) and parathyroid hormone related protein (PTHrP) in the human growth plate during pubertal development." J Endocrinol **174**(2): R1-6.

Koide, Y., S. Morikawa, Y. Mabuchi, Y. Muguruma, E. Hiratsu, K. Hasegawa, M. Kobayashi, K. Ando, K. Kinjo, H. Okano and Y. Matsuzaki (2007). "Two distinct stem cell lineages in murine bone marrow." Stem Cells **25**(5): 1213-1221.

Kondo, M. (2010). "Lymphoid and myeloid lineage commitment in multipotent hematopoietic progenitors." Immunol Rev **238**(1): 37-46.

Kozhemyakina, E., A. B. Lassar and E. Zelzer (2015). "A pathway to bone: signaling molecules and transcription factors involved in chondrocyte development and maturation." Development **142**(5): 817-831.

Kronenberg, H. M. (2003). "Developmental regulation of the growth plate." Nature **423**(6937): 332-336.

Le Blanc, K. and D. Mougiakakos (2012). "Multipotent mesenchymal stromal cells and the innate immune system." Nat Rev Immunol **12**(5): 383-396.

Le Blanc, K. and O. Ringden (2007). "Immunomodulation by mesenchymal stem cells and clinical experience." J Intern Med **262**(5): 509-525.

Lehmann, J. M., J. M. Lenhard, B. B. Oliver, G. M. Ringold and S. A. Kliewer (1997). "Peroxisome proliferator-activated receptors alpha and gamma are activated by indomethacin and other non-steroidal anti-inflammatory drugs." J Biol Chem **272**(6): 3406-3410.

Lepperdinger, G. (2011). "Inflammation and mesenchymal stem cell aging." Curr Opin Immunol **23**(4): 518-524.

Li, D. Y., L. K. Sorensen, B. S. Brooke, L. D. Urness, E. C. Davis, D. G. Taylor, B. B. Boak and D. P. Wendel (1999). "Defective angiogenesis in mice lacking endoglin." Science **284**(5419): 1534-1537.

Logan, M., J. F. Martin, A. Nagy, C. Lobe, E. N. Olson and C. J. Tabin (2002). "Expression of Cre Recombinase in the developing mouse limb bud driven by a Prxl enhancer." Genesis **33**(2): 77-80.

Long, F., U. I. Chung, S. Ohba, J. McMahon, H. M. Kronenberg and A. P. McMahon (2004). "Ihh signaling is directly required for the osteoblast lineage in the endochondral skeleton." Development **131**(6): 1309-1318.

Long, F. and D. M. Ornitz (2013). "Development of the endochondral skeleton." Cold Spring Harb Perspect Biol **5**(1): a008334.

Lorda-Diez, C. I., J. A. Montero, C. Martinez-Cue, J. A. Garcia-Porrero and J. M. Hurle (2009). "Transforming growth factors beta coordinate cartilage and tendon differentiation in the developing limb mesenchyme." J Biol Chem **284**(43): 29988-29996.

Luna, G., J. Paez and J. E. Cardier (2004). "Expression of the hematopoietic stem cell antigen Sca-1 (LY-6A/E) in liver sinusoidal endothelial cells: possible function of Sca-1 in endothelial cells." Stem Cells Dev **13**(5): 528-535.

Mabuchi, Y., D. D. Houlihan, C. Akazawa, H. Okano and Y. Matsuzaki (2013). "Prospective isolation of murine and human bone marrow mesenchymal stem cells based on surface markers." Stem Cells Int **2013**: 507301.

Mackie, E. J., L. Tatarczuch and M. Mirams (2011). "The skeleton: a multi-functional complex organ: the growth plate chondrocyte and endochondral ossification." J Endocrinol **211**(2): 109-121.

Mak, K. K., H. M. Kronenberg, P. T. Chuang, S. Mackem and Y. Yang (2008). "Indian hedgehog signals independently of PTHrP to promote chondrocyte hypertrophy." Development **135**(11): 1947-1956.

Maleki, M., F. Ghanbarvand, M. Reza Behvarz, M. Ejtemaei and E. Ghadirkhomi (2014). "Comparison of mesenchymal stem cell markers in multiple human adult stem cells." Int J Stem Cells **7**(2): 118-126.

Manilay, J. O. and M. Zouali (2014). "Tight relationships between B lymphocytes and the skeletal system." Trends Mol Med **20**(7): 405-412.

Mariani, F. V., C. P. Ahn and G. R. Martin (2008). "Genetic evidence that FGFs have an instructive role in limb proximal-distal patterning." Nature **453**(7193): 401-405.

Mendez-Ferrer, S., T. V. Michurina, F. Ferraro, A. R. Mazloom, B. D. Macarthur, S. A. Lira, D. T. Scadden, A. Ma'ayan, G. N. Enikolopov and P. S. Frenette (2010). "Mesenchymal and haematopoietic stem cells form a unique bone marrow niche." Nature **466**(7308): 829-834.

Merino, R., J. Rodriguez-Leon, D. Macias, Y. Ganan, A. N. Economides and J. M. Hurle (1999). "The BMP antagonist Gremlin regulates outgrowth, chondrogenesis and programmed cell death in the developing limb." Development **126**(23): 5515-5522.

Mikkola, H. K. and S. H. Orkin (2006). "The journey of developing hematopoietic stem cells." Development **133**(19): 3733-3744.

Miyamoto, T., Iwasaki, H., Reizis, B., Ye, M., Graf, T., Weissman, I. L., Akashi, K. (2002). "Myeloid or lymphoid promiscuity as a critical step in hematopoietic lineage commitment." Dev Cell **3**(1): 137-147.

Mizoguchi, T., S. Pinho, J. Ahmed, Y. Kunisaki, M. Hanoun, A. Mendelson, N. Ono, H. M. Kronenberg and P. S. Frenette (2014). "Osterix marks distinct waves of primitive and definitive stromal progenitors during bone marrow development." Dev Cell **29**(3): 340-349.

Morikawa, S., Y. Mabuchi, Y. Kubota, Y. Nagai, K. Niibe, E. Hiratsu, S. Suzuki, C. Miyauchi-Hara, N. Nagoshi, T. Sunabori, S. Shimmura, A. Miyawaki, T. Nakagawa, T. Suda, H. Okano and Y. Matsuzaki (2009). "Prospective identification, isolation, and systemic transplantation of multipotent mesenchymal stem cells in murine bone marrow." J Exp Med **206**(11): 2483-2496.

Muruganandan, S., A. A. Roman and C. J. Sinal (2009). "Adipocyte differentiation of bone marrow-derived mesenchymal stem cells: cross talk with the osteoblastogenic program." Cell Mol Life Sci **66**(2): 236-253.

Nakada, D., H. Oguro, B. P. Levi, N. Ryan, A. Kitano, Y. Saitoh, M. Takeichi, G. R. Wendt and S. J. Morrison (2014). "Oestrogen increases haematopoietic stem-cell self-renewal in females and during pregnancy." Nature **505**(7484): 555-558.

Nakamura, Y., F. Arai, H. Iwasaki, K. Hosokawa, I. Kobayashi, Y. Gomei, Y. Matsumoto, H. Yoshihara and T. Suda (2010). "Isolation and characterization of endosteal niche cell populations that regulate hematopoietic stem cells." Blood **116**(9): 1422-1432.

Nakashima, K., X. Zhou, G. Kunkel, Z. Zhang, J. M. Deng, R. R. Behringer and B. de Crombrugghe (2002). "The novel zinc finger-containing transcription factor osterix is required for osteoblast differentiation and bone formation." Cell **108**(1): 17-29.

Nauta, A. J. and W. E. Fibbe (2007). "Immunomodulatory properties of mesenchymal stromal cells." Blood **110**(10): 3499-3506.

Ng, L. J., S. Wheatley, G. E. Muscat, J. Conway-Campbell, J. Bowles, E. Wright, D. M. Bell, P. P. Tam, K. S. Cheah and P. Koopman (1997). "SOX9 binds DNA, activates transcription, and coexpresses with type II collagen during chondrogenesis in the mouse." Dev Biol **183**(1): 108-121.

Nifuji, A. and M. Noda (1999). "Coordinated expression of noggin and bone morphogenetic proteins (BMPs) during early skeletogenesis and induction of noggin expression by BMP-7." J Bone Miner Res **14**(12): 2057-2066.

Niswander, L., S. Jeffrey, G. R. Martin and C. Tickle (1994). "A positive feedback loop coordinates growth and patterning in the vertebrate limb." Nature **371**(6498): 609-612.

Ode, A., J. Schoon, A. Kurtz, M. Gaetjen, J. E. Ode, S. Geissler and G. N. Duda (2013). "CD73/5'-ecto-nucleotidase acts as a regulatory factor in osteo-

/chondrogenic differentiation of mechanically stimulated mesenchymal stromal cells." Eur Cell Mater **25**: 37-47.

Ohyama, A., F. Saito, H. Ohuchi and S. Noji (2001). "Differential expression of two BMP antagonists, gremlin and Follistatin, during development of the chick feather bud." Mech Dev **100**(2): 331-333.

Okabe, M., M. Ikawa, K. Kominami, T. Nakanishi and Y. Nishimune (1997). "Green mice' as a source of ubiquitous green cells." FEBS Lett **407**(3): 313-319.

Ornitz, D. M. and P. J. Marie (2002). "FGF signaling pathways in endochondral and intramembranous bone development and human genetic disease." Genes Dev **16**(12): 1446-1465.

Ortega, G., P. E. Korty, E. M. Shevach and T. R. Malek (1986). "Role of Ly-6 in lymphocyte activation. I. Characterization of a monoclonal antibody to a nonpolymorphic Ly-6 specificity." J Immunol **137**(10): 3240-3246.

Osyczka, A. M., D. L. Diefenderfer, G. Bhargave and P. S. Leboy (2004). "Different effects of BMP-2 on marrow stromal cells from human and rat bone." Cells Tissues Organs **176**(1-3): 109-119.

Ovchinnikov, D. A., J. Selever, Y. Wang, Y. T. Chen, Y. Mishina, J. F. Martin and R. R. Behringer (2006). "BMP receptor type IA in limb bud mesenchyme regulates distal outgrowth and patterning." Dev Biol **295**(1): 103-115.

Park, D., J. A. Spencer, B. I. Koh, T. Kobayashi, J. Fujisaki, T. L. Clemens, C. P. Lin, H. M. Kronenberg and D. T. Scadden (2012). "Endogenous bone marrow MSCs are dynamic, fate-restricted participants in bone maintenance and regeneration." Cell Stem Cell **10**(3): 259-272.

Pei, L. and P. Tontonoz (2004). "Fat's loss is bone's gain." J Clin Invest **113**(6): 805-806.

Peister, A., J. A. Mellad, B. L. Larson, B. M. Hall, L. F. Gibson and D. J. Prockop (2004). "Adult stem cells from bone marrow (MSCs) isolated from different strains of inbred mice vary in surface epitopes, rates of proliferation, and differentiation potential." Blood **103**(5): 1662-1668.

Pelttari, K., E. Steck and W. Richter (2008). "The use of mesenchymal stem cells for chondrogenesis." Injury **39 Suppl 1**: S58-65.

Pelttari, K., A. Winter, E. Steck, K. Goetzke, T. Hennig, B. G. Ochs, T. Aigner and W. Richter (2006). "Premature induction of hypertrophy during in vitro chondrogenesis of human mesenchymal stem cells correlates with calcification and vascular invasion after ectopic transplantation in SCID mice." Arthritis Rheum **54**(10): 3254-3266.

Peters, K. G., S. Werner, G. Chen and L. T. Williams (1992). "Two FGF receptor genes are differentially expressed in epithelial and mesenchymal tissues during limb formation and organogenesis in the mouse." Development **114**(1): 233-243.

Phinney, D. G., G. Kopen, R. L. Isaacson and D. J. Prockop (1999). "Plastic adherent stromal cells from the bone marrow of commonly used strains of inbred mice: variations in yield, growth, and differentiation." J Cell Biochem **72**(4): 570-585.

Pinho, S., J. Lacombe, M. Hanoun, T. Mizoguchi, I. Bruns, Y. Kunisaki and P. S. Frenette (2013). "PDGFRalpha and CD51 mark human nestin+ sphere-forming mesenchymal stem cells capable of hematopoietic progenitor cell expansion." J Exp Med **210**(7): 1351-1367.

Pittenger, M. F., A. M. Mackay, S. C. Beck, R. K. Jaiswal, R. Douglas, J. D. Mosca, M. A. Moorman, D. W. Simonetti, S. Craig and D. R. Marshak (1999). "Multilineage potential of adult human mesenchymal stem cells." Science **284**(5411): 143-147.

Pizette, S. and L. Niswander (2000). "BMPs are required at two steps of limb chondrogenesis: formation of prechondrogenic condensations and their differentiation into chondrocytes." Dev Biol **219**(2): 237-249.

Qiu, W., T. E. Andersen, J. Bollerslev, S. Mandrup, B. M. Abdallah and M. Kassem (2007). "Patients with high bone mass phenotype exhibit enhanced osteoblast differentiation and inhibition of adipogenesis of human mesenchymal stem cells." J Bone Miner Res **22**(11): 1720-1731.

Rebel, V. I., C. L. Miller, G. R. Thornbury, W. H. Dragowska, C. J. Eaves and P. M. Lansdorp (1996). "A comparison of long-term repopulating hematopoietic stem cells in fetal liver and adult bone marrow from the mouse." Exp Hematol **24**(5): 638-648.

Reif, A. E. and J. M. Allen (1963). "Specificity of Isoantisera against Leukaemic and Thymic Lymphocytes." Nature **200**: 1332-1333.

Retting, K. N., B. Song, B. S. Yoon and K. M. Lyons (2009). "BMP canonical Smad signaling through Smad1 and Smad5 is required for endochondral bone formation." Development **136**(7): 1093-1104.

Rodriguez, J. I., S. Razquin, J. Palacios and V. Rubio (1992). "Human growth plate development in the fetal and neonatal period." J Orthop Res **10**(1): 62-71.

Rombouts, W. J. and R. E. Ploemacher (2003). "Primary murine MSC show highly efficient homing to the bone marrow but lose homing ability following culture." Leukemia **17**(1): 160-170.

Rosen, E. D. (2005). "The transcriptional basis of adipocyte development." Prostaglandins Leukot Essent Fatty Acids **73**(1): 31-34.

Sabatini, F., L. Petecchia, M. Tavian, V. Jodon de Villeroche, G. A. Rossi and D. Brouty-Boye (2005). "Human bronchial fibroblasts exhibit a mesenchymal stem cell phenotype and multilineage differentiating potentialities." Lab Invest **85**(8): 962-971.

Sacchetti, B., A. Funari, S. Michienzi, S. Di Cesare, S. Piersanti, I. Saggio, E. Tagliafico, S. Ferrari, P. G. Robey, M. Riminucci and P. Bianco (2007). "Self-renewing osteoprogenitors in bone marrow sinusoids can organize a hematopoietic microenvironment." Cell **131**(2): 324-336.

Sarugaser, R., L. Hanoun, A. Keating, W. L. Stanford and J. E. Davies (2009). "Human mesenchymal stem cells self-renew and differentiate according to a deterministic hierarchy." PLoS One **4**(8): e6498.

Sasaki, J., T. Matsumoto, H. Egusa, M. Matsusaki, A. Nishiguchi, T. Nakano, M. Akashi, S. Imazato and H. Yatani (2012). "In vitro reproduction of endochondral ossification using a 3D mesenchymal stem cell construct." Integr Biol (Camb) **4**(10): 1207-1214.

Schmitt, B., J. Ringe, T. Haupl, M. Notter, R. Manz, G. R. Burmester, M. Sittinger and C. Kaps (2003). "BMP2 initiates chondrogenic lineage development of adult human mesenchymal stem cells in high-density culture." Differentiation **71**(9-10): 567-577.

Schwenk, F., U. Baron and K. Rajewsky (1995). "A cre-transgenic mouse strain for the ubiquitous deletion of loxP-flanked gene segments including deletion in germ cells." Nucleic Acids Res **23**(24): 5080-5081.

Scotti, C., E. Piccinini, H. Takizawa, A. Todorov, P. Bourgine, A. Papadimitropoulos, A. Barbero, M. G. Manz and I. Martin (2013). "Engineering of a functional bone organ through endochondral ossification." Proc Natl Acad Sci U S A **110**(10): 3997-4002.

Scotti, C., B. Tonnarelli, A. Papadimitropoulos, A. Scherberich, S. Schaeren, A. Schauerte, J. Lopez-Rios, R. Zeller, A. Barbero and I. Martin (2010). "Recapitulation of endochondral bone formation using human adult mesenchymal stem cells as a paradigm for developmental engineering." Proc Natl Acad Sci U S A **107**(16): 7251-7256.

Sekiya, I., J. T. Vuoristo, B. L. Larson and D. J. Prockop (2002). "In vitro cartilage formation by human adult stem cells from bone marrow stroma defines the sequence of cellular and molecular events during chondrogenesis." Proc Natl Acad Sci U S A **99**(7): 4397-4402.

Seo, H. S. and R. Serra (2007). "Deletion of Tgfbr2 in Prx1-cre expressing mesenchyme results in defects in development of the long bones and joints." Dev Biol **310**(2): 304-316.

Serafini, M., B. Sacchetti, A. Pievani, D. Redaelli, C. Remoli, A. Biondi, M. Riminucci and P. Bianco (2014). "Establishment of bone marrow and hematopoietic niches in vivo by reversion of chondrocyte differentiation of human bone marrow stromal cells." Stem Cell Res **12**(3): 659-672.

Shi, Y. and J. Massague (2003). "Mechanisms of TGF-beta signaling from cell membrane to the nucleus." Cell **113**(6): 685-700.

Shih, D. T., D. C. Lee, S. C. Chen, R. Y. Tsai, C. T. Huang, C. C. Tsai, E. Y. Shen and W. T. Chiu (2005). "Isolation and characterization of neurogenic mesenchymal stem cells in human scalp tissue." Stem Cells **23**(7): 1012-1020.

Simmons, P. J. and B. Torok-Storb (1991). "Identification of stromal cell precursors in human bone marrow by a novel monoclonal antibody, STRO-1." Blood **78**(1): 55-62.

Smits, P., P. Li, J. Mandel, Z. Zhang, J. M. Deng, R. R. Behringer, B. de Crombrugghe and V. Lefebvre (2001). "The transcription factors L-Sox5 and Sox6 are essential for cartilage formation." Dev Cell **1**(2): 277-290.

Solchaga, L. A., K. J. Penick and J. F. Welter (2011). "Chondrogenic differentiation of bone marrow-derived mesenchymal stem cells: tips and tricks." Methods Mol Biol **698**: 253-278.

Song, J., M. J. Kiel, Z. Wang, J. Wang, R. S. Taichman, S. J. Morrison and P. H. Krebsbach (2010). "An in vivo model to study and manipulate the hematopoietic stem cell niche." Blood **115**(13): 2592-2600.

St-Jacques, B., M. Hammerschmidt and A. P. McMahon (1999). "Indian hedgehog signaling regulates proliferation and differentiation of chondrocytes and is essential for bone formation." Genes Dev **13**(16): 2072-2086.

Starlinger, P., P. Brugger, C. Reiter, D. Schauer, S. Sommerfeldt, D. Tamandl, I. Kuehrer, S. F. Schoppmann, M. Gnant and C. Brostjan (2011). "Discrimination between circulating endothelial cells and blood cell populations with overlapping phenotype reveals distinct regulation and predictive potential in cancer therapy." Neoplasia **13**(10): 980-990.

Steinert, A. F., B. Proffen, M. Kunz, C. Hendrich, S. C. Ghivizzani, U. Noth, A. Rethwilm, J. Eulert and C. H. Evans (2009). "Hypertrophy is induced during the in vitro chondrogenic differentiation of human mesenchymal stem cells by bone morphogenetic protein-2 and bone morphogenetic protein-4 gene transfer." Arthritis Res Ther **11**(5): R148.

Takakura, N., H. Yoshida, Y. Ogura, H. Kataoka, S. Nishikawa and S. Nishikawa (1997). "PDGFR alpha expression during mouse embryogenesis: immunolocalization analyzed by whole-mount immunohistostaining using the

monoclonal anti-mouse PDGFR alpha antibody APA5." J Histochem Cytochem **45**(6): 883-893.

Tavassoli, M. and W. H. Crosby (1968). "Transplantation of marrow to extramedullary sites." Science **161**(3836): 54-56.

Ten Berge, D., S. A. Brugmann, J. A. Helms and R. Nusse (2008). "Wnt and FGF signals interact to coordinate growth with cell fate specification during limb development." Development **135**(19): 3247-3257.

Tian, H., S. Yang, L. Xu, Y. Zhang and W. Xu (2007). "Chondrogenic differentiation of mouse bone marrow mesenchymal stem cells induced by cartilage-derived morphogenetic protein-2 in vitro." J Huazhong Univ Sci Technolog Med Sci **27**(4): 429-432.

Tokoyoda, K., T. Egawa, T. Sugiyama, B. I. Choi and T. Nagasawa (2004). "Cellular niches controlling B lymphocyte behavior within bone marrow during development." Immunity **20**(6): 707-718.

Tokunaga, A., T. Oya, Y. Ishii, H. Motomura, C. Nakamura, S. Ishizawa, T. Fujimori, Y. Nabeshima, A. Umezawa, M. Kanamori, T. Kimura and M. Sasahara (2008). "PDGF receptor beta is a potent regulator of mesenchymal stromal cell function." J Bone Miner Res **23**(9): 1519-1528.

Tolar, J., K. Le Blanc, A. Keating and B. R. Blazar (2010). "Concise review: hitting the right spot with mesenchymal stromal cells." Stem Cells **28**(8): 1446-1455.

Uccelli, A., L. Moretta and V. Pistoia (2008). "Mesenchymal stem cells in health and disease." Nat Rev Immunol **8**(9): 726-736.

van den Heuvel, M. and P. W. Ingham (1996). "smoothened encodes a receptor-like serpentine protein required for hedgehog signalling." Nature **382**(6591): 547-551.

Van der Stok, J., M. K. Koolen, H. Jahr, N. Kops, J. H. Waarsing, H. Weinans and O. P. van der Jagt (2014). "Chondrogenically differentiated mesenchymal stromal cell pellets stimulate endochondral bone regeneration in critical-sized bone defects." Eur Cell Mater **27**: 137-148; discussion 148.

Vintersten, K., C. Monetti, M. Gertsenstein, P. Zhang, L. Laszlo, S. Biechele and A. Nagy (2004). "Mouse in red: red fluorescent protein expression in mouse ES cells, embryos, and adult animals." Genesis **40**(4): 241-246.

Weissman, I. L., Shizuru, J. A. (2008). "The origins of the identification and isolation of hematopoietic stem cells, and their capability to induce donor-specific transplantation tolerance and treat autoimmune diseases." Blood **112**(9): 3543-3553.

Wijgerde, M., S. Karp, J. McMahon and A. P. McMahon (2005). "Noggin antagonism of BMP4 signaling controls development of the axial skeleton in the mouse." Dev Biol **286**(1): 149-157.

Worthley, D. L., M. Churchill, J. T. Compton, Y. Tailor, M. Rao, Y. Si, D. Levin, M. G. Schwartz, A. Uygur, Y. Hayakawa, S. Gross, B. W. Renz, W. Setlik, A. N. Martinez, X. Chen, S. Nizami, H. G. Lee, H. P. Kang, J. M. Caldwell, S. Asfaha, C. B. Westphalen, T. Graham, G. Jin, K. Nagar, H. Wang, M. A. Kheirbek, A. Kolhe, J. Carpenter, M. Glaire, A. Nair, S. Renders, N. Manieri, S. Muthupalani, J. G. Fox, M. Reichert, A. S. Giraud, R. F. Schwabe, J. P. Pradere, K. Walton, A. Prakash, D. Gumucio, A. K. Rustgi, T. S. Stappenbeck, R. A. Friedman, M. D. Gershon, P. Sims, T. Grikscheit, F. Y. Lee, G. Karsenty, S. Mukherjee and T. C. Wang (2015). "Gremlin 1 identifies a skeletal stem cell with bone, cartilage, and reticular stromal potential." Cell **160**(1-2): 269-284.

Yamamoto, M., H. Nakata, J. Hao, J. Chou, S. Kasugai and S. Kuroda (2014). "Osteogenic Potential of Mouse Adipose-Derived Stem Cells Sorted for CD90 and CD105 In Vitro." Stem Cells Int **2014**: 576358.

Yi, S. E., A. Daluiski, R. Pederson, V. Rosen and K. M. Lyons (2000). "The type I BMP receptor BMPRIB is required for chondrogenesis in the mouse limb." Development **127**(3): 621-630.

Yoo, J. U., T. S. Barthel, K. Nishimura, L. Solchaga, A. I. Caplan, V. M. Goldberg and B. Johnstone (1998). "The chondrogenic potential of human bone-marrow-derived mesenchymal progenitor cells." J Bone Joint Surg Am **80**(12): 1745-1757.

Yoon, B. S., D. A. Ovchinnikov, I. Yoshii, Y. Mishina, R. R. Behringer and K. M. Lyons (2005). "Bmpr1a and Bmpr1b have overlapping functions and are essential for chondrogenesis in vivo." Proc Natl Acad Sci U S A **102**(14): 5062-5067.

Young, K., B. Conley, D. Romero, E. Tweedie, C. O'Neill, I. Pinz, L. Brogan, V. Lindner, L. Liaw and C. P. Vary (2012). "BMP9 regulates endoglin-dependent chemokine responses in endothelial cells." Blood **120**(20): 4263-4273.

Zeller, R., J. Lopez-Rios and A. Zuniga (2009). "Vertebrate limb bud development: moving towards integrative analysis of organogenesis." Nat Rev Genet **10**(12): 845-858.

Zhang, Y., D. Khan, J. Delling and E. Tobiasch (2012). "Mechanisms underlying the osteo- and adipo-differentiation of human mesenchymal stem cells." ScientificWorldJournal **2012**: 793823.

Zhao, Q., H. Eberspaecher, V. Lefebvre and B. De Crombrugghe (1997). "Parallel expression of Sox9 and Col2a1 in cells undergoing chondrogenesis." Dev Dyn **209**(4): 377-386.

Zhou, B. O., R. Yue, M. M. Murphy, J. G. Peyer and S. J. Morrison (2014). "Leptin-receptor-expressing mesenchymal stromal cells represent the main source of bone formed by adult bone marrow." Cell Stem Cell **15**(2): 154-168.

Zuk, P. A., M. Zhu, P. Ashjian, D. A. De Ugarte, J. I. Huang, H. Mizuno, Z. C. Alfonso, J. K. Fraser, P. Benhaim and M. H. Hedrick (2002). "Human adipose tissue is a source of multipotent stem cells." Mol Biol Cell **13**(12): 4279-4295.

Zuniga, A. (2015). "Next generation limb development and evolution: old questions, new perspectives." Development **142**(22): 3810-3820.

Zuniga, A., A. P. Haramis, A. P. McMahon and R. Zeller (1999). "Signal relay by BMP antagonism controls the SHH/FGF4 feedback loop in vertebrate limb buds." Nature **401**(6753): 598-602.

12. Appendix

I: Cell cycle analysis of PαS cells in culture by BrdU incorporation and 7AAD DNA content
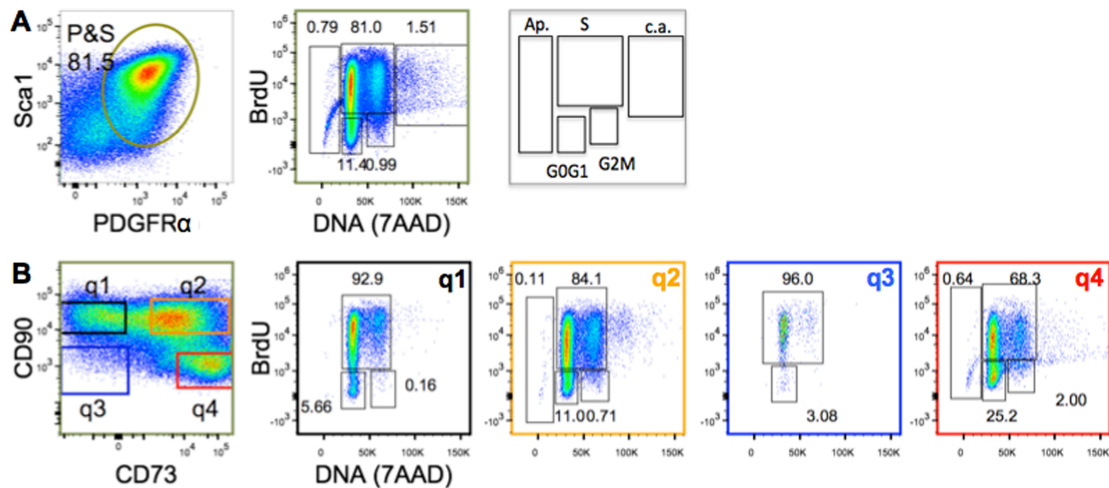

Fig. I (A) Cell cycle analysis of PαS cells expanded in vitro by BrdU incorporation and DNA content (stained with 7AAD). This combination detects apoptotic cells (Ap.) and resolves cell cycle phases into S, G_0/G_1, and G_2/M phases as shown in the right panel. c.a. = cell aggregates. **(B)** Phases of cell cycle in the 4 subpopulations of PαS cells (q1, q2, q3 and q4). A cells from q3 subset shows maximum BrdU incorporation (S phase 96%), followed by q1 (93%), q2 (84%) and q4 (68%).

II: Development of HSCs/HPCs pool from fetal liver till postnatal bone
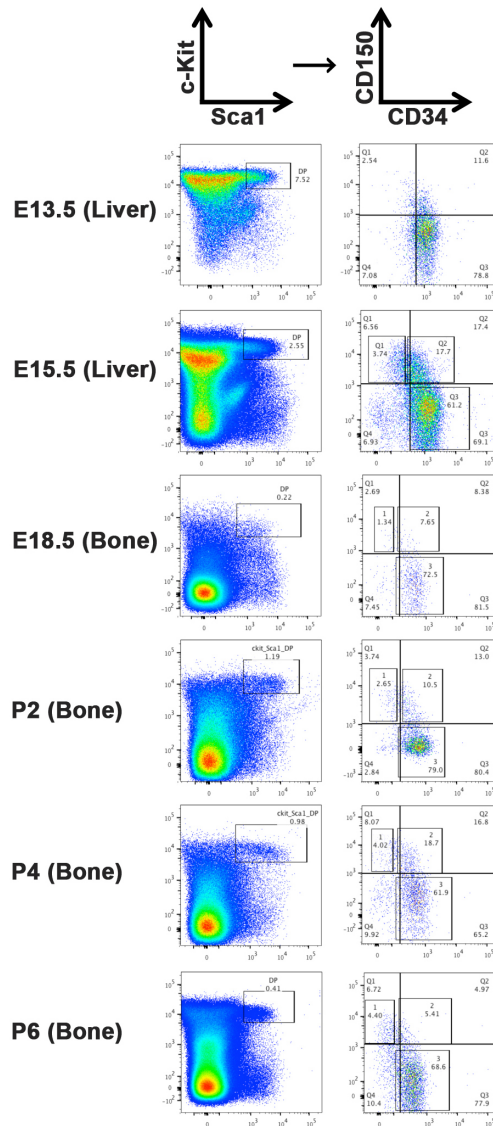
Fig. II: Representative gatings on LSK cells (Sca1$^+$c-Kit$^+$ fraction from Lin$^-$ fraction) of from liver and crushed bone are shown in the left panels. Combination of CD150 (SLAM) and CD34 splits the LSK cells into long term (which lies in LSKCD34$^-$ subset) and short term (which lies in LSKCD34$^+$ subset) HSCs, shown in the right panel. 'Lin' fraction constitute of cells positive for: CD3, Gr-1, FLK-1, PDGFRα, CD31, CD11b, and Ter119.

III: PαS cells maintain the expression of CD90 and CD73 for few days in culture

The in vitro and in vivo assays with PαS cells (and their subpopulations) were performed after a short-term expansion (5 days) of these cells in serum-based culture medium. This period of time for expansion of cells was chosen after establishing that the CD signature of these cells do not change over a short time of expansion and hence would not compromise the multilineage potential in trilineage assays.
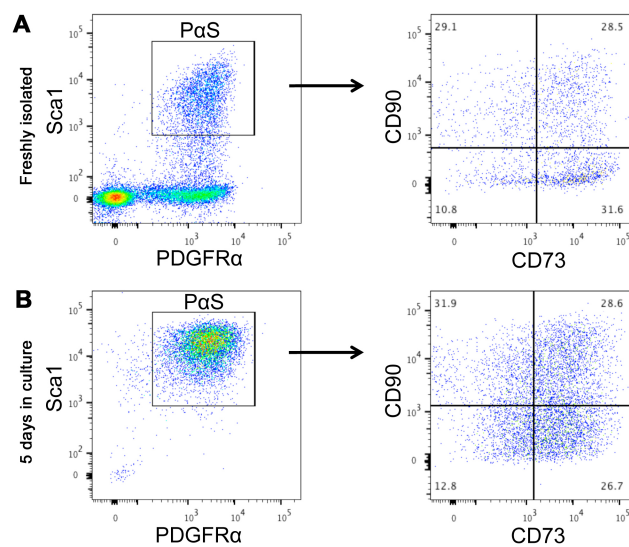

Fig. III: (A) Representative gatings for CD90 and CD73 expression on freshly isolated PαS cells from P2 mice. **(B)** Representative gatings for CD90 and CD73 expression on PαS cells (from A) after 5 days in culture.

IV: In vitro chondrogenic differentiation of PαS cells do not mature to hypertrophy during the time of chondrogenic differentiation
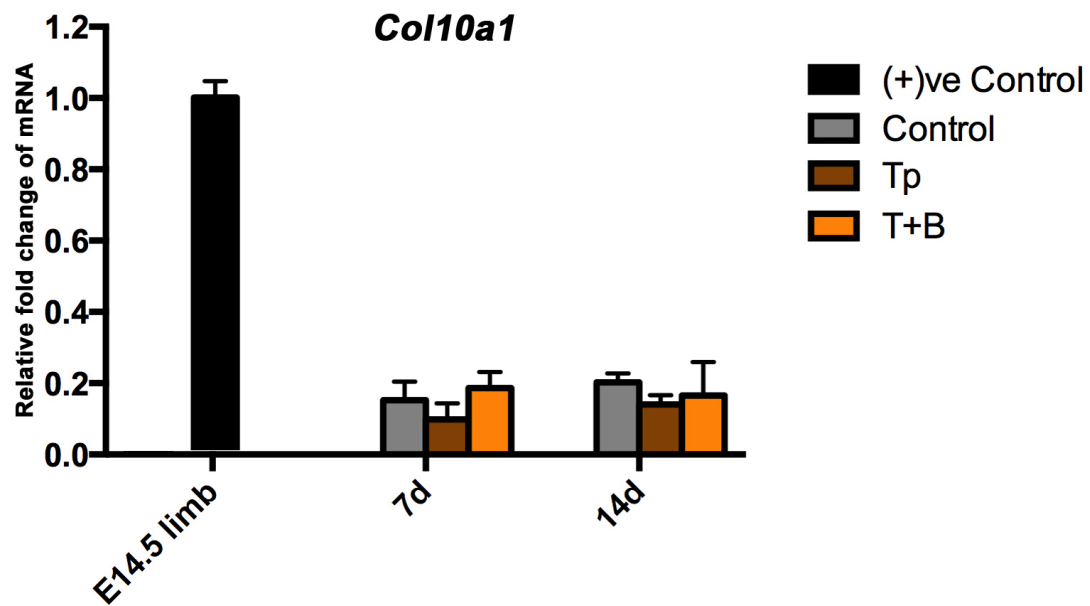

Fig. IV: mRNA fold change of *Col10a1* in adult PαS cells during chondrogenic differentiation at day 7 and day 14. E14.5 Limb is set as positive control to set *Col10a1* expression to 1.0. Control = PαS cells at high density in expansion medium; (+)ve Control is limb cells from E14.5. Tp = PαS cells at high density in 'Tp' differentiation medium; T+B = PαS cells at high density in 'T+B' differentiation medium.

V: PαS cells that express CD15 (Stage-Specific Embryonic Antigen-1 or SSEA-1) lie as a small fraction of q3 (PαS$^+$CD90$^-$CD73) subpopulation
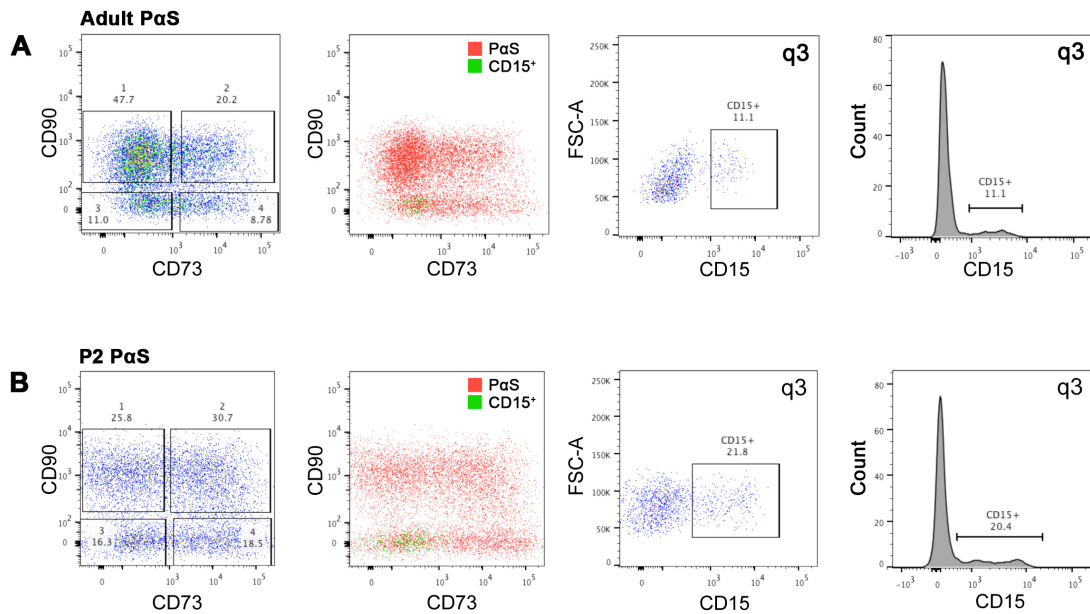

Fig. V: (A) Representative gatings and histogram of CD15$^+$ cells in PαS subpopulations (q1-q4, left panel) of adult mice. CD15$^+$ cells (shown in green) are located in the q3 subpopulation of PαS cells (shown in red). CD15$^+$ cells constitute ~10% of q3 subpopulation (3rd panel and histogram) **(B)** Representative gatings and histogram of CD15$^+$ cells in PαS subpopulations (q1-q4, left panel) of P2 mice. CD15$^+$ cells (shown in green) are located in the q3 subpopulation of PαS cells (shown in red). CD15$^+$ cells constitute ~20% of q3 subpopulation (3rd panel and histogram).

VI: In vivo fate of PαS, PαS⁺CD90⁺ and PαS⁺CD90⁻ subsets from E18.5

(a)
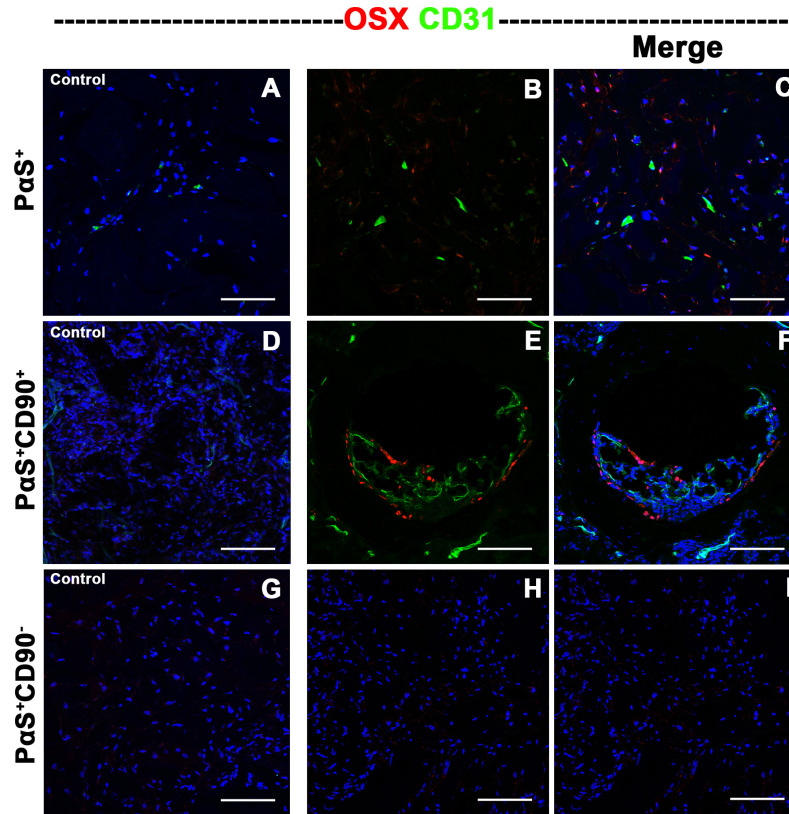
Fig. VI (a). Cartilage templates derived from perinatal (E18.5) PαS$^+$CD90$^+$ cells are only partially remodeled into bone, which attracts endothelial cells (A, D, F) Undifferentiated control implants. **(B, C, E, F, H, I)** Immunofluorescence analysis of the Osterix (OSX in red) and CD31 (green) distributions in implants derived from PαS (B, C), PαS$^+$CD90$^+$ (E, F) and PαS$^+$CD90$^+$ cells (H, I). Nuclei are detected by Hoechst (blue). Scale bar = 100 μm. (n= 3 independent experiments).

(b)
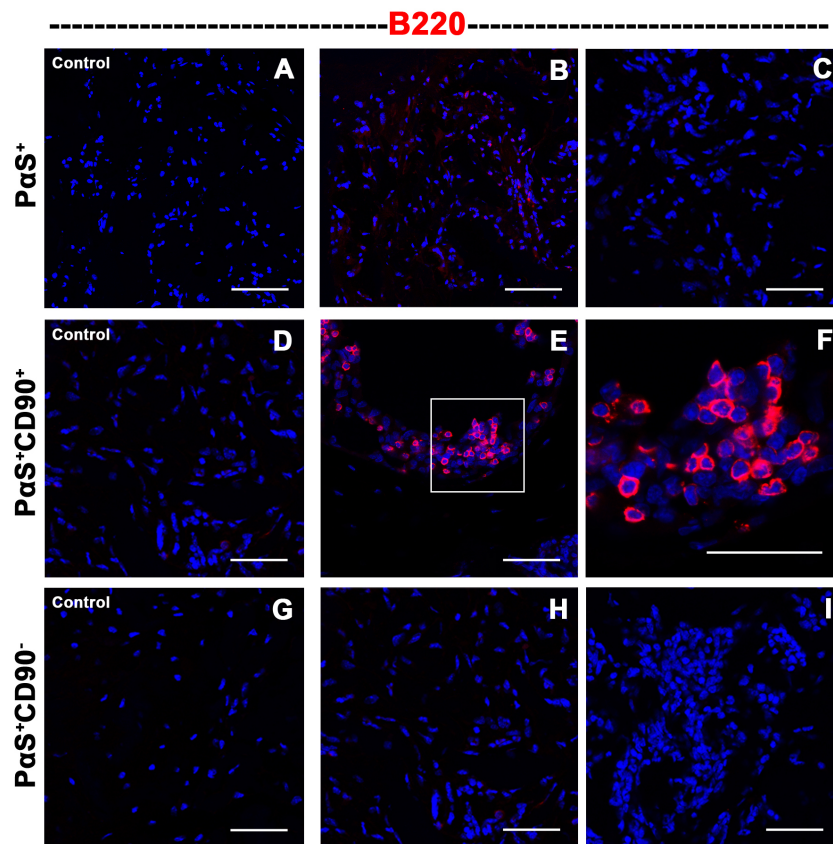
Fig. VI (b). PαS⁺CD90⁺ derived implants support B-cell development at the site of bone formation. (A, D, F) Representative area of undifferentiated control implants **(B, C, E, F, H, I)** immunofluorescent analysis of the B220 (red) distribution in implants of PαS (B, C), PαS⁺CD90⁺ (E, F) and PαS⁺CD90⁺ cells (H, I). Nuclei are detected by Hoechst (blue). Scale bar = 100μm. (n= 3 independent experiments).

(c)
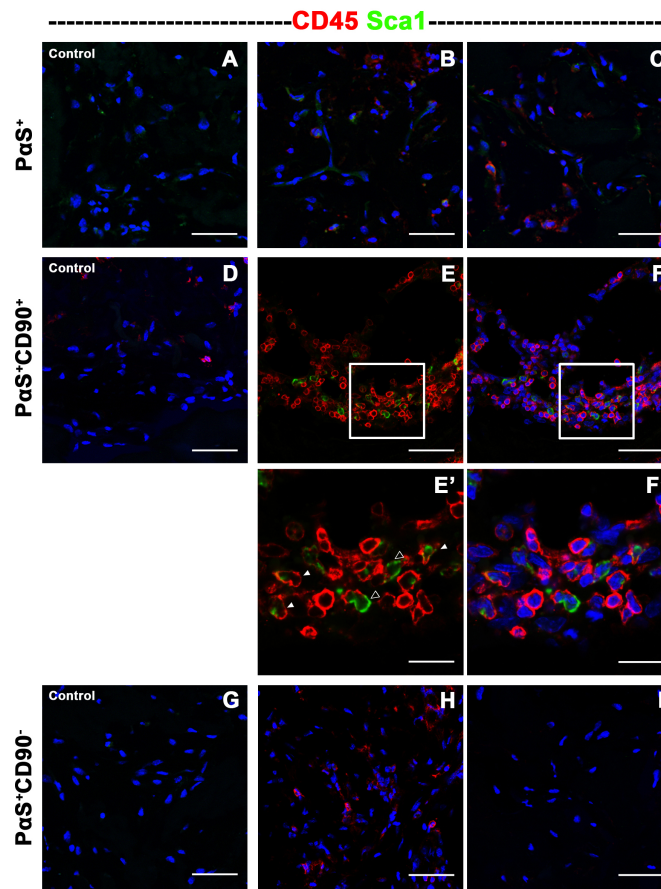
Fig. VI (c). Implants from PαS⁺CD90⁺ derived implants support hematopoiesis (HPCs) at sites of bone formation. (**A, D, G**) Representative area of undifferentiated control implants. (**B, C, E, E', F, F', H, I**) Immunofluorescent analysis of the distribution of the CD45 (red) and Sca1 (green) on sections of implants derived from PαS (B, C), PαS⁺CD90⁺ (E, E', F, F') and PαS⁺CD90⁺ cells (H, I). Cells co-expressing Sca1 and CD45 were detected (E', solid arrowhead. In addition, Sca1 single positive cells were also detected (E', hollow arrowhead). (**H, I**) Only few CD45-positive cells were detected in PαS⁺CD90⁻ derived implants and controls. Nuclei are detected by Hoechst (blue). Scale bar = 50µm. Scale bars for enlargements (E', F') = 10µm. (n= 3 independent experiments).

VII: Manuscript in preparation (1)

"Characterization of early mouse mesenchymal stem/progenitor cells for generating cartilage and study their role in endochondral ossification"

Sumit Jaiswal[1*], Gretel Nusspaumer[1*], Andrea Barbero[1], Atanas Todorov[1], Dana Ronen[1], Gerhard Christofori[1] Ivan Martin[1], Rolf Zeller[1]

[1]Departement of Biomedicine, University of Basel, Switzerland

*The project details are discussed as a part of this thesis work.

VIII: Manuscript in preparation (2)

"Quantitative analysis of vertebrate limb bud growth and proliferation kinetics"

Erkan Ünal[1,2,3], Jannik Vollmer[2,3], Gretel Nusspaumer[1], Sumit Jaiswal[1], Rolf Zeller[1]*, Dagmar Iber[2,3]*

[1]Department of Biomedicine, University of Basel, Mattenstrasse 28, 4058, Basel, Switzerland

[2]Department of Biosystems, Science and Engineering (D-BSSE), ETH Zurich, Switzerland

[3]Swiss Institute of Bioinformatics (SIB), Mattenstraße 26, 4058 Basel, Switzerland

Abstract: The cellular and molecular mechanisms controlling organ size have remained rather elusive and quantitative data are largely missing to evaluate models and hypotheses in mammalian systems. We combined limb bud mesenchyme specific reporter gene expression with FACS (fluorescent-activated cell sorting) analysis and 3D imaging to generate quantitative datasets for mouse and chicken limb buds. In particular, with have quantitated mesenchymal cells numbers for mouse forelimb buds. This analysis reveals the striking biphasic behaviour of limb bud growth in both species. In spite of the growth rates being higher in chicken than mouse forelimb buds, the switch in growth behaviour occurs upon reaching similar mesenchymal cell numbers in both species. This switch point coincides with the time window during which the autopod primordia (hand plate) forms, but the slower proliferation of the SOX9-positive osteo-chondrogenic progenitors cannot account for the observed switch to lower limb bud growth. Rather, the biphasic growth behaviour is the result of the continuous decline in proliferation of all limb bud mesenchymal cells. The experimental results are computationally analysis using different growth laws for simulations. Intriguingly, the growth behaviour of the *Drosophila* wing disc can be described with the same growth laws. This raises the possibility of an evolutionary conserved mechanism for growth control that is not *per se* linked to a specific tissue-patterning program.

My contribution to this project was to perform the BrdU incorporation studies in mouse embryonic limb bud at different somite stages and analyse them through fluorescent microscopy. I analysed the limb progenitor cells that were in proliferative state (BrdU labelling) and that were committed towards osteo-chondro-lineage (Sox9$^+$) (Fig. VIII). These results validated the flow cytometry based analysis performed at same somite stages of mouse limb buds and hence contributed to the datasets in the manuscript.
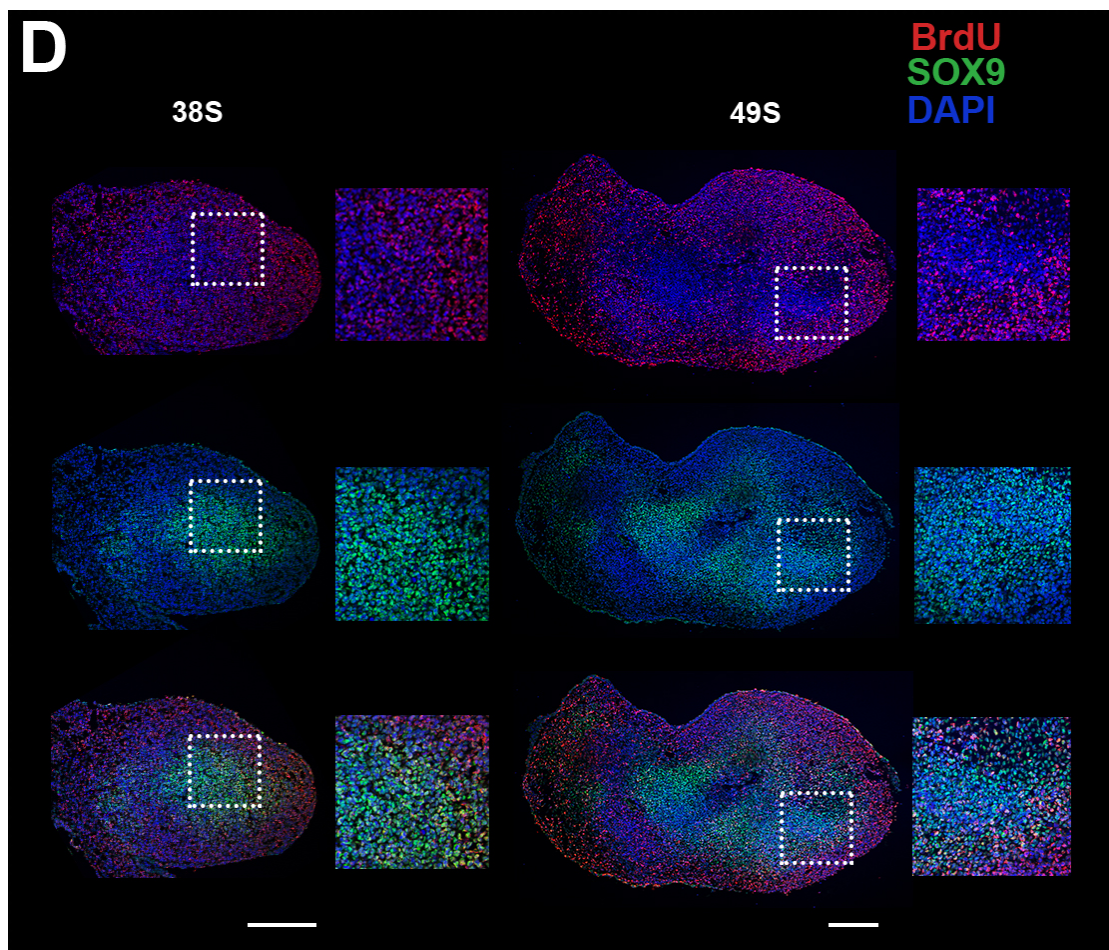

Fig. VIII. Immunofluorescent analysis of BrdU labelling (red), together with SOX9 (green), and DAPI (blue) staining in mouse limb buds at the indicated somite stages (S). Scale bar = 200 µm. (n ≥ 5 independent experiments).